NTNU

Norwegian University of
Science and Technology

Feasibility study of high-rise timber buildings using moment resisting frames

Vegard Klund
Paal Greva Skovdahl
Kristine Hansine Ullsfoss
Torp

Civil and Environmental Engineering
Submission date: June 2017
Supervisor: Kjell A Malo, KT

Norwegian University of Science and Technology
Department of Structural Engineering

Department of Structural Engineering
Faculty of Engineering Science and Technology
NTNU- Norwegian University of Science and Technology

ACCESSIBILITY

Open

MASTER THESIS 2017

SUBJECT AREA:	DATE:	NO. OF PAGES:
Structural Engineering	10.06.2017	109 + 37 Appendix

TITLE

Feasibility study of high-rise timber buildings using moment resisting frames

Mulighetsstudie av høyhus i tre ved bruk av momentstive rammer

BY:

Vegard Klund

Paal Greva Skovdahl

Kristine Ullsfoss Torp



SUMMARY:
This master thesis is a part of the WoodSol project, a research project coordinated by NTNU, Department of Structural Engineering. This study includes an investigation of the serviceability state issues on high-rise timber buildings. The buildings studied have a structural system where moment resisting frames are used for horizontal bracing in one direction. The bracing is enhanced by the stiffness from composite wood slabs. The work is limited to examine the acceleration, deflection and the fire capacity of the system.

The first part of the thesis describes wood as a construction material, and the requirements and design considerations for the structural system. The models investigated were based on two main designs. One simple design with rectangular footprint and one unsymmetrical, hence more complicated, T-shape design. The finite element program *Abaqus* was used for the modelling. A verification process was preformed to ensure the validity of the numerical simulations.

A parametric study was done to map the response and robustness of the structural system. For each model, properties of different building components, e.g. cross sections dimensions, the rotational stiffness in the connections and the boundary conditions were changed. Then, a modal analysis was done to find the dynamic properties of the models. The natural frequency and mass were used to calculate the acceleration and the structural factor, $c_s c_d$, which is used to calculate the wind loads affecting the model. Both ULS and SLS load combinations have been checked, giving results for evaluating the fire design and the deflections in the top of the building, respectively.

Acceleration was found to be the governing requirement, which was expected based on previous work done on high-rise timber buildings. From the findings of this work, it can be concluded that it will be possible to build high-rise timber buildings using the structural system with moment resisting frames bracing the building in one direction. To meet the requirements for acceleration, deflection and fire capacity, modifications have to be done. Like adding extra mass, increasing column sections and connecting shafts to the structural system. With the right modifications, it is possible to build eight storey high buildings, and probably higher.

RESPONSIBLE TEACHER: Kjell Arne Malo

SUPERVISOR(S): Kjell Arne Malo, Haris Stamatopoulos

CARRIED OUT AT: Department of Structural Engineering, NTNU

Preface

This master thesis is a part of the 5-year study program, Civil and Environmental Engineering. This thesis is written at the Department of Structural Engineering at the Norwegian University of Science and Technology (NTNU), during the spring semester of 2017. The work done is a part of the research project WoodSol, *Wood frame solutions for free space design in urban buildings*, at NTNU.

The work consisted of doing numerical analysis and a parametric study of structural systems for a five to 10 storey timber building. The work has given us a greater understanding on structural systems in high-rise buildings, and the challenges and advantages for building with wood. We have learned more on the complexity of the peak acceleration calculation, and how the results depend on changes to the building through a parametric study. Due to little prior experience, a lot of time was spent learning the FEM-program *Abaqus* and we are now familiar with many of the programs functions and possibilities.

We are very grateful to supervisor Kjell Arne Malo and co-supervisor Haris Stamatopoulos for all the guidance and helpful discussions through the entire semester. Further we would like to thank the rest of the WoodSol group for help and inspiration, and hope our work is found useful. Finally, we would like to thank all our classmates for making the years here at NTNU so memorable.

Trondheim, 10th June 2017

Vegard Klund

Paal Greva Skovdahl

Kristine Ullsfoss Torp

Abstract

This master thesis is a part of the WoodSol project, a research project coordinated by NTNU, Department of Structural Engineering. This study includes an investigation of the serviceability state issues on high-rise timber buildings. The buildings studied have a structural system where moment resisting frames are used for horizontal bracing in one direction. The bracing is enhanced by the stiffness from composite wood slabs. The work is limited to examine the acceleration, deflection and the fire capacity of the system.

The first part of the thesis describes wood as a construction material, and the requirements and design considerations for the structural system. The models investigated were based on two main designs. One simple design with rectangular footprint and one unsymmetrical, hence more complicated, T-shape design. The finite element program *Abaqus* was used for the modelling. A verification process was preformed to ensure the validity of the numerical simulations.

A parametric study was done to map the response and robustness of the structural system. For each model, properties of different building components, e.g. cross sections dimensions, the rotational stiffness in the connections and the boundary conditions were changed. Then, a modal analysis was done to find the dynamic properties of the models. The natural frequency and mass were used to calculate the acceleration and the structural factor, $c_s c_d$, which is used to calculate the wind loads affecting the model. Both ULS and SLS load combinations have been checked, giving results for evaluating the fire design and the deflections in the top of the building, respectively.

Acceleration was found to be the governing requirement, which was expected based on previous work done on high-rise timber buildings. From the findings of this work, it can be concluded that it will be possible to build high-rise timber buildings using the structural system with moment resisting frames bracing the building in one direction. To meet the requirements for acceleration, deflection and fire capacity, modifications have to be done. Like adding extra mass, increasing column sections and connecting shafts to the structural system. With the right modifications, it is possible to build eight storey high buildings, and probably higher.

Sammendrag

Denne masteroppgaven er skrevet som en del av forskningsprosjektet WoodSol, som er ledet av NTNU ved Instituttet for konstruksjonsteknikk. Oppgaven innholder et studie av bruksgrensetilstanden til høyhus i tre, der et bæresystem basert på momentstive rammer bidrar til horisontal avstivning. Studiet er begrenset til å undersøke akselerasjonen, utbøyningen og brannkapasiteten til konstruksjonen.

Den første delen av oppgaven beskriver tre som konstruksjonsmateriale og går gjennom kravene konstruksjonssystemet må tilfredsstille. Modellene som er undersøkt er basert på to hoveddesign. Et enkelt, med et rektangulært fotavtrykk, og et mer komplekst og usymmertisk T-formet design. *Abaqus*, som er et program som utfører numeriske simuleringer, ble brukt til modellering og analyser. For å sikre korrekt modellering, ble det utført en verifiserinsprosess.

Et paramterstudie ble gjennomført for å kartlegge ytelsen og robustheten til bæresystemet. For hver modell er det blitt gjort endringer av egenskaper for utvalgte bygningskomponenter, og utført modale analyser for å finne dens dynamiske egenskaper. Modellens egenmoder og masse ble brukt til å regne ut akselerasjon, mens konstruksjonsfaktoren, $c_s c_d$, ble brukt til å regne ut vindlasten som modellene ble utsatt for. Lastkombinasjoner for både brudd- og bruksgrensetilstand er brukt til henholdsvis å vurdere bygningens brannkapasitet, og utbøyning i øverste etasje.

Akselerasjonskriteriet viste seg å være vanskeligst å nå. Dette var forventet, da tidligere arbeid som omhandler høyhus i tre har indikert det samme. Basert på resultater fra arbeidet med denne rapporten, kan man konkludere med at det er mulig å bygge høyhus i tre med konstruksjonssystemer som bruker momentstive rammer til avsivning i en retning. For å nå akseptable verdier for akselerasjon, utbøyning og brannkapasitet, kan modifikasjoner som å legge til masse i bygningen, øke søylers tverrsnittsstørrelser og koble en sjakt til det stabiliserende systemet gjøres. Med de riktige modifikasjonene kan man bygge åtte etasjers høyhus i tre, og sannsynligvis høyere, med dette konstruksjonssystemet.

Contents

Chapter 1

Introduction

1.1 Starting point

This master thesis is a part the WoodSol project. The project is coordinated by NTNU, Department of Structural Engineering, and was started in 2016. The main goal of WoodSol is to *develop industrialised structural solutions, based on rigid wooden frames, for use in urban buildings having five to 10 storeys open architecture* [42].

The increasing urbanisation have created a demand for more high-rise buildings, but to meet the environmental challenges of today the building industry needs to cut their carbon emissions. A solution to this problem can be the use of more environmental friendly materials, like wood, which is considered to be carbon neutral. There has been a growing interest among developers and architects to use more wood products. A study conducted for *Statsbygg* disclosed that there is a lack of knowledge and standardised solutions for high-rise timber buildings, which makes it a bigger risk to choose wood over more traditional and familiar structural systems based on concrete and steel [37]. For this to change, there needs to be developed industrialised structural concepts that are robust and flexible with low economic risk. Prior work done on high-rise buildings in timber, show that satisfying the serviceability limit state requirements can be challenging [40] [3]. A light material like wood can result in high accelerations and horizontal deflection at the top floor.

1.2 Objectives and limitations

This work includes studying several different building designs, where the structural system is based on the use of moment resisting frames. Their natural frequencies, mode shapes and response to wind load is evaluated. Subsequently looking at the acceleration, deflection and response to fire load. The objective of this master thesis is to develop an understanding, with help of a parametric study, of the global response in the serviceability limit state, and how the different geometries and change of parameters effect the results.

The focus of this work has been a global analysis of the serviceability limit state of the buildings, and it will not include

- seismic performance
- vertical deflection and response of the slabs
- detailing of solutions
- acoustic evaluation
- evaluation of erection and assembly
- Life Cycle Cost (LCC) and Life Cycle Analysis (LCA)

1.3 Approach and structure of thesis

The thesis starts with an overview of the requirements and design considerations. The relevant work done in WoodSol is presented, followed by some background on the use of wood as the material in a structural system. The typologies of the buildings are decided and the requirements they are to satisfy are presented. Then there is performed a verification of the numerical model. This to validate the simplifications of the model used for analysis in the finite element program *Abaqus*. The result from the analysis is presented for each model and discussed further, before some conclusive remarks are made. At last, some recommendations for further work are presented.

Chapter 2

Background

This chapter gives the basis for the structural system and the requirements that should be considered in the design and modelling process.

2.1 Typology

Some guidelines for the typology must be established as basis for the structural system. The typology of a building concerns its shape, height and footprint, as well as the need for open spaces and the sectioning of the building. These parameters are essential for how the structural system should be, deciding the placement of supporting elements and how the loads are carried through the building. Some examples of footprints are shown in Figure 2.1.

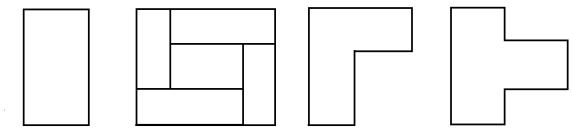

Figure 2.1: Examples of footprints

In this thesis, the premise for the building is to meet the volume market, focusing on residential and office buildings in urban areas. As the population is growing and more people move into cities, it is likely that cities develop towards getting a higher population density. To enable this, the cities need to be more compact, and this can be done by building higher or by adding storeys on top of existing buildings. The structural system should be robust and flexible to allow open architecture and future changes of

use, preferably with repetitive prefabricated elements and a symmetrical layout. If this is successful, the assembly of the building will be fast and uncomplicated. Variations as cantilever elements, balconies and different roof structures should be easily implemented to the simple and robust structural system. For future flexibility it is tried to use as few inner columns and shear walls as possible, creating big open spaces. Based on the prestudy done by the WoodSol project and the interviews done in the context of this thesis[1], some constrains and guidelines are defined, see Table 2.1.

Table 2.1: Constrains of structural lay-out of components

Number of storeys	5 to 10 stricter fire regulation over 8 storeys
Net storey height	min. 2.4 m (residential) min. 2.6 - 2.7 m (offices etc.)
Span length of floor elements	8 to 10 m
Maximum size of components (due to transport)	width: 2.4 m length: 35 m

[1] Veidekke att: Sigbjørn Faanes, Kjeldsberg att: Harald Bjørlykke and Trondheim kommune att: Arve Arstad

2.2 Wood as construction material

Wood is an anisotropic material, meaning that the properties are dependent on directions. The stiffness in the longitudinal direction is 10-15 times higher than the radial, and 20-30 times higher than the tangential [6]. The material directions are illustrated in Figure 2.2.

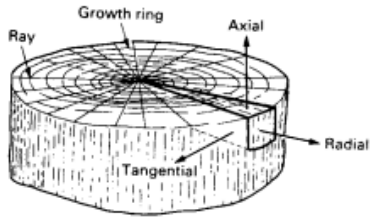

Figure 2.2: Material orientation of wood
[7]

Wood is a material with high strength and stiffness compared to its weight. The modulus of elasticity (E) is low compared to steel and concrete, but the specific stiffness is similar to steel, see Table 2.2.

Table 2.2: Material properties for steel, concrete[2] and wood [24]

Material	E [MPa]	ρ [kg/m^3]	**Specific stiffness** E/ρ
Steel	210000	7800	27
Concrete	35000	2400	14
Wood (C24)	11000	420	26

Construction elements where large portions of the load comes from its own self-weight, like slabs, will be a lot lighter using wood compared to concrete or steel. A building with low self-weigh is beneficial in urban areas, where the possibility for foundation can be limited, or when wanting to add more storeys on top of an existing building [32]. Development of more engineered wood products utilise the advantages of the material properties and make the use of wood more suitable for tall buildings.

[2] Depending on the concrete class

(a) GLT [19] (b) CLT [1] (c) LVL [18]

Figure 2.3: Construction materials in wood

Glue Laminated Timber, GLT

Figure 2.3a shows a GLT beam. GLT, or glulam, consists of wood panel layers glued and compressed together. Either homogeneous, with the same strength in all layers, or in-homogeneous, with varying strength. The material properties are better than for construction timber and it is used for both buildings and bridges. Glulam beams can be curved, have large spans and be produced with almost any dimension of cross section. There are several big producers in Norway, among other, Moelven and Splitcon.

Cross Laminated Timber, CLT

Figure 2.3b shows typical CLT panels. Developed in the 1990s, CLT created new opportunities for the use of wood as a building material [1]. CLT panels are normally composed with three, five or seven layers, connected with glue or wooden pegs and stacked in layers rotated 90 or 45 degrees with respect to each other. The layers can have different thickness and wood quality. The lay-up makes the panels able to better carry load in two directions, making them suitable as floor and wall panels. Total thickness is normally between 60 and 300 mm. The elements can have large cut-outs and are prefabricated with millimetres precision, cutting the installation time on site. There are some smaller producers of CLT elements in Norway, but for bigger projects the elements are today imported from manufacturers in Southern Europe[3].

Laminated Veneer Lumber, LVL

Figure 2.3c shows LVL products. LVL is a product of multiple 3 mm veneer layers, and is the strongest wood product on the marked [18]. Normally, all fibres are in the same

[3] Veidekke att: Sigbjørn Faanes, project director *Moholt 50|50*

direction and the total thickness of a plate or beam is between 21 mm and 90 mm. MestäWood in Finland is the producer of Kerto, which is a LVL product.

2.2.1 Environmental advantages

The focus has for a long time been to reduce the energy use in the operational phase of a building, building more passive and low energy buildings. More recent studies show that the material choice have relatively greater importance caused by this development [10]. This is illustrated by Figure 2.4. Emissions related to materials can be responsible for almost 50 % of the total energy use.

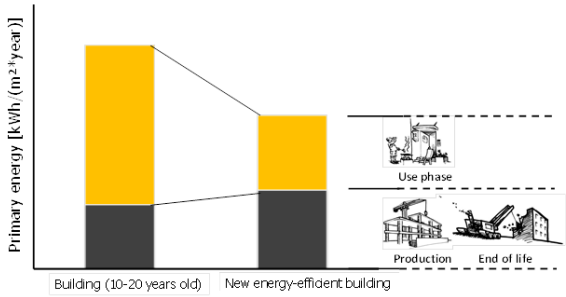

Figure 2.4: Energy use of a new energy-efficient building [10]

Low density of wood products reduces the transport and assembly costs. It also have a positive effect on the amount of concrete foundation needed. Figure 2.5 shows a simple comparison of the GWP-value, the global warming potential, of different wood products compared with concrete.

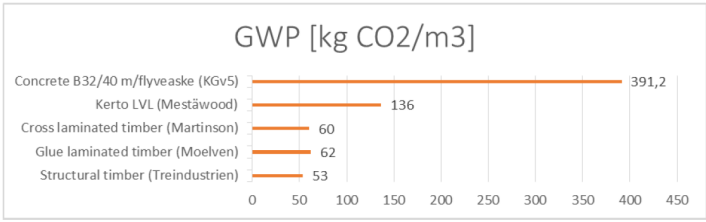

Figure 2.5: The emission of CO_2 in the production phase of different materials [39]

2.3 Structural system

Wood has not traditionally been used in the structural system of high-rise buildings, but for the last couple of decades there has been an increasing interest and development on the matter. Because wood is a flexible and light material, there are some dynamic challenges when building higher structures. Solving these challenges, a structural system based on wood can mean both economic and environmental advantages over systems in concrete and steel.

(a) *Treet* in Bergen

(b) *Moholt 50|50* in Trondheim

Figure 2.6: Examples of high-rise timber structures

Figure 2.6a shows *Treet* in Bergen, which is an example of a new way to build high-rise buildings using wood. Where the horizontal stabilisation is provided by glulam trusses, inspired by the method used for timber bridges. The same truss structure will be used in *Mjøstårnet* in Brumunddalen, finished in 2018. It will with its 66 metres become the highest timber building in the world [8]. Another structural system is based on CLT elements, and is used in many of the new tall timber buildings in Norway. Figure 2.6b shows *Moholt 50|50*, which is the biggest element structure of CLT in Europe, located in Trondheim and finished in 2016 [17]. The CLT elements act both as load bearing and horizontal stabilisers. The wall elements become part of the support system, restricting the floor spans to 5-6 metres. Another approach is *Trä8*. This is a building system developed by Moelven, with continuous columns, beams, prefabricated composite walls and prefabricated floors [42].

The system investigated in this work is based on glulam columns and beams, and cassette floor solutions. The columns are continuous and the the column-beam-connections have a high rotational stiffness. This will be the horizontal stabilisation in one direction. The other direction will be stabilised with shear walls or a stiff core. Figure 2.7 is an early proposal for a possible lay-out [14].

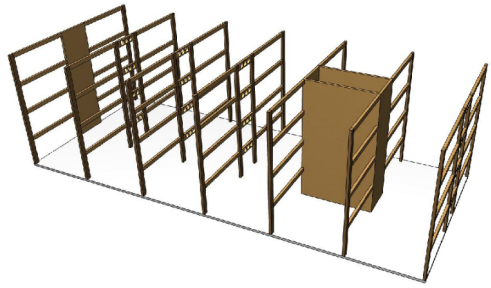

Figure 2.7: Structural system of moment resisting frames

2.3.1 Moment resisting frames, MRF

Moment resisting frames are the basis for the structural system in this work. They allow bigger spans and open architecture, provided that the connections have the necessary strength and stiffness. This will also enhance lateral building stiffness and improve comfort properties of floors [13].

This was the basis for the preliminary analysis done by Malo and Stamatopoulos (2016). Their analysis show that the minimum rotational stiffness required for a moment resisting connection is about 10 000 kNm/rad for a 10 storey building [13]. Figure 2.8a show the case study; a 30 m high, 10 storey building, with floor spans of 8, 3, and 8 m. Spacing the frames 2.4 m apart and having 140 mm x 450 mm cross sections of strength class GL30c.

Through experimental testing, Lied and Nordal achieved connections with rotational stiffness of 5 000 to 10 000 kNm/rad and moment capacity between 80 to 130 kNm in their master thesis. This is for a single cross-section beam and column GL30c, both with dimensions 140 mm × 450 mm. In the case of a doubled cross section, the stiffness would be doubled and the required rotational stiffness is possible to achieve [20]. Figure 2.8b shows a prototype of the connection. Threaded rods with a diameter of 20-25 mm are screwed into the glulam beam and column and connected using a steel ring. Investigation of this solution concluded that the assembly was feasible, but the design is still in development.

Slabs

The structural system should have slab solutions that can span up to 10 metres, without increased storey heights. The elements should be prefabricated for easy mounting on site. The slabs will probably be a cassette type design. Compared to CLT floor elements, these type of floors have higher stiffness, making it possible for longer spans. The slabs

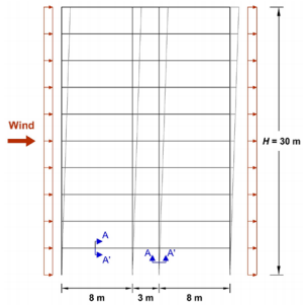

(a) Preliminary analysis of MRF [13]

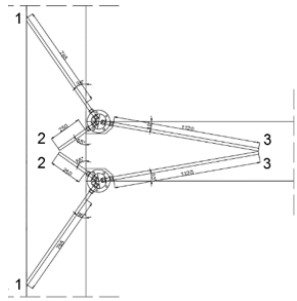

(b) Technical solution for MRF [20]

Figure 2.8: Moment resisting frames

are expected to contribute to the global stability and load carrying of the building together with the moment resisting frames.

Figure 2.9 show some examples of solutions, where a variation of the cassette design (upper right) is the most likely solution. In this thesis there will be no further investigation of slab solutions and their properties, but a design proposal from WoodSol will be used as base.

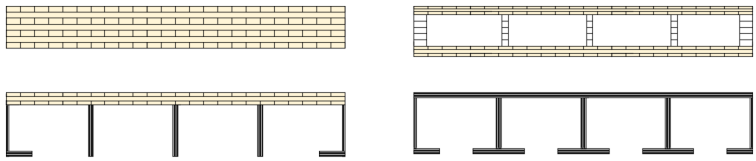

Figure 2.9: Different design and materials of slab solutions [39]. CLT-plates, rib-slabs and a cassette solution

2.4 Loads

This section gives an overview of relevant loads and load combinations. The load actions are determined using NS-EN 1991 [24] and combined accordring to NS-EN 1990 [23] .

2.4.1 Dead load

The dead load of the buildings is dependent upon the material choices for the structural system. Glulam for beams and columns, and CLT for shear walls. Their densities are listed in Table 2.3. No load from permanent technical installations, facades, balconies or inner walls are included. For the slabs the dead load is based on the work done by Bjørge and Kristoffersen for the WoodSol project [4]. They used dead load of 200 kg/m^2. The same is done in this thesis. The effect of higher mass is evaluated in the Discussion, Chapter 5.

Table 2.3: Density of wood materials

Material	[kg/m^3]	**Source**
GLT (glue laminated timber)	430	Moelven [19]
CLT (cross laminted timber)	400	Martinsons [35]
LVL (laminated veneer lumber)	480	Kerto, Moelven [18]

2.4.2 Live load

The live load is decided by the building category, which describes the intended use. The buildings in this thesis may be used for offices, as well as apartments, giving a distributed live load of q_k = 3 kN/m^2. This load is used on all floors except the roof, according to Eurocode [23]. The relevant categories and associated loads are listed in Appendix A.2.

2.4.3 Snow load

The roof has a distributed snow load. The load is dependent on the geographical location, typology of the building and its roof slopes. The snow load used is valid for buildings with flat roofs in the biggest cities in Norway, s_k = 2.8 kN/m^2. The equations for calculating snow load are found in Appendix A.3.

2.4.4 Wind load

The wind load is depended upon the buildings geographical location and geometry. The wind loads are calculated in accordance to NS-EN 1991-1-4 [26], which treats the wind as a static load. This method is a simplification, but gives reasonable results for deflection and accelerations and is assumed to be the most feasible way to calculate the wind loads for this work.

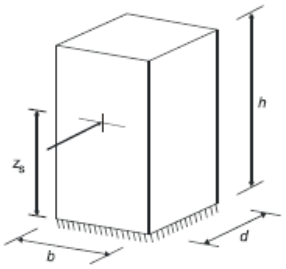

Figure 2.10: Structural dimensions and reference height [26]

When using the method in NS-EN 1991-1-4 the geometry needs to be simplified to a box-like structure. Figure 2.10 shows the approved geometry of the building that wind loads should be calculated for. For complex geometries the method in Eurocode is not satisfactory.

To find the resulting wind force on buildings, the external and internal forces are added, Equation (2.1). Friction forces are neglected. The buildings are only considered for an urban environment, terrain category IV. A building in more open areas would have higher wind loads and the horizontal displacements would increase. The formulas for the complete calculation of the wind loads are found in Appendix A.4.

External and internal forces:

$$F_{w,e} = c_s c_d \sum_{surfaces} w_e \cdot A_{ref} \tag{2.1a}$$

$$F_{w,i} = \sum_{surfaces} w_i \cdot A_{ref} \tag{2.1b}$$

where

$c_s c_d$ is the structural factor, formulas for calculation in Appendix A.4.2

w_e is the wind pressure on external surface at reference height z_e

w_i is the wind pressure on internal surface at reference height z_i

A_{ref} is the reference area

External and internal wind pressure:

$$w_e = q_p(z_e) \cdot c_{pe} \tag{2.2a}$$

$$w_i = q_p(z_i) \cdot c_{pi} \tag{2.2b}$$

where

$q_p(z)$ is the peak velocity pressure at reference height, formulas for calculation in Appendix A.4.1. $q_p(z)$ is calculated for Trondheim, where the reference wind speed is 26 m/s.

c_p is the pressure coefficient, formulas for calculation in Appendix A.4.3

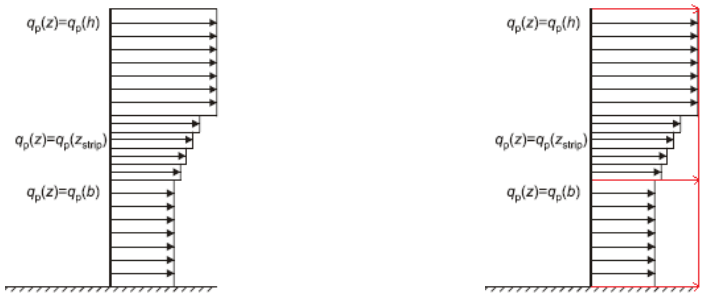

(a) From Eurocode (b) Simplified

Figure 2.11: Wind pressure over the height, $q_p(z)$

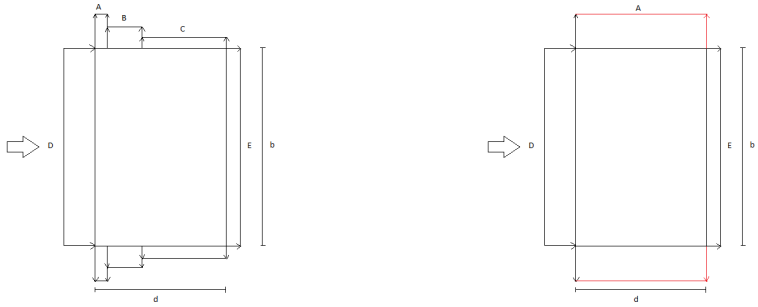

(a) Wind zones as in Eurocode (b) Simplified

Figure 2.12: Wind zones on walls

The velocity profile vary both vertically and horizontally, illustrated by Figure 2.11 and 2.12. A conservative simplification in this work, is not to vary the pressure profile over the height of the building and only use $q_p(h)$. Another simplification is that the walls parallel to the wind direction only use the velocity pressure from the zone with the highest pressures, zone A. This leaves to calculate wind for zone A, D and E at height h. The wind loads are then applied as line loads on the external columns of the building, see Figure 2.13.

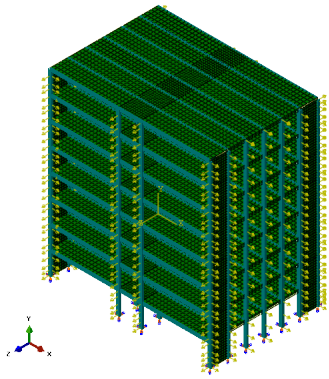

Figure 2.13: Distribution of wind load in *Abagus*

The roof is also sectioned into different wind zones, but the effect from the wind load on the roof is has little effect on the horizontal displacement, and is thus neglected. Exemplified in Appendix A.4. The wind loads used in the different models are listed in Appendix A.4.4.

2.4.5 Limit states

Ultimate limit state, ULS

The fire load is checked in accordance with the ULS requirements for design of construction parts. The capacity is determined with the least favorable combination of the following load combinations:

$$\sum \gamma_{G,j} \cdot G_{k,j} + \gamma_{Q,1}\psi_{0,1} \cdot Q_{k,1} + \sum \gamma_{Q,i}\psi_{0i} \cdot Q_{k,i} \tag{2.3a}$$

$$\sum \xi \cdot \gamma_{G,j} \cdot G_{k,j} + \gamma_{Q,1} \cdot Q_{k,1} + \sum \gamma_{Q,i}\psi_{0,i} \cdot Q_{k,i} \tag{2.3b}$$

The load factors are defined in Appendix A.1. For this work, Equation (2.3a) is used: $1.35 \cdot G + 1.05 \cdot Q + 1.05 \cdot S + 0.9 \cdot W$,

where

G	is the permanent load
Q	is the live load
S	is the snow load
W	is the wind load

Serviceability limit state, SLS

For multi-storey timber buildings, serviceability requirements, as deformation and comfort properties, may govern the design.

$$\sum G_{k,j} + Q_{k,1} + \sum \gamma_{Qi}\psi_{0,i}Q_{k,i} \tag{2.4}$$

In this work the characteristic load combination, Equation (2.4), is used for serviceability calculation: $G + W + 0.7 \cdot Q + 0.7 \cdot S$, with wind being the dominant variable load. 0.7 is used as a factor because the live load and the snow load will have a positive effect on the horizontal deflections.

There is no maximum limit for horizontal displacement stated in the Eurocodes. Each project defines their own limit. For WoodSol the limit is $H/500$, where H is the total height of the building. The maximum peak acceleration at the top floor of the building should be within the guidelines of ISO 10137 [9], see Section 2.5.1. For the calculation

of the acceleration, 30 % of the live load can be added as mass in the modal analysis. This comes from the assumption that some of the live load is quasi-permanent. The quasi-permanent factor of live load is, $\psi_2 = 0.3$ for office areas and residential buildings [23]. The effect of this is investigated in the thesis, but not included in all calculations.

2.5 Acceleration

Structural response due to wind loading is a complex phenomenon. Partially because of the complexity of the wind itself, but also because of how the flow pattern is distributed around the building. Especially vibrations of high-rise buildings have to be given careful attention, and it is important to be aware of the weaknesses and limitations of the chosen method. The along-wind response of a building can be divided into a mean component and a fluctuating component. The mean component is a result of the mean wind speed, and can be dealt with in a static manner. The fluctuating component is wind-speed variations from the mean, often referred to as turbulence. This is a random process which is dependant upon the shape of the building, surrounding terrain and wind profile, among other things. The aerodynamic effects due to turbulence results in vibrations of the structure in translation and torsional modes. The level of vibrations is measured by the accelerations of the top floor. The two most common methods to find accelerations are listed below.

1. Wind tunnel testing

2. Gust factor approach

Wind tunnel testing is suitable for large, irregular buildings or very flexible buildings where the aerodynamic effects becomes greater. In wind tunnel testing, the test model is equipped with sensors that measures accelerations.

The gust factor approach is based on the separation of wind loads into mean and fluctuating components [16]. The fluctuating component is taken into account by the intensity of turbulence and dynamic amplification. NS-EN 1991-1-4 [26] uses the gust factor approach to calculate the accelerations of the top floor as it includes the turbulence effects in resonance with the considered vibration mode. When the gust factor approach is used to calculate the acceleration, one can predict the dynamic response of the building with reasonable accuracy [16]. Even though the method in NS-EN 1991-1-4 is considered satisfactory to predict accelerations, is it important to know the limitations and assumptions which the method is built upon. For instance does the method require a pure translation vibration mode in the wind direction. It is recommended to perform a wind tunnel test if the fundamental vibration mode is a torsional mode, or a translation mode in the cross-wind direction. The same goes for buildings with irregular shape. The approved shapes are shown in Figure 2.14.

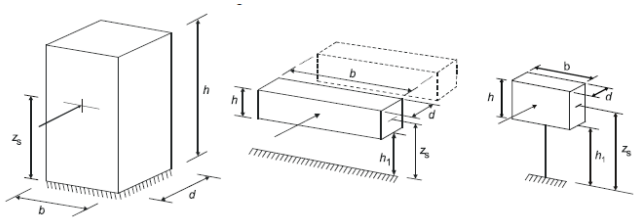

Figure 2.14: Approved shapes for calculation of acceleration [26]

2.5.1 Acceleration criteria

Today, there is no internationally agreed comfort criteria when it comes to vibrations. Each project can define its own comfort criteria and limits for deflection in the serviceability limit state. The main reason for this is that the perception of acceleration differ from person to person, as some people are more sensitive to vibrations than others. However, the evaluation curves for wind-induced vibrations in ISO 10137 [9] has been frequently used, see Figure 2.15. The curve shows that the comfort criteria varies with the fundamental frequency of the building, and shows the strictest criteria for a frequency range between 1 and 2 Hz, where the peak acceleration should not exceed 0.04 m/s^2.

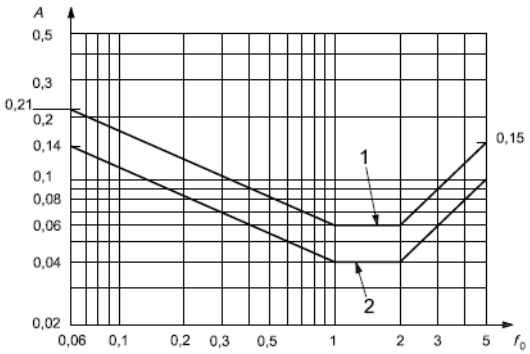

Figure 2.15: Evaluation curves for wind-induced vibrations [9]

where

A	is the peak acceleration
f_0	is the natural frequency of the building
1	is the curve for offices
2	is the curve for residences

Numerous researchers have tried to predict motion threshold levels for humans due to vibrations. Boggs [5] found that the lower limit for perception of acceleration is 0.02 m/s^2, but only 2% of the population are able to feel that, while a less strict limit of 0.05 m/s^2 can be felt by half of the population. Mendis, Ngo, Haritos, Hira, Samali and Cheung [16] suggests different perception levels, summarised i Table 2.4. Depending of the usage of the building and the project specific limits, one can define a comfort criteria for acceleration which is either higher or lower than the ISO-curve, if Boggs' or Mendis' et. al. criteria is used.

Table 2.4: Human perception levels [16]

Acceleration [m/s^2]	**Effect**
< 0.05	Humans cannot perceive motion
0.05 - 0.10	Sensitive people can perceive motion and hanging objects may move slightly
0.10 - 0.25	Majority of people will perceive motion
0.25 - 0.40	Desk work becomes difficult
> 0.85	Objects begin to fall and people may be injured

All of the above acceleration limits are given as peak acceleration, rather than root-mean-square (RMS) acceleration. The difference between the two is that the peak acceleration neglect the smaller amplitudes of vibrations and focus on the peak value over a given period of time. RMS acceleration focus on some average effects over the same time period. As a consequence of this, RMS gives a lower limit than the peak acceleration. For a sinusoidal wave, the RMS is a factor $\sqrt{2}$ lower than the peak value. Today, the peak acceleration is preferred, even though one can argue to use the mean value of the RMS and the peak value [5]. The peak acceleration is used in this thesis.

2.5.2 Acceleration calculation in accordance to NS-EN 1991-1-4

The acceleration of the building can be calculated using Equations (2.5) and (2.6).

$$a = \sigma_{a,x} \cdot k_p \tag{2.5}$$

where

$\sigma_{a,x}$ is the standard deviation of the wind induced acceleration

k_p is the peak velocity factor

$$\sigma_{a,x}(z) = \frac{c_f \cdot \rho \cdot b \cdot I_v(z_s) \cdot v_m(z_s)^2}{m_e} \cdot R \cdot K_x \cdot \phi_{1,x}(z) \tag{2.6}$$

where

c_f	is the force coefficient
ρ	is the air density, $\rho = 1.25\ \mathrm{kg/m^3}$
b	is the width of the structure
$I_v(z_s)$	is the turbulence intensity
$v_m(z_s)$	is the mean wind velocity, calculated with a return period of 2 years
z_s	is the reference height, $z_s = 0.6 \cdot h \geq z_{min}$, see Figure 2.14
R	is the square root of the resonance response
K_x	is the non-dimensional coefficient
m_e	is the along wind fundamental equivalent mass
$\Phi_{1,x}(z)$	is the fundamental along wind modal shape

The equivalent mass, m_e, can be calculated in two different ways. Either with the exact integral i Equation (2.7), or in a simplified manner based on properties of the upper third of the building, shown in Equation (2.8).

$$m_e = \frac{\int_0^l m(s) \cdot \Phi^2(s)\,\mathrm{d}s}{\int_0^l \Phi^2(s)\,\mathrm{d}s} \tag{2.7}$$

where

$m(s)$	is the mass per unit length
$\Phi(s)$	is the considered mode shape

$$m_e = \frac{m_3}{h_3} \tag{2.8}$$

where

m_3	is the average value of the mass over the upper third of the building
h_3	is the height of the upper third of the building

The rest of the variables used to calculate the acceleration are defined in Appendix B.

2.6 Structural fire design

Wood is a combustible material, and between 1907 and 1997 multi-storey timber buildings were not allowed in Norway, due to the risk of city fires [11]. Improved knowledge of fire design in timber buildings and development in technical measures like sprinklers and smoke detection systems opened for a wider use of wood as a construction material.

Fire safety is depended on the structural system. It is important that the occupants of the building can be rescued. To help this, the building should be designed in a way reducing spread of fire and smoke, and ensuring that the load-bearing structure parts resist fire for a minimum duration of time. This section summarize the relevant fire safety requirements for designing the structural system for high-rise timber buildings. The fire design method for construction parts in wood can be found in NS-EN 1995-1-2 [28], and the Norwegian fire regulations are from the *Byggteknisk forskrift*, TEK10.

2.6.1 Requirements

The fire resistance of a building component is classified as the load carrying capacity (R), integrity (E) and insulation (I), followed by the resistance time required in minutes. How materials react to fire are described by their inflammability (A-F), the smoke development (s1-3) and admittance of burning droplets (d0-2). A product used as fire protective cladding is classified by K_1 (10 min) or K_2 (10, 30 or 60 min) [21].

The fire safety requirements of a building are governed by the risk and fire class. A buildings risk class describes the use of the building, and the fire class is a measure of how critical the consequences would be in a case of fire, with respect to human lives and interests of the society. Buildings over five storeys, with a risk class between two and five (includes residences, offices and stores), are **fire class 3** [38, §11-2 and §11-3]. This risk class will apply to all buildings investigated in this thesis.

Table 2.5: Fire protection requirements [38, §11-4]

Load carrying building component	**Fire class 3**
Main load carrying system	R90 A2-s1, d0
Secondary load carrying system (floor separators, roof)	R60 A2-s1, d0
Stairwell	R30 A2-s1, d0

Table 2.5 list the preaccepted requirements in TEK 10. For buildings lower than eight storeys the floor separators can have fire resistance of R60 A2-s1, d0, even though they

are a part of the global stabilisation of the building [38, §11-4(4)]. For buildings over eight storeys, an additional staircase is required [38, §11-13], as well as elevated pressure in escape stairways. The maximum distance from the exit of a fire compartment to the staircase is 15 metres [38, §11-14]. The additional costs for building higher than eight storeys makes it more reasonable to build e.g. 12 instead of nine storeys in total, if the "eight storey limit" should be exceeded in the first place[4].

For buildings in risk class four or higher, an automatic fire extinguishing system is required, and is satisfied by e.g. a sprinkling system [38, §11-12]. In addition, a building should be sectioned into fire compartments that can help delay the spread and contribute to safe escape and rescue. A typical fire compartment would be one apartment. Each compartment should have the resistance of EI60, A2-s1, d0 [38, §11-8]. That means no exposed wood. To allow exposed wood surfaces, the building needs to be considered as a whole, and the fire energy from wood needs to be accounted for. Type of surfaces is not considered any further, but needs to be considered in a complete design process.

2.6.2 Fire design

To address the performance of the structural system the *reduced cross section method* is used. The main load carrying system are the slabs, the shear walls, the beams and columns. This assignment only look at the columns near the foundations. The performance is satisfied when the load-bearing function of the columns is maintained after 90 minutes of fire exposure.

Protective cladding, like fire gypsum, will delay the charring of the columns, but this is not considered in this assignment. All surfaces exposed to fire will char. The char will act insulating, maintaining the temperature on the underlying wood surface. The core of the wood maintains its ability to carry load. The cross section is illustrated by Figure 2.16.

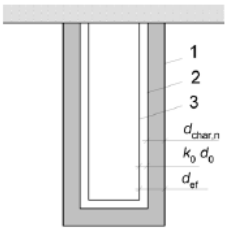

Figure 2.16: Reduced cross section [28]. 1 - initial surface, 2 - residual cross section, 3 - effective cross section

[4] Kjeldsberg att: Harald Bjørlykke

The remaining effective cross section is decided by the formulas in NS-EN 1995-1-2 [28]:

$$d_{ef} = d_{char,n} + k_0 d_0 \tag{2.9a}$$

$$d_{char,n} = \beta_n \cdot t \tag{2.9b}$$

where

$d_{char,n}$	is the charring rate for glulam $\beta_n = 0.7$ mm/min
d_0	$d_0 = 7$ mm
k_0	$k_0 = 1$ when $t \geq 20$ minutes

For $t = 90$ minutes, $d_{ef} = 70$mm. This needs to be withdrawn from all sides exposed to fire of the initial cross section. The remaining cross section have to carry 60 % of the design load of the building [28]. Formulas for calculating the capacity of the cross section is given in Appendix C. Note that with one layer of fire gypsum (class K_1), d_{ef} would be reduces to 63 mm.

Chapter 3

Modelling and Analysis

The different layouts of the structural system have been modelled in the finite element program *Abaqus*. The goal of the study is to develop an understanding of the global stability in the serviceability limit state of tall timber buildings built with moment resisting frames. Thus, the modelling has been simplified to only account for what is essential regarding load bearing and stability. The simplifications, assumptions and considerations made during the modelling are discussed in this chapter, as is the case building and the analysis of the model.

3.1 Case building

The main goal for the WoodSol project is to develop industrialised structural solutions based on moment resisting frames having five to 10 storeys open architecture [14]. As the same structural solutions will be used in several different buildings, the solutions should be robust and adaptable for small changes. The models from Section 3.5 vary in numbers of storeys and geometry, but should be built by the same principles on a construction site. Based on this, the modelling will also follow the same principles for all models, meaning all *Abaqus*-models are assembled with the same parts and after the same guidelines:

- Continuous timber columns in full building height
- Slabs merged with beams making the horizontal areas of the floors
- CLT shear walls
- CLT walls to represent stair and elevator shafts
- Nodal masses to represent extra mass

The buildings vary from four to 12 storeys and have footprints varying from roughly 260 to 830 m^2. The slabs span from 3 to 9.6 m, and are not wider than 2.4 m. This means that two neighbouring frames can not be farther apart than 2.4 m if the slab between them is meant to contribute to horizontal stiffening in the frame direction. If the distance is larger, the slabs have to be positioned with their span direction orthogonal to the frame direction, and thus be connected to the frame beams and not the columns. See Figure 3.1 for examples of both span directions.

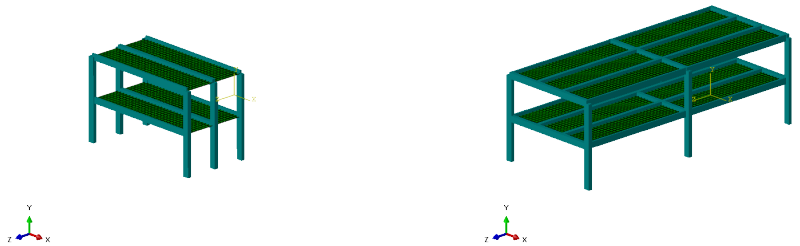

(a) Slab span direction parallell to frame (b) Slab span direction orthogonal to frame

Figure 3.1: Span directions of slabs

3.2 Modelling in *Abaqus*

Abaqus is a general purpose finite element analysis program with a wide range of opportunities. By a combination of modelling in CAE[1], manipulation through the keyword function and usage of input files, almost anything can be modelled. *Abaqus* lets the user be in control by giving a wide range of options throughout every step of the modelling process and the possibility to customise input. The program also lets the user run *Python* scripts, which makes parameter studies easier. *Abaqus* was chosen on the basis of its wide range of possibilities and customisation options.

Features and elements

All beams and columns are modelled as wire features and meshed with B31 elements. The B31 element is a Timoshenko element, allowing transverse shear deformation. The

[1] This is the GUI of *Abaqus*

element can be used in stout, as well as slender beams, it uses lumped mass representation and is linearly integrated [33].

Shear walls and slabs are modelled as shell elements. The slabs are in general meshed with S4R elements. S4R is a general-purpose shell element with four nodes that uses reduced integration with hourglass control to calculate its stiffness contribution. It provides accurate solutions for all loading situations. The shear walls are meshed with S4 elements, which is stiffer than the S4R element because it exhibit shear locking. S4 is used to avoid hourglass modes in the shear walls. In special cases, e.g. corridors, where short slabs results in a slab thickness larger than 1/15 of the slab span, the S8R element is used. This element is a 8-node doubly curved thick shell with reduced integration. It is recommended for use in regular mesh geometries for thick shell applications [33] [34].

Wire features, with assigned connector sections, are used to represent the connections between columns and slabs and between columns and shafts. Wire features are also used between columns and the ground to model a semi-stiff connection as a parametric study of the boundary condition.

Model assembly

The steps of the assembly of the models are summarised in Figure 3.3. It starts by setting out column pairs where slabs should be put in between. The shear walls are placed out and merged to columns to give the right continuity. The slabs are placed out as continuous shell features with partition areas to represent the connection between each slab, see Figure 3.2a. The slabs are merged with a layer of beams over each partition line to give the right stiffness and bending shape, see Figure 3.2b. This is done because the shell elements used in the slabs do not have rotational degrees of freedom. For the modelling of moment resisting frames to be successful, it is important that the connection nodes between columns and slabs both have rotational degrees of freedom, making manually assigned rotational stiffness between those parts possible. Each slab is connected to four columns, one in each corner, with connection points between the partition and the slab section. This means that every column connected to two slabs in the model has a doubled cross section. Tie constraints are also used to keep the building continuous, typically between building parts not connected by wires, e.g. building parts with different span direction, see Figure 3.4a. In models containing an elevator shaft, the shaft is put between cut out slabs and surrounded by columns, see Figure 3.4b.

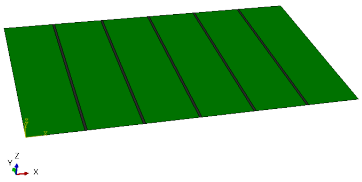

(a) Slabs with partition area

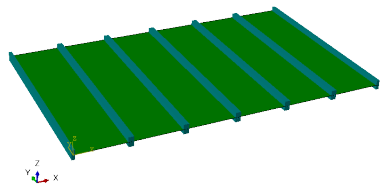

(b) Slabs merged with beams

Figure 3.2: Slab modelleling

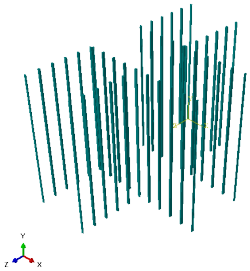

(a) Columns are set out

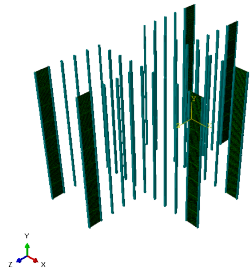

(b) Shear walls merged with columns

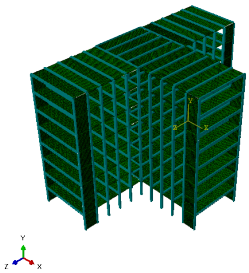

(c) Slab parts added

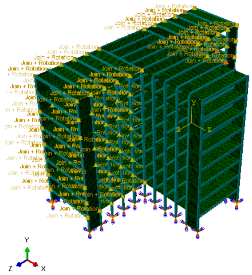

(d) Connections and boundary conditions added

Figure 3.3: Assembly of models

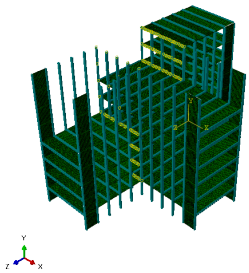

(a) Yellow rings represent TIE constraints between building parts

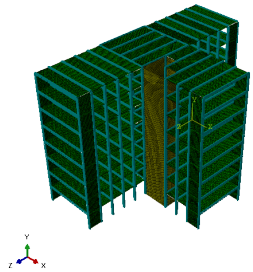

(b) Complete building with shaft

Figure 3.4: Assembling details

Connections

The slabs are connected to the columns by wire features, so that translations are constrained and rotations are released in two directions. The third rotation direction has a semi-rigid constraint, with rotational stiffness of 10 000 kNm/rad. The direction of this stiffness is such that it reduces rotation between the column and slab beam about the strong axis of the beam section, i.e. rotational stiffness about the z-axis in Figure 3.5.

For shafts, all rotations are released, while translations are constrained.

To check for semi-rigid boundary conditions, there has been used pinned boundary conditions accompanied with assigned rotational stiffness of 10 000 kNm/rad about the ground plane axes.

When modelling a wire connection in *Abaqus*, it has to be a gap between the two connected nodes. To ease the modelling, this gap is large during the modelling and set shorter during simulations. Figure 3.5 visualises the gap, as well as presenting the result that the model seems to stiffen with the gap decreasing. The influence is small, with a deviation of 2.2 %. In the modelling, the gap is set to one, and the influence of change is not investigated further.

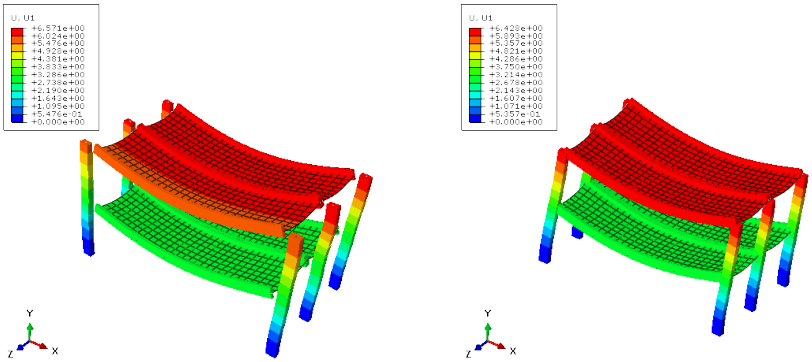

(a) Model with gap = 500 mm

(b) Model with gap = 1 mm

Figure 3.5: Connection gaps

Simplifications

In order to use numerical programming to effectively analyse a multiple storey building, simplifications have to be made. If all details (as connection details, screws, walls, etc.) were to be modelled, both simulations and the modelling process would be very time consuming. The main simplifications made are listed below and discussed in Section 5.2.5.

- Slabs are modelled as shell elements merged with beam elements. The modelling is based on an *Abaqus* model from the master thesis by Bjørge and Kristoffersen [4].
- Only building parts that contribute to the global stability of the building are included. Facades, inner walls etc. are not modelled.
- Multiple slabs are modelled as one part, making the connection between them simplified as an isotropic section with low strength
- Shear walls merged to columns
- Wind load modelled as uniform line load

3.3 Verification of numerical modelling

The complexity of modelling a 3D model in *Abaqus* makes it hard to keep track of every step during creating a model. To ensure the validity of the computations done in *Abaqus*, a verification process has been completed.

To do so, hand calculations and *fap2D* have been used. *fap2D* is a program for static and dynamic analysis of 2D frame structures developed at NTNU at the Department of structural engineering [30]. *fap2D* has been used to calculate the responses of simple frames for comparison to *Abaqus* models, while hand calculations have been used to compare the energy balance between 3D and 2D models.

The following tests have been done to validate the computations done in *Abaqus*:

- Comparison of 2D models modelled in *Abaqus* and *fap2D*
- Comparison of bracing between frames modelled in *Abaqus* and *fap2D*
- Conversion from 3D in *Abaqus* to 2D in *fap2D*
- Energy balance comparison between models

The comparisons between *Abaqus* and *fap2D* models are done using steel as the material. This because steel has isotropic properties, and it is easier to ensuring the same representation in the two programs. Wood, on the other hand, is defined with material properties in three independent directions in *Abaqus*, but only one direction in *fap2D*.

3.3.1 2D model comparison

To compare results from *Abaqus* and *fap2D*, it is important to ensure that the modelling done in the two programs gives the same results for the *same* model.

This test was done by modelling a 2D frame of five storeys with columns and beams. The columns are encastred to the ground, and the beams are connected to the columns with translations constrained and rotation stiffness of 20 000 kNm/rad[2]. The rotational stiffness reduces the rotation between beam and column, with stiffness about the z-axis in the *Abaqus* model and about the out-of-plane axis in *fap2D*. See Figure 3.6 and Table 3.1 for the model representation.

[2] The test is done to verify the 2D modelling and that the moment resisting connection works. Using 20 000 kNm/rad or 10 000kNm/rad is not important, as long as similar values are used in both programs

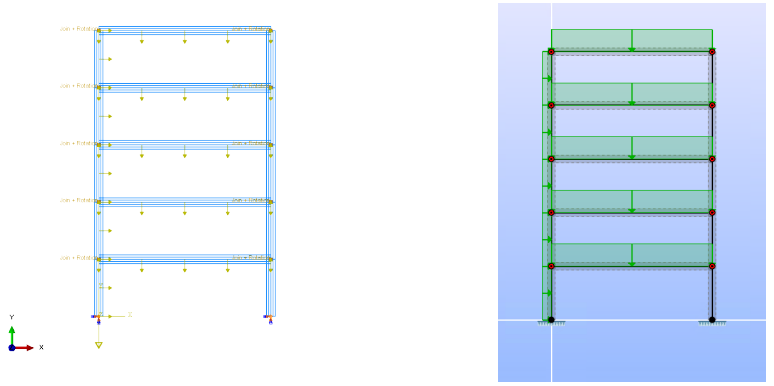

(a) *Abaqus* model (b) *fap2D* model

Figure 3.6: 2D frame, five storeys

Table 3.1: Model input for 2D comparison models

	Abaqus and *fap2D*
Storey height [m]	3
Beam length [m]	9
Line load on column [N/mm]	5
Line load on beam [N/mm]	12
Gravity constant [m/s^2]	9.81
Rotational stiffness [kNm/rad]	20 000
Boundary condition	encastred
Material	steel, see Table 3.2

Table 3.2: Steel material properties

	ρ [kg/m^3]	E [MPa]	ν
Steel	7850	210 000	0.3

The results from the two models and the deviations between results from *fap2D* and *Abaqus* in percent are listed in Table 3.3. It is expected that the differences are minimal as the two models in principle are the same model. As shown in the table, there are some small deviations. These may arise from different round-off in the two programs. The differences in results are very small, leading to the conclusion that the simulation of connections are correct.

Table 3.3: Results from comparison between *Abaqus* and *fap2D*

Output	*Abaqus*	*fap2D*	**Deviation**
U1 floor 5 [mm]	14.9185	14.92	0.010 %
U1 floor 3 [mm]	8.2262	8.23	0.047 %
U1 floor 1 [mm]	1.4274	1.43	0.181 %
U2 floor 5 [mm]	2.8666	2.87	0.118 %
U2 floor 3 [mm]	2.7138	2.72	0.228 %
U2 floor 1 [mm]	2.3542	2.36	0.246 %
RF1L [kN]	38.129	38.22	0.239 %
RF1R [kN]	36.871	36.78	-0.247 %
RF2L [kN]	2263.490	2265.34	0.082 %
RF2R [kN]	2310.210	2312.06	0.080 %
Natural frequencies [Hz] Mode	*Abaqus*	fap2D	**Deviation**
1	0.5798	0.5797	-0.024 %
2	2.6884	2.6879	-0.019 %
3	6.9833	6.9807	-0.037 %

where

$U1$ is the displacement in the x-direction

$U2$ is the negative displacement in the y-direction

$RF1L$ is the reaction force on the left column in the x-direction

$RF1R$ is the reaction force on the right column in the x-direction

$RF2L$ is the reaction force on the left column in the y-direction

$RF2R$ is the reaction force on the right column in the y-direction

with directions from Figure 3.6a.

3.3.2 Bracing by shear walls

There is done a test validating the modelling of shear walls in *Abaqus*. An eight storey 2D wall is modelled with shear walls merged to columns in *Abaqus*. This model is converted to a model with cross bracing of circular beam sections in *Abaqus*, so that it can easily be checked by a similar model in *fap2D*. The models are presented in Figure 3.7.

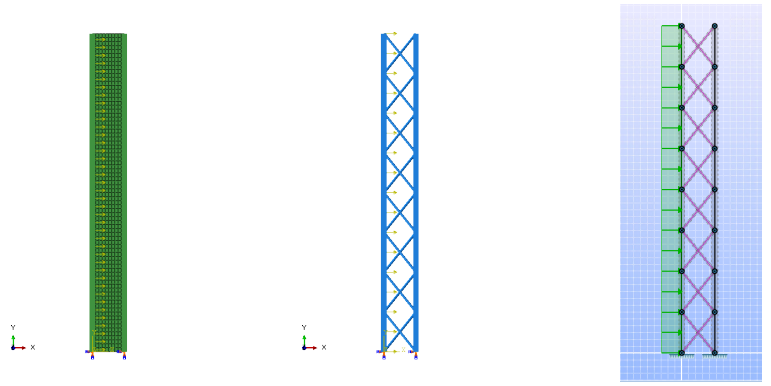

(a) *Abaqus*, shear wall (b) *Abaqus*, cross bracing (c) *fap2D* model

Figure 3.7: Models of bracing

The model in Figure 3.7a is modelled with material properties according to Table 3.4. The model shown in Figure 3.7b, with material properties from Table 3.5 is compared to the this model to make sure the cross bracing model can represent a compact shear wall. These material properties are found by iteration. The results from this comparison are presented in Table 3.6.

Table 3.4: Material properties shear wall model

	ρ [kg/m^3]	E_1 [MPa]	E_2 [MPa]	E_3 [MPa]	ν_{12}	ν_{13}	ν_{23}	G_{12} [MPa]	G_{13} [MPa]	G_{23} [MPa]
Frame	450	13 000	300	300	0.6	0.6	0.6	650	650	65
Shear wall	450	13 000	300	300	0.6	0.6	0.6	650	650	65

Table 3.5: Material properties cross bracing model

	ρ [kg/m^3]	E_1 [MPa]	E_2 [MPa]	E_3 [MPa]	ν_{12}	ν_{13}	ν_{23}	G_{12} [MPa]	G_{13} [MPa]	G_{23} [MPa]
Frame	450	13 000	300	300	0.6	0.6	0.6	650	650	65
Cross beams	1345.5	9 000	4000	4000	0.6	0.6	0.6	650	650	65

Table 3.6: Results from *Abaqus* models 3.7a and 3.7b

Output	**Shear wall**	**Cross bracing**	**Deviation**
U1 top [mm]	51.98	51.28	1.347 %
Natural frequencies [Hz] Mode	**Shear wall**	**Cross bracing**	**Deviation**
1	4.055	4.0862	0.769 %
2	17.478	17.819	1.951 %
3	37.288	37.013	-0.738 %

The results show that the cross bracing model can represent the compact shear wall model in *Abaqus*.

The cross bracing model is then compared to a similar model in *fap2D*, and the results are presented in Table 3.7. The material choice is steel, with properties from Table 3.2. The small deviations leads to the conclusion that the simulation of shear walls is correct.

Table 3.7: Results from comparison

Output	*Abaqus*	*fap2D*	**Deviation**
U1 top [mm]	3.022	3.04	0.006 %
Natural frequencies [Hz] Mode	*Abaqus*	*fap2D*	**Deviation**
1	4.920	4.897	-0.005 %
2	23.013	22.748	0.012 %
3	46.671	46.581	-0.002 %

3.3.3 From 3D to 2D

This comparison is done to make sure that the simulation of a 3D model gives logical values for deformations and reaction forces. It is expected that the results will vary when one dimension is taken away because of effects that happen in 3D and not in 2D, and also simplifications done in the 2D model. Two 3D models from *Abaqus* have been checked against 2D models from *fap2D*, one with five storeys and one with two storeys, both six slabs wide. This is done to check for accumulation of errors. Figure 3.8 visualises how the sections from the 3D models are transferred to 2D, where the sections are marked in Figures 3.8c and 3.8d. Model input are shown in Table 3.8.

The results for these simulations are presented in Table 3.9 and 3.10.

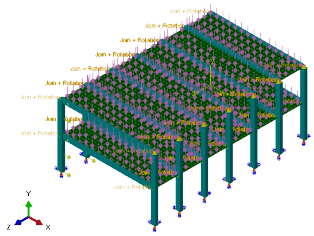

(a) 3D model, two storeys

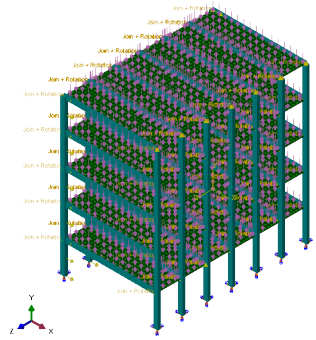

(b) 3D model, five storeys

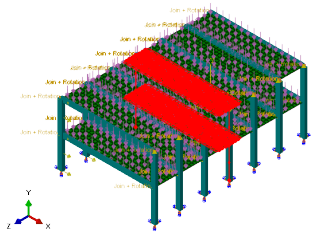

(c) Section transfered to 2D

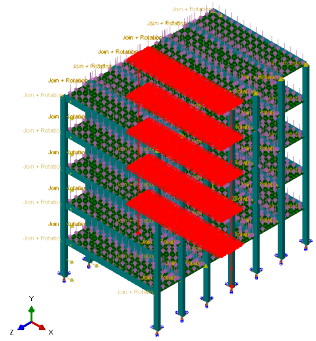

(d) Section transfered to 2D

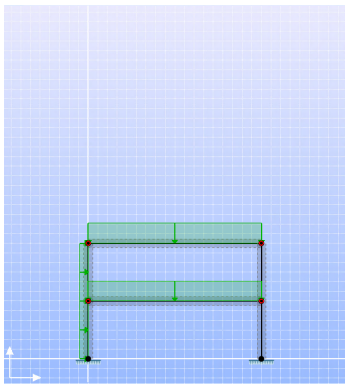

(e) 2D model, two storeys

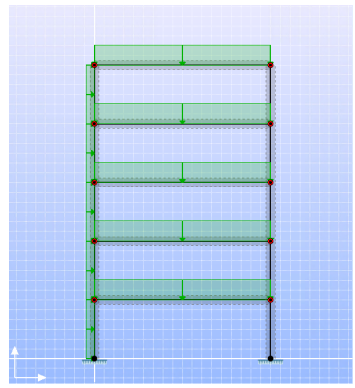

(f) 2D model, 5 storeys

Figure 3.8: Overview of models

Table 3.8: Model input for 3D to 2D comparison models

	Abaqus	*fap2D*
Storey height [m]	3	3
Slab(beam) length [m]	9	9
Slab width [m]	2.4	-
Slab thickness [mm]	450	-
Beam section (h × b) [mm]	-	450 × 2 400
Line load on column [N/mm]	5	5
Line load on beam [N/mm]	-	12
Pressure on floors [N/mm^2]	0.005	-
Gravity constant [m/s^2]	9.81	9.81
Rotational stiffness [kNm/rad]	10 000 per connection	20 000
Boundary condition	encastred	encastred
Material	steel, see Table 3.2	steel, see Table 3.2

Table 3.9: Results from comparison, two storeys

Output	*Abaqus*	*fap2D*	**Deviation**
U1 floor 2 [mm]	0.7383	0.71	-3.833 %
U1 floor 1 [mm]	0.2760	0.26	-5.790 %
U2 floor 2 [mm]	1.7563	2.24	27.544 %
U2 floor 1 [mm]	1.7066	2.19	28.329 %
RF1L [kN]	16.840	16.37	-2.791 %
RF1R [kN]	13.280	13.63	-2.636 %
RF2L [kN]	931.500	914.23	-1.854 %
RF2R [kN]	934.100	916.73	-1.860 %
Natural frequencies [Hz]	*Abaqus*	*fap2D*	**Deviation**
Mode			
1	2.1727	2.1567	-0.7364 %
2	12.6680	12.4621	-1.6254 %
3	13.5870	12.7113	-6.4451 %

Table 3.10: Results from comparison, five storeys

Output	*Abaqus*	*fap2D*	**Deviation**
U1 floor 5 [mm]	16.2200	14.92	-8.015 %
U1 floor 3 [mm]	8.8000	8.23	-6.477 %
U1 floor 1 [mm]	1.5026	1.43	-4.828 %
U2 floor 5 [mm]	2.3729	2.87	20.948 %
U2 floor 3 [mm]	2.2227	2.72	22.374 %
U2 floor 1 [mm]	1.8683	2.36	26.318 %
RF1L [kN]	39.271	38.22	-2.676 %
RF1R [kN]	36.669	36.78	0.303 %
RF2L [kN]	2 298.100	2 265.34	-1.426 %
RF2R [kN]	2 352.310	2 312.06	-1.711 %
Natural frequencies [Hz] Mode	*Abaqus*	*fap2D*	**Deviation**
1	0.5700	0.5797	1.707 %
2	2.7101	2.6879	-0.819 %
3	7.0988	6.9807	-1.664 %

where

$U1$ is the displacement in the x-direction

$U2$ is the negative displacement in the y-direction

$RF1L$ is the reaction force on the left column in the x-direction

$RF1R$ is the reaction force on the right column in the x-direction

$RF2L$ is the reaction force on the left column in the y-direction

$RF2R$ is the reaction force on the right column in the y-direction

with directions from Figure 3.8a.

The results show that the deviations between the two and five storey models does not seem to accumulate. The deviation in downward deformation is quite high. This might be because of the different force propagation paths from a 3D model versus a 2D model. In the *Abaqus* models, the slabs are plates, while in *fap2D*, they are modelled as beams. To convert the Youngs modulus, E, to a corresponding value in *fap2D* the formula for downward deformation in a slab has been used, see Equation (3.1) through (3.3), and the deflection is collected from the point shown in Figure 3.9. To fulfill the require-

ments for Equation (3.1), this model has pinned connections between the top slab and the columns. The point of deflection is chosen because it is the midpoint between the largest and the lowest deflection in the model, as the deflection is higher toward the short ends of the model.

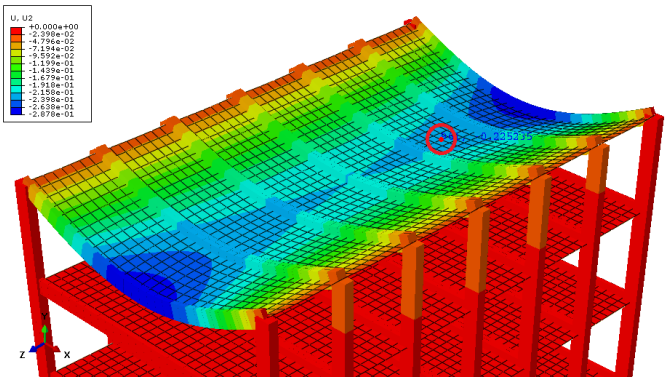

Figure 3.9: Red dot marking where the deflection was collected

$$w = \frac{5 \cdot qL^4}{384 \cdot D} \tag{3.1}$$

with

$$D = \frac{Et^3}{12 \cdot (1 - \nu^2)} \tag{3.2}$$

which gives

$$E = \frac{60 \cdot qL^4 \cdot (1 - \nu^2)}{384 \cdot w} \tag{3.3}$$

where

w	is the downward deflection of the slab.
q	is the pressure load on the slab
L	is the span length of the slab
ν	is the poisson ratio of the material

This gives E = 227 000 MPa, which is used in an updated *fap2D* five storey model to give the new results of Table 3.11. These results are more even, but they deviate from

each other with up to 16.7 % for the downward deflection in the first floor. The U1 deformations are higher in *Abaqus* while the U2 deformations are lower. This indicates that the model is less stiff than the *fap2D* model in the x-direction and more stiff in the y-direction. For the purpose of this thesis, the downward deformation of slabs is not relevant, as it is the frequencies, reaction forces and the horizontal deformation which is important to check for acceleration, fire and top deflection requirements. The reaction forces and natural frequencies do not deviate by much, while the deviation of the deflection in x-direction is about 10 %. These deviations are not considered alarming. It is concluded that the modelling technique is valid, and it is used throughout the modelling process of this thesis.

Table 3.11: Results from comparison, five storey

Output	*Abaqus*	*fap2D*	**Deviation**
U1 floor 5 [mm]	16.2200	14.38	-11.344 %
U1 floor 3 [mm]	8.8000	7.87	-10.568 %
U1 floor 1 [mm]	1.5026	1.35	-10.153 %
U2 floor 5 [mm]	2.3729	2.66	12.098 %
U2 floor 3 [mm]	2.2227	2.52	13.376 %
U2 floor 1 [mm]	1.8683	2.18	16.684 %
RF1L [kN]	39.271	38.44	-2.116 %
RF1R [kN]	36.669	36.56	-0.297 %
RF2L [kN]	2298.100	2266.11	-1.392 %
RF2R [kN]	2352.310	2311.43	-1.738 %
Natural frequencies [Hz] Mode	*Abaqus*	*fap2D*	**Deviation**
1	0.5700	0.5908	3.655 %
2	2.7101	2.7730	2.321 %
3	7.0988	7.2341	1.906 %

3.3.4 Energy comparison

This test validates the modelling of the connections in *Abaqus* by comparison of both strain energy in the connection, and total internal energy of the system in *Abaqus* with hand calculations. The considered model is a simple frame, shown in Figure 3.10. The frame is loaded with a point load of 10 kN in the top left corner.

Simplified, the energy balance can be written as shown Equation (3.4).

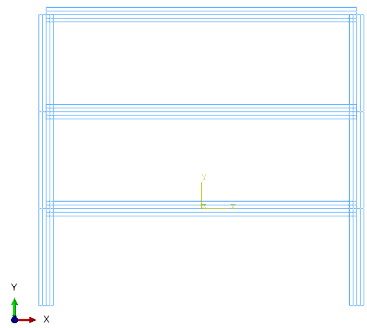

Figure 3.10: 2D model in *Abaqus*

$$E_{tot} = E_{int} + E_{ext} = (E_b + E_{col} + E_{con}) + E_{ext} \tag{3.4}$$

where

E_{tot}	is the total energy in the system
E_{int}	is the internal energy
E_{ext}	is the external energy
E_b	is the strain energy from beams
E_{col}	is the strain energy from columns
E_{con}	is the strain energy from connections

Strain energy contributions from beams and columns are defined in Equations (3.5), (3.6) and (3.7), for moment, shear force and axial force, respectively. Strain energy from the connections are defined in Equation (3.8).

$$E_{b/col} = \frac{1}{2}\int_0^L M(x)\frac{M(x)}{EI}dx \tag{3.5}$$

$$E_{b/col} = \frac{1}{2}\int_0^L k_y V(x)\frac{V(x)}{GA}dx \tag{3.6}$$

$$E_{b/col} = \frac{1}{2}\int_0^L N(x)\frac{N(x)}{EA}dx \tag{3.7}$$

$$E_{con} = \frac{1}{2} k_{rot} \phi^2 \tag{3.8}$$

where

L	is the length of the beam/column
$M(x)$	is the moment distribution for the actual beam/column
$V(x)$	is the shear force distribution for the actual beam/column
$N(x)$	is the axial force distribution for the actual beam/column
E	is the Youngs modulus
G	is the shear modulus
I	is the moment of inertia
A	is the cross-sectional area
k_{rot}	is the rotational stiffness of the connection, 10 000 kNm/rad
k_y	is the cross-sectional factor, for rectangular cross section, k_y = 1.2
ϕ	is the rotation of each connection

Table 3.12 shows negligible deviations between *Abaqus* and hand calculations, which strongly indicates that the physical behavior of the connections are modelled correctly. In addition, since the deviations in displacement are under one percent, as seen in Table 3.3, the validity of the modelling technique is approved.

Table 3.12: Strain energy

Output	*Abaqus* [J]	**Hand calculation** [J]	**Deviation**
E_b	-	20 570	-
E_{col}	-	18 833	-
E_{con}	23 478	23 477	0.004 %
E_{int}	62 352	62 880	0.84 %

3.3.5 Modelling of Slab

As mentioned in Section 3.2, the modelling of the slabs is a simplification, where the material properties are fictitious. The simplified slab is based on the master thesis by Bjørge and Kristoffersen [4], hereafter called the reference slab. The conversion from the reference slab to a simplified slab was done by comparing single slab elements. The considered slab has a dimension of 9 m × 2.4 m. Figures 3.11 and 3.12 shows the reference slab and the simplified model, respectively.

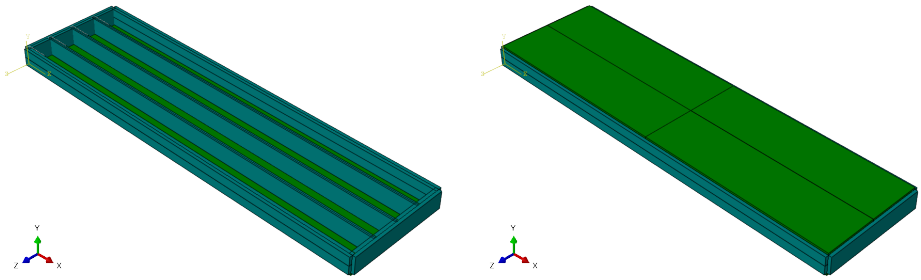

(a) Bottom plate and girders (b) Complete slab

Figure 3.11: Reference slab

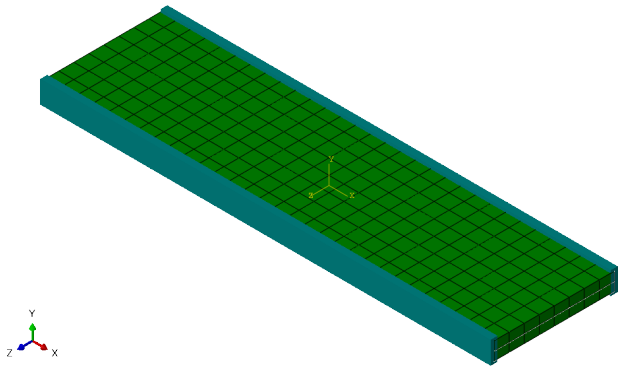

Figure 3.12: Simplified slab

As shown in Table 3.13, the simplified slab is able to represent the natural frequencies of the reference slab. The first mode shape is the first bending mode about the weak axis, the second mode is a torsional mode, the third one is translation in the cross direction, while the fourth mode shape is the second bending mode about the weak axis.

The mode shapes are illustrated in Figure 3.13. All of the modes have less than 10 % deviation from the reference model, which is acceptable. Table 3.14 shows a maximum deviation in deflection of 4.5 %, which increase the validity of the simplified model. Even though the simplified slabs give approximately the same resulting frequency and deflection as the reference slab, the total mass is too low compared to the reference slab. This makes it necessary to add extra mass when calculating the accelerations. For a slab of dimension 9 m × 2.4 m, 523 kg has to be added per slab.

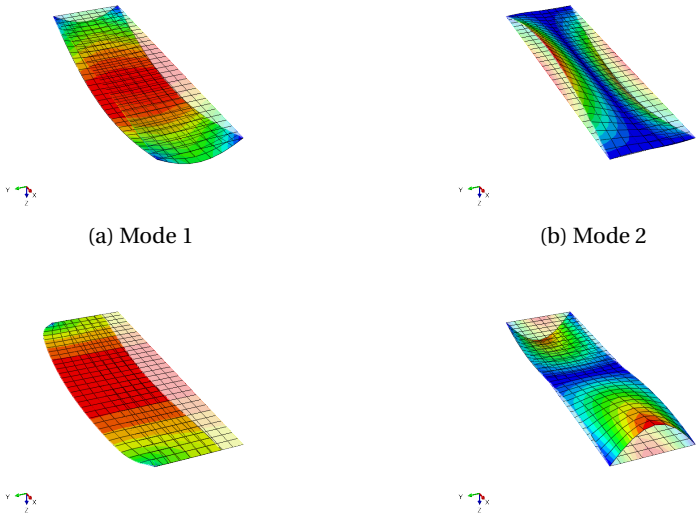

(a) Mode 1

(b) Mode 2

(c) Mode 3

(d) Mode 4

Figure 3.13: Mode shapes for the simplified slab

Table 3.13: Comparison of natural frequencies

Mode	**Reference model** [Hz]	**Simplified model** [Hz]	**Deviation**
1	9.2934	9.3597	0.71 %
2	14.4570	13.9130	3.76 %
3	19.6440	19.5020	0.72 %
4	23.3800	21.6380	7.45 %

Table 3.14: Comparison of deflection

Load case	**Reference model** [mm]	**Simplified model** [mm]	**Deviation**
Evenly distributed	13.58	14.00	3.09 %
Concentrated (center)	3.94	4.12	4.54 %

3.4 Material properties in *Abaqus*

All wood materials in the simulations are modelled as transversely isotropic with linear elastic behaviour.

Wood is an anisotropic material, but can be approximated to an orthotropic behaviour. A research by Stamatopoulos and Malo [36] show that there is little difference in modelling the material as fully orthotropic and transversely isotropic, giving the material equal proprieties in the radial and tangential direction. Transversely isotropic is considered a good approximation of the material behaviour for this work. Figure 3.14 illustrate models of cylindrical orthotropic, transversely orthotropic, and the particular directions in a datum with three perpendicular axes: longitudinal (L), radial (R) and tangential (T).

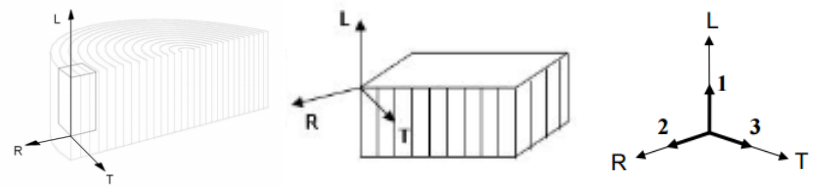

Figure 3.14: Wood models[12] and the particular material directions[6]

Glue Laminated Timber

Table 3.15 list the material properties for glulam used in the analysis. The density and modules of elasticity are from the manufacturer, Moelven [19] and represent quality GL30C. The remaining values are from the study by Stamatopoulos and Malo [36], which based their Poisson ratios on Dahl's study on mechanical properties of Norway spruce [6].

Table 3.15: Material properties GLT

	ρ [kg/m^3]	E_1 [MPa]	E_2 [MPa]	E_3 [MPa]	ν_{12}	ν_{13}	ν_{23}	G_{12} [MPa]	G_{13} [MPa]	G_{23} [MPa]
GL30C	430	13 000	300	300	0.6	0.6	0.6	650	650	65

Cross Laminated Timber

CLT is represented as a composite cross section, modelled in layers of quality C14 and C24. The material stiffness and density are from NS-EN 338 [29] and the manufacturer,

Martinsons [35]. The Poisson ratios are from Dahl [6]. Table 3.16 list the material properties for CLT used in the analysis.

Table 3.16: Material properties CLT

	ρ [kg/m^3]	E_1 [MPa]	E_2 [MPa]	E_3 [MPa]	ν_{12}	ν_{13}	ν_{23}	G_{12} [MPa]	G_{13} [MPa]	G_{23} [MPa]
C14	350	7 000	230	230	0.48	0.42	0.50	440	440	50
C24	420	11 000	370	370	0.48	0.42	0.50	690	690	50

The thickness of the plies and the layout are inspired by the elements produced by Martinsons [15]. C24 is used in the load carrying direction and C14 in the other. Table 3.17 lists type of material, thickness and orientation of a three ply CLT element. CLT is used in both the modelling of shear walls and shafts.

Table 3.17: Stacking direction of the CLT elements

Ply	**Material**	**Thickness**	**Orientation**
1	C24	30 mm	0°
2	C14	30 mm	90°
3	C24	30 mm	0°

Slabs

The modelling of the slabs is described in Section 3.3.5 and the material properties are presented in Table 3.18.

Table 3.18: Material properties of the slabs

	ρ [kg/m^3]	E_1 [MPa]	E_2 [MPa]	E_3 [MPa]	ν_{12}	ν_{13}	ν_{23}	G_{12} [MPa]	G_{13} [MPa]	G_{23} [MPa]
Slab	450	15000	300	265	0.6	0.6	0.8	175	150	385

Partition

The slabs are connected with each other. This connection is in the global analysis represented by a partition that has a low stiffness compared to the slabs. The material of the partition is isotropic, and presented in Table 3.19. See Appendix D for more.

Table 3.19: Material properties of the partition in slabs

	ρ [kg/m^3]	E [MPa]	ν
Partition	430	30	0.3

3.5 Models

This section gives a brief presentation of the different geometries of the analysed models. The models investigated can be divided into two main designs, which have been modified further in a parametric study. The first main design is a building containing two larger open areas separated by a corridor, hereafter called Room Corridor Room, RCR for short. The second main design is a building with a T-section shape, containing two blocks in the flange direction, separated by a third block spanning in the orthogonal direction, the web. This design is hereafter called the T-design. In each of the main designs, there is a base model. This model is used as a reference to learn what affects the building the most with respect to a parametric study. The main models are modelled without a shaft contributing to stability. This is based on the goal of robustness, and to investigate if the requirements can be reached without being dependent on a shaft. The geometric changes concern

- number of storeys
- number of slabs
- shear wall layout
- the presence of a shaft connected to the structural system

The main model in each design and its variations can be found in Section 3.5.1 and 3.5.2.

3.5.1 Room Corridor Room, *RCR*

Main model

The main model is eight storeys high and six slabs wide, and is presented in Figure 3.15. The number of storeys are chosen based on the WoodSol project guidelines and on stricter fire regulations for buildings higher than eight storeys. The number of slabs were chosen to set a basis for comparison. The input for this model is summarised in Table 3.20, which also is the input for all modifications labelled *Base* for the RCR design.

Table 3.20: Main model and base input

Property		Values
Dimenssion of cross sections	mid frames	280 mm × 450 mm
	end frames	140 mm × 450 mm
	beams	140 mm × 450 mm
Dimenssions of slabs	room	9.15 m × 2.40 m
	corridor	3.00 m × 2.4 mm
Thickness of slabs		350 mm
Thickness of shear walls		90 m
Heigth of storeys		3 m
Spacing of frames		2.4 m
Rotational stiffness connections		10 000 kNm/rad
Boundary condition		encastred
Material properties		see Section 3.4

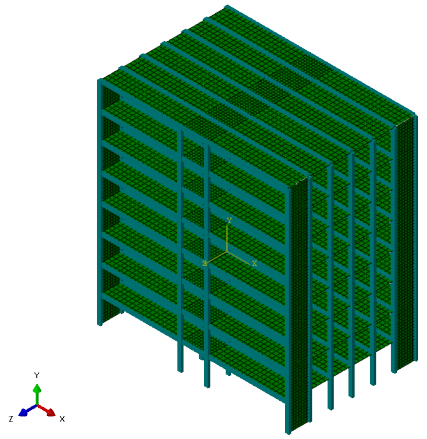

Figure 3.15: Main model of design RCR. Table 3.20 for input

Variations of storeys

By adding storeys, the total mass of a structure will rise, while the stiffness will be reduced as the columns length increases. The impact of influence on the natural frequencies of the structure is investigated by simulating models with varying number of storeys. The variations are shown in Figure 3.16.

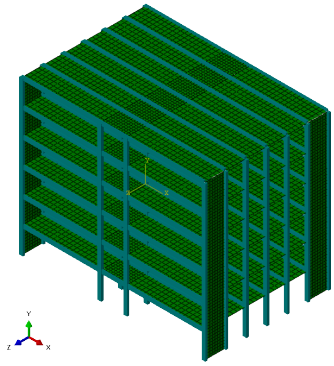

(a) Six storeys, n6d6

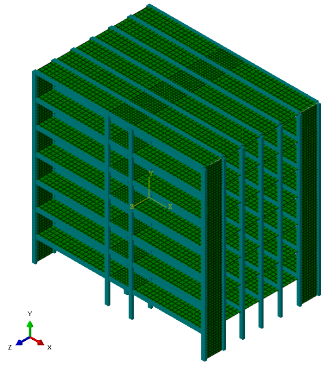

(b) Seven storeys, n7d6

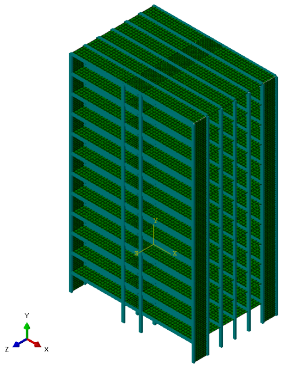

(c) 12 storeys, n12d6

Figure 3.16: Variations in number of storeys

Variation of slabs

Two models with added slabs in the direction orthogonal to the frames are shown in Figure 3.17a and 3.17b. These models are made to investigate how the results are affected by changing the slenderness of the building, and also the impact of adding more moment resisting frames. Figure 3.17c shows a model without the corridor and one of the "room"-blocks. The evaluation of this model will tell how adding or removing frames in their span direction affects the response.

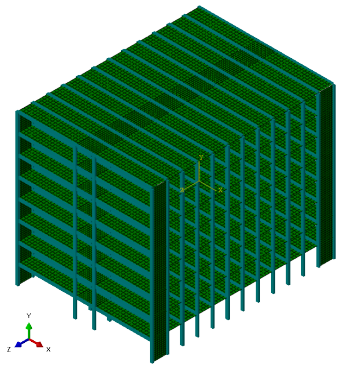

(a) 12 slabs wide, n8d12

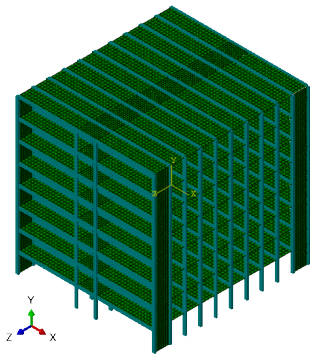

(b) 10 slabs wide, n8d10

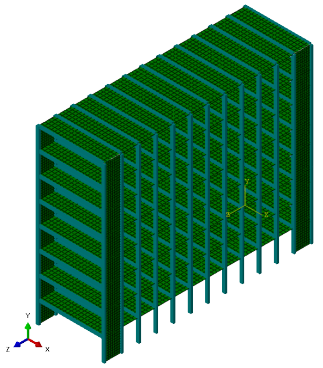

(c) One open section isolated, n8d12-room

Figure 3.17: Variation of slabs

Shaft added

Every building with more than three storeys must have an elevator, as well as a stairway [38]. The influence of a wooden shaft as a part of the structural system, is investigated through the model shown in Figure 3.18. The shaft in this model is modelled using three ply CLT.

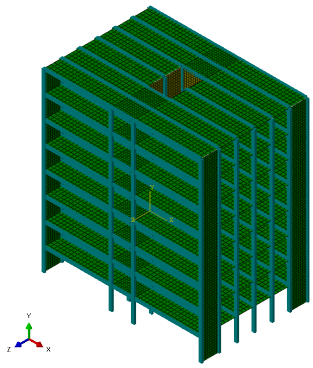

Figure 3.18: Wooden shaft added, n8-shaft

Slab and shear walls added

Figure 3.19 shows a model with four additional shear walls added, two in each direction. A slab has also been added to maintain symmetry. The influence of extra shear walls is investigated using this model.

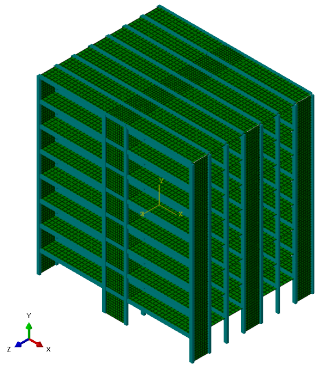

Figure 3.19: Seven slabs wide with extra shear walls, n8d7-shear

Special customisations

In some cases, a high first floor is wanted for e.g. a lobby or an reception area. Figure 3.20a and 3.20b show seven storey buildings with the same height as the main model. These models are investigated to learn the consequences of removing a lower floor from the structural system, checking for the contributions from slabs, beams and column height.

Figure 3.20c shows a four storey model which is placed on top of a virtual existing concrete building. The results from this model are used in a short introductory discussion on the application of light timber structures used to expand existing buildings.

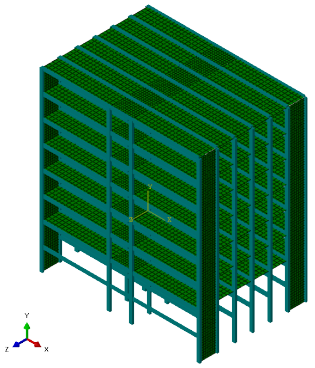

(a) First floor slabs from main model stripped off, n8-open1

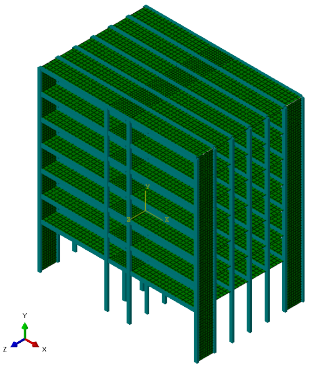

(b) First floor from main model stripped off entirely, n8-open2

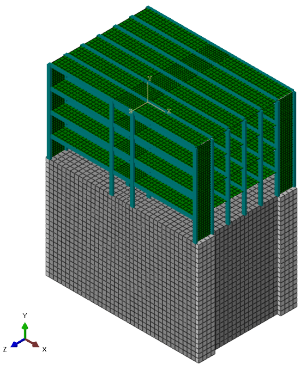

(c) Expanding an existing building, n4-ontop

Figure 3.20: Special customisations of RCR

3.5.2 The T-design

Main model

The main model have five slabs in each of the blocks making the flange, and nine slabs making the web, see Figure 3.21. As for the RCR design, this model also has eight storeys. This design is more complicated than the RCR design, due to lack of symmetry about one plane axis, this is discussed in more detail in the Discussion chapter, 5. The input for this model is summarised in Table 3.21, which also gives the input for all modifications labelled *Base* for the T-design.

Table 3.21: Main model and base input

Property		Values
Dimenssion of cross sections	mid frames	280 mm × 450 mm
	end frames	140 mm × 450 mm
	beams	140 mm × 450 mm
Dimenssions of slabs		9.6 m × 2.4 m
Thickness of slabs		350 mm
Thickness of shear walls		90 mm
Heigth of storeys		3 m
Spacing of frames		2.4 m
Rotational stiffness connections		10 000 kNm/rad
Boundary condition		encastred
Material properties		see Section 3.4

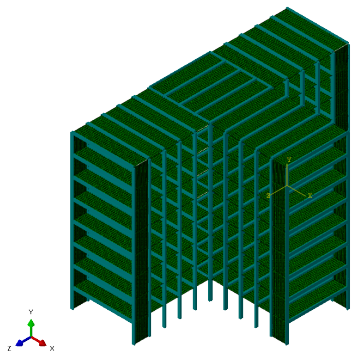

Figure 3.21: Main design of the T-model. Table 3.21 for input

Slabs added in the web

The number of slabs in the web is increased to 15, see Figure 3.22. This will alter the footprint of the building, and the influence on results are investigated.

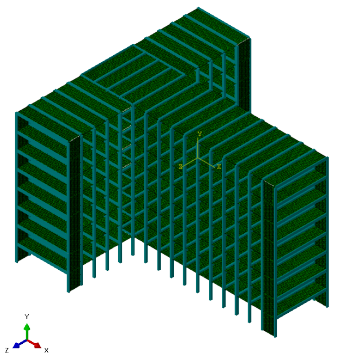

Figure 3.22: Six slabs added to the web, n8-long-web

Shaft added

The influence of a wooden shaft is investigated through the models shown in Figure 3.23. The shaft in this model is modelled using five ply CLT. The shaft is added where the web meets the flange because this is a plausible position for an entrance. It may also increase the stiffness of the web, influencing the torsional eigenmodes of the design.

A model with a shaft added as well as a shear wall on the opposite side of the web has been made, see Figure 3.23b. The results for this model are used to discuss the extra contribution to the models stiffness, when a shaft is already added.

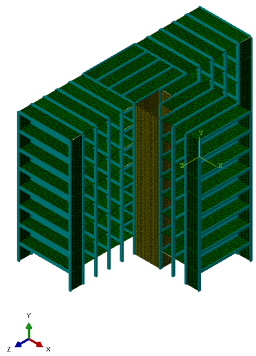

(a) With shaft, n8-shaft

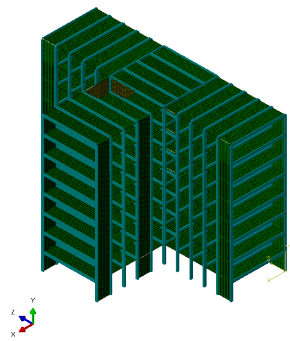

(b) With shaft and extra shear wall, n8-shaft-shear

Figure 3.23: T-design with wooden shaft

Six storey models

A six storey variation of the design is shown in Figure 3.24a. Figure 3.24b shows same the model with added shear walls. These models are used to investigate the influence of both lowering the building, and adding shear walls.

Figure 3.25a shows a different shape of the six storey model. In this model, six slabs have been added to the flange, while two slabs have been removed from the web. This is to understand the change in response due to changing the shape toward a more slender building. This configuration is also checked with added shear walls, see Figure 3.25b

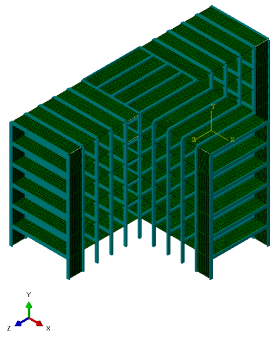

(a) Six storeys, n6

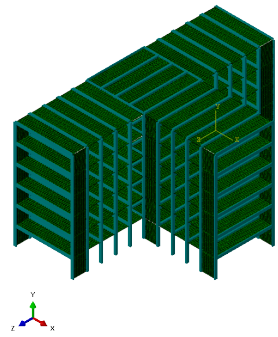

(b) Six storeys with extra shear walls, n6-shear

Figure 3.24: Six storey variations of the T-design

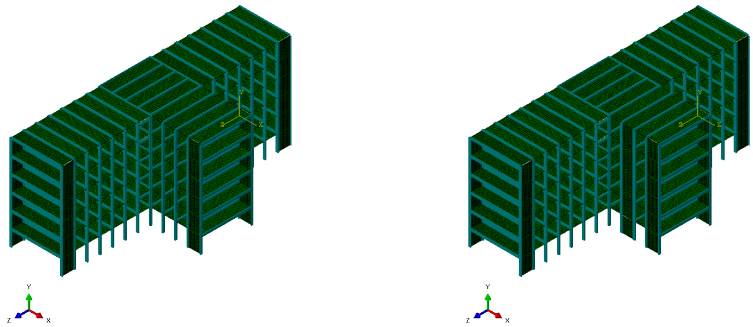

(a) Without extra shear walls, n6-wide (b) With extra shear walls, n6-wide-shear

Figure 3.25: Six slabs added in the flange and two removed from the web for a six storey model

3.5.3 Summary

Table 3.22 and 3.23 summarises the geometrical differences between the submodels in the RCR design and the T-design, respectively. The geometrical similarities between the submodels have been presented in Table 3.20 and 3.21.

Table 3.22: Variations in RCR design

Model	**Storeys**	**Height**	**# of Slabs**	**Span**		**Extra shear**	**Shaft**
	n	H [m]	d	x-dir [m]	z-dir [m]		
Main	**8**	**24**	**6**	**14.4**	**21.3**	**no**	**no**
n6d6	6	18	6	14.4	21.3	no	no
n7d6	7	21	6	14.4	21.3	no	no
n12d6	12	36	6	14.4	21.3	no	no
n8d10	8	24	10	24.0	21.3	no	no
n8d12	8	24	12	28.8	21.3	no	no
n8d12-room	8	24	12	28.8	9.2	no	no
n8-shaft	8	24	6	14.4	21.3	no	yes
n8d7-shear	8	24	7	16.8	21.3	yes	no
						Special customisation	
n7-open1	7	24	6	14.4	21.3	Stripped first floor slabs	
n7-open2	7	24	6	14.4	21.3	Stripped first floor entirely	
n4-ontop	4	12	6	14.4	21.3	Add-on building	

Table 3.23: Variations in the T-design

Model	**Storeys**	**Height**	**# of Slabs**		**Span**		**Extra shear**	**Shaft**
	n	H [m]	d_{web}	d_{flange}	x-dir [m]	z-dir [m]		
Main	**8**	**24**	**9**	**2 × 5**	**14.4**	**21.3**	**no**	**no**
n8-long-web	8	24	15	2 × 5	36.0	33.6	no	no
n8-shaft	8	24	9	2 × 5	21.6	33.6	no	yes
n8-shaft-shear	8	24	9	2 × 5	21.6	33.6	yes	yes
n6	6	18	9	2 × 5	21.6	33.6	no	no
n6-shear	6	18	9	2 × 5	21.6	33.6	no	no
n6-wide	6	18	8	2 × 7	19.2	43.2	no	no
n6-wide-shear	6	18	8	2 × 7	19.2	43.2	yes	no

3.6 Analysis

Approach

For each model and customisation, the same formula is followed. First, a modal analysis is done to find the models dynamic properties. This is done by executing a linear perturbation step in *Abaqus* with Lanczos as the iteration method. The outputs from this step are the systems natural frequencies and their associated eigenmodes. The natural frequencies and masses of the models are used to calculate the acceleration and the structural factor $c_s c_d$ as explained in Appendix A.4. $c_s c_d$ is then used to calculate the static wind loads in both the x- and the z-direction, which are included in load combinations applied to the model in a static linear perturbation step. Both ULS and SLS load combinations are checked, giving results for evaluating the fire design and the deflections in the top of the building. All simulations are in the linear domain.

The calculated wind loads for each model can be found in Appendix A.4 together with the formulas for wind load from NS-EN 1991-1-4 [26]. The deflection is only evaluated in the direction of the wind force, while the deflection perpendicular to the wind direction is neglectable in comparison.

Parametric study

A parametric study is done on the main model of each design. The parameters tested are

- column sections
- shear wall thickness
- rotation stiffness in connections between frames and beams
- different boundary conditions
- added mass in all the floors, or in the top floors of the building

The results from the parametric study for the main models decide what modifications will be done for the other models, aiming for an improvement on the results regarding acceleration, deflection and fire durability. This means that only the most effective modifications are investigated for the other models of each design, as well as combinations of these modifications.

Fire design

To check for the fire design requirements, the columns are sorted into groups. Columns with the same cross section size and the same sides exposed to a potential fire will fall

into the same group. The maximum reaction forces for each group are used to check if the sections are sufficient to withstand a 90 minute fire.

The design fire load and utilisation of capacity for the most vulnerable cross section are listed in tables throughout Chapter 4. The results are only listed for modifications where the acceleration is at a low level for the given model, or for the modifications where the columns are most affected by strong reaction forces. This way, the most critical modification is checked.

Remarks on main designs

The T-design has a more complex geometry compared to the RCR design. Where the RCR models are symmetric about both the x and the z-axis, the T-design models are only symmetric about the x-axis (with the exceptions of models including a shaft[3], which are unsymmetrical). This results in torsional eigenmodes. As described in Section 2.5, the formula for calculating accelerations is only valid for translation eigenmodes. The consequence is that only the x-direction, where a translation eigenmode can be found, is checked for acceleration for the T-design models. The torsional eigenmode with most mass contribution in z-direction is however used to calculate the $c_s c_d$ factor to find the wind loads in this direction, as presentet in Appendix A.4. For more comprehensive investigation of accelerations and behavior for the T-design models, wind tunnel testing is recommended.

[3] The shaft models have a eigenmode which is close to translational, which is used to investigate accelerations.

Chapter 4

Results

This chapter presents the results from the parametric study done on the different models. The frequencies, acceleration, deflection and reaction forces are evaluated for different modifications of the models, and the most important values are presented. Not all requirements are evaluated for every modification. Evaluation of deflection and fire design are leaved out in some of the simulations as the acceleration is the governing requirement. A summary and discussion of the results are found in Chapter 5.

4.1 Design: Room Corridor Room, RCR

This section presents the results from the analyses of the Room Corridor Room design, RCR. The main model is presented thoroughly with results for many modifications. The main model is followed by presentations of the most important results for the variation of number of storeys, number of slabs, additional shafts and shear walls and the special configurations.

4.1.1 Main model

Acceleration

Table 4.1 gives an overview of the different modifications of parameters and the resulting frequencies and accelerations. The deviation from the acceleration of the base model is also included. The base model has the properties represented in Table 3.20. The total and equivalent mass, m_e, are listed for every modification and used in the

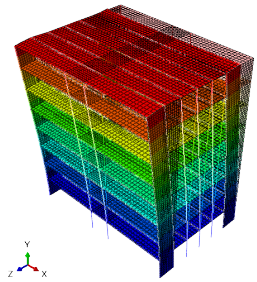

(a) Mode shape 1

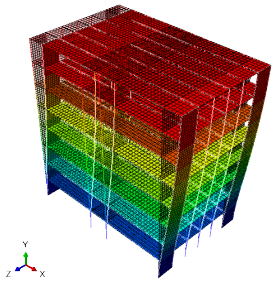

(b) Mode shape 2

Figure 4.1: The two first mode shapes of the RCR main model, *Base*

calculation of the acceleration, see equations in Section 2.5. For the base model the acceleration is 0.080 m/s^2 in the direction of the frames (x-dir) and 0.134 m/s^2 in the shear wall direction (z-dir). Figure 4.1 show the mode shapes of the base model for the two first modes. A combination of increasing the cross section of the columns and adding mass in the top two floors will decrease the acceleration to 0.041 m/s^2 in the x-direction and 0.065 m/s^{2}in z-direction. The maximum acceleration for a residential building with frequencies between 1 and 2 Hz is 0.04 m/s^2, according to ISO-10137 [9].

Table 4.1: Frequencies and accelerations, RCR main model

	Modification	**Mass** [kg]		**Frequency** [Hz]		**Acceleration** [m/s^2]			
		Total	m_e	x-dir	z-dir	x-dir	$\Delta a/a_{base}$	z-dir	$\Delta a/a_{base}$
1	**Base**[1]	494 298	27 334	0.834	0.793	**0.080**	0 %	**0.134**	0 %
2	t_{shear} =180 mm	502 523	27 919	0.828	0.850	0.079	-2 %	0.121	-9 %
3	k_{rot} = 20 000 kNm/rad[2]	494 298	27 334	0.946	0.795	0.070	-13 %	0.133	-1 %
4	Cross section 280×900[3]	603 525	33 027	1.150	1.176	0.047	-41 %	0.073	-46 %
5	Cross section 270×675	555 413	30 553	1.016	1.104	0.057	-29 %	0.084	-38 %
6	ρ doubled top two floors	590 925	38 622	0.704	0.647	0.065	-19 %	0.120	-10 %
7	30 % of live load as added mass	724 466	38 973	0.683	0.657	0.069	-13 %	0.118	-12 %
8	Extra shear wall, Figure 4.2	499 453	27 766	1.031	0.796	0.062	-23 %	0.132	-1 %
9	Combination 4 + 6	708 243	44 062	0.996	1.001	0.041	-49 %	0.065	-51 %
10	Combination 5 + 8	560 658	30 815	1.236	1.099	0.045	-44 %	0.083	-44 %
11	Combination 5 + 7 + 8	790 737	42 274	1.035	0.920	0.041	-49 %	0.075	-44 %
12	BC: k_{rot} = 10 000 kNm/rad	494 298	27 334	0.769	0.788	0.087	8 %	0.134	0 %
13	BC: pinned	494 298	27 334	0.692	0.784	0.097	21 %	0.135	1 %

[1] For the following sections the **Base** is referred to the *Main model*.
[2] The rotational stiffness for one single connection.
[3] The dimensions for one single cross section.

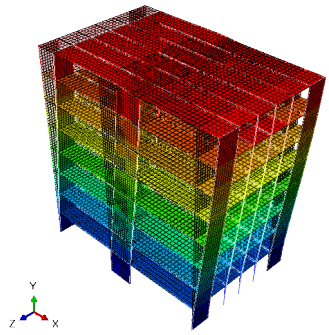

Figure 4.2: The RCR main model, *Base*, with an extra shearwall in the corridor

Deflection

The deflections under the SLS load combination are listed in Table 4.2, together with the deviation from the accepted deflection. The maximum deflection for a 24 m high building is 48 mm. The deflection in U1 is the deflection in the x-direction from wind load in x-direction. U3 is for the z-direction under wind load in z-direction. The different modifications are from Table 4.1.

Table 4.2: Deflection, RCR main model

	Modification	**Deflection** [mm]			
		U1	$^{\Delta U1}/_{max}$	U3	$^{\Delta U3}/_{max}$
1	**Base**	**38.8**	-19 %	**61.0**	27 %
2	t_{shear} =180 mm	38.8	-19 %	52.7	10 %
3	k_{rot} = 20 000 kNm/rad	30.1	-37 %	60.7	27 %
4	Cross section 280×900	18.4	-62 %	23.2	-52 %
6	ρ doubled top two floors	38.9	-19 %	61.0	27 %
9	Combination 4 + 6	18.4	-62 %	23.2	-52 %
12	BC: k_{rot} = 10 000 kNm/rad	45.7	-6 %	61.8	29 %
13	BC: pinned	56.1	17 %	62.7	31 %

Fire design

The fire design loads are 60 % of the ULS load combination. Table 4.3 lists the fire loads for the base model. The capacity is evaluated for the worst affected columns. The loads do not necessarily occur on the same column, but are the maximum loads for the col-

umn group[4]. The formulas for calculating the capacity of the cross section are listed in Appendix C. The cross sections are checked for shear, combined bending and tension, combined bending, compression and buckling. The capacity control regarding lateral torsional instability has only been checked for the main models. This is justified by a control of the increased cross sections, showing that lateral torsional instability is prevented, see Appendix C.

For the Room Corridor Room design, the most vulnerable columns are the corner columns and the exterior corridor columns, illustrated in Figure 4.3a. These columns have initial cross sections with dimensions 140mm × 450 mm. The corner columns are reduced by fire load on two sides, and the exterior columns in the corridor, reduced by fire load on three sides. The utilisation of the capacity is shown in Table 4.4. Figure 4.3b illustrates the axis system used for fire design.

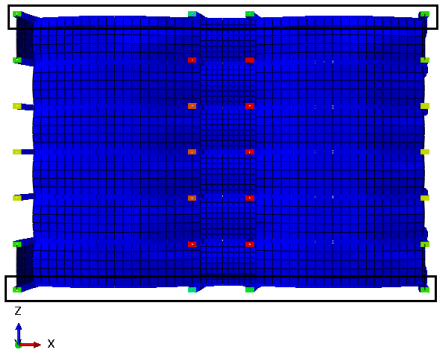

(a) The most vulnerable columns to fire load for the RCR models. Seen from below.

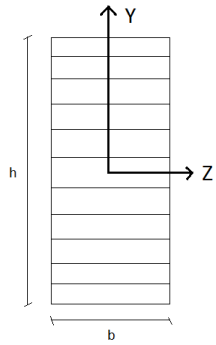

(b) Axis system of the cross section

Figure 4.3: Column grouping and axis system

Table 4.3: Fire design loads, RCR main model, *Base*

Column **eff. cross section** [mm×mm]		M_z [kNm]	M_y [kNm]	V_z [kN]	V_y [kN]	N[5] [kN]	P[6] [kN]
Corridor, exterior, 70×310	x-dir	22.6	4.1	6.2	9.5	0.0	205.7
	z-dir	1.1	8.1	4.2	1.5	0.0	188.6
Outer corner, 70×380	x-dir	22.6	2.0	14.6	9.3	0.0	235.6
	z-dir	2.8	13.4	40.5	6.0	105.1	610.4

Table 4.5 lists the loads for *Combination 4 + 6* (from Table 4.1), an increase of the cross

[4]Column group, e.g. corner columns, exterior mid columns, exterior corridor columns, inner corridor columns.

[5]Tensile force

[6]Compression force

Table 4.4: Utilisation of cross section, RCR main model, *Base*

	Corridor, ext.		Outer corner	
	x-dir	**z-dir**	**x-dir**	**z-dir**
Shear				
C.7a	24 %	4 %	19 %	9 %
C.7b	16 %	11 %	30 %	91 %
Bending and tension				
C.9a	87 %	95 %	45 %	153 %
C.9b	91 %	68 %	51 %	117 %
Bending, comp. and buckling				
C.11a	305 %	294 %	248 %	634 %
C.11b	91 %	68 %	83 %	171 %
Lateral torsional instability				
C.14	281 %	203 %	245 %	512 %

section and double mass in the two top floors. The utilisation of this cross section is listed in Table 4.6.

Table 4.5: Fire design loads, RCR main model, *Combination 4 + 6*

Column **eff. cross section** [mm×mm]		M_z [kNm]	M_y [kNm]	V_z [kN]	V_y [kN]	N [kN]	P [kN]
Corridor, exterior, 210×760	x-dir	55.7	12.4	9.5	9.6	0.0	243.7
	z-dir	69.5	34.1	8.3	1.5	0.0	232.1
Outer corner, 210×830	x-dir	55.7	7.8	10.6	10.3	0.0	252.7
	z-dir	4.1	43.9	29.1	5.3	68.0	544.5

Table 4.6: Utilisation of cross section, RCR main model, *Combination 4 + 6*

	Corridor ext.		Outer corner	
	x-dir	**z-dir**	**x-dir**	**z-dir**
Shear				
C.7a	3 %	1 %	3 %	2 %
C.7b	3 %	3 %	3 %	9 %
Bending and tension				
C.9a	12 %	18 %	8 %	23 %
C.9b	12 %	12 %	9 %	17 %
Bending, comp. and buckling				
C.11a	18 %	24 %	14 %	34 %
C.11b	18 %	18 %	14 %	26 %

4.1.2 Variation of storeys

Table 4.7 presents an overview of the different modifications for the six, seven and 12 storey model. The total and equivalent mass are listed, together with the frequency, acceleration and the deviation of acceleration from the base model.

Acceleration

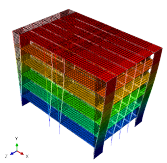

(a) Six storeys

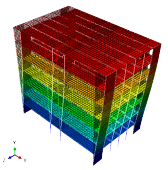

(b) Seven storeys

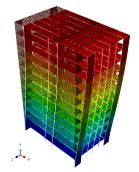

(c) 12 storeys

Figure 4.4: The first mode shape (in x-direction) for the six, seven and 12 storey model

Table 4.7: Frequencies and accelerations, n6d6, n7d6, n12d6

	Modification	**Mass** [kg]		**Frequency** [Hz]		**Acceleration** [m/s^2]			
		Total	m_e	x-dir	z-dir	x-dir	$\Delta a / a_{base}$	z-dir	$\Delta a / a_{base}$
	Main model (eight storeys)	494 298	27 334	0.827	0.796	0.080	-	0.134	-
	Six storeys, n6d6, Figure 4.4a								
1	Base	364 872	28 677	1.130	1.250	0.062	0 %	0.088	0 %
2	ρ doubled top floor	415 231	37 069	0.991	1.064	0.056	-10 %	0.083	-6 %
3	30 % of live load as added mass	537 499	40 798	0.928	1.026	0.054	-12 %	0.079	-11 %
4	Cross section 270×675	416 560	32 306	1.444	1.677	0.041	-33 %	0.056	-37 %
5	Combination 3 + 4	590 357	44 510	1.214	1.403	0.037	-40 %	0.050	-43 %
	Seven storeys, n7d6, Figure 4.4b								
1	Base	425 684	27 783	0.958	0.988	0.071	0 %	0.110	0 %
2	ρ doubled top floor	476 043	34 976	0.855	0.853	0.065	-9 %	0.104	-5 %
3	30% of live load as added mass	627 082	39 526	0.787	0.811	0.063	-12 %	0.098	-11 %
4	Cross section 270×810	504 419	32 374	1.291	1.395	0.044	-39 %	0.064	-42 %
5	Combination 3 + 4	705 817	44 117	1.084	1.170	0.039	-45 %	0.058	-47 %
	12 storeys, n12d6, Figure 4.4c								
1	Base	741 447	25 971	0.542	0.407	0.132	0 %	0.269	0 %
2	ρ double top four floors	934 677	38 967	0.442	0.320	0.109	-17 %	0.233	-14 %
3	30 % live load as added mass	1 086 699	36 794	0.447	0.336	0.114	-14 %	0.235	-13 %
4	Cross section 280×900	905 287	31 107	0.687	0.626	0.087	-34 %	0.149	-45 %
5	Combination 3 + 4	1 250 540	41 930	0.582	0.530	0.077	-42 %	0.135	-50 %
6	Combination 2 + 3 + 4	1 443 770	54 925	0.504	0.450	0.069	-47 %	0.123	-54 %

Deflection

The deflections of the combinations from Table 4.7 are listed in Table 4.8, alongside the deviation from the requirement. For six storeys the requirement is 36 mm, for seven it is 42 mm and for 12 it is 72 mm. The results from the main model (eight storeys) are presented for comparison.

Table 4.8: Deflections, n6d6, n7d6, n12d6

Modification	**Deflection** [mm]			
	U1	$^{\Delta U1}/_{max}$	U3	$^{\Delta U3}/_{max}$
Main model (eight storeys)	38.8	-19 %	61.0	27 %
Six storeys, n6d6				
Base	13.3	-63 %	18.0	-50 %
Combination 3 + 4	7.6	-79 %	9.2	-74 %
Seven storeys, n7d6				
Base	21.9	-48 %	34.0	-19 %
Combination 3 + 4	11.0	-74 %	14.5	-65 %
12 storeys, n12d6				
Base	126.1	75 %	338.5	370 %
Combination 2 + 3 + 4	69.4	-4 %	118.2	64 %

Fire design

The fire design loads for the 12 storey model, *Combination 2 + 3 + 4* (from Table 4.7), are listed in Table 4.9. Only the worst effected columns are looked at, and the utilisations of the cross sections are found in Table 4.10. Tables for loads and utilisation for the six and seven storey model are found in Appendix C.

Table 4.9: Fire design loads, **12 storeys** n12d6, *Combination 2 + 3 + 4*

Column		M_z	M_y	V_z	V_y	N	P
eff. cross section [mm×mm]		[kNm]	[kNm]	[kN]	[kN]	[kN]	[kN]
Corridor, exterior, 210×760	x-dir	124.6	14.8	11.4	18.2	0.0	467.3
	z-dir	0.9	79.6	16.7	1.9	0.0	427.1
Outer corner, 210×830	x-dir	124.6	9.4	13.9	18.7	0.0	475.1
	z-dir	6.7	102.1	60.7	7.2	554.8	1 438.8

Table 4.10: Utilisation of cross section, **12 storeys**, *Combination 2 + 3 + 4*

	Corridor, ext.		Outer corner	
	x-dir	**z-dir**	**x-dir**	**z-dir**
Shear				
C.7a	6%	1%	6%	2%
C.7b	4%	6%	4%	19%
Bending and tension				
C.9a	20%	41%	15%	63%
C.9b	23%	29%	18%	49%
Bending, comp. and buckling				
C.11a	32%	33%	26%	82%
C.11b	33%	38%	28%	64%

4.1.3 Variation of slabs

The footprint of the main model is altered by adding and removing slabs. The first variation is adding slabs in the z-direction, maintaining the Room Corridor Room Design. Then there is looked at a variation with only one open section (only "Room") for 12 slabs.

Acceleration

Table 4.11 and 4.12 lists the frequencies and accelerations for the different modifications.

Table 4.11: Frequencies and accelerations, n8d10, n8d12

	Modification	**Mass** [kg]		**Frequency** [Hz]		**Acceleration** [m/s^2]			
		Total	m_e	x-dir	z-dir	x-dir	$\Delta a / a_{base}$	z-dir	$\Delta a / a_{base}$
	Main model (RCR six slabs)	494 298	27 334	0.827	0.796	0.080	-	0.134	-
	10 slabs, n8d10, Figure 4.5a								
1	Base	801 876	45 720	0.828	0.631	0.074	0 %	0.094	0 %
2	ρ doubled top floor	885 807	56 209	0.748	0.551	0.070	-8 %	0.089	-5 %
3	30 % of live load as added mass	1 185 476	64 825	0.680	0.518	0.066	-11 %	0.083	-12 %
4	Extra mass on the roof[7]	975 025	67 365	0.682	0.491	0.046	-15 %	0.084	-10 %
5	Cross section 280×900	973 518	52 475	1.141	0.962	0.044	-42 %	0.052	-45 %
6	Cross section 270×855	954 311	52 348	1.112	0.939	0.046	-37 %	0.053	-44 %
7	Cross section 270×675	910 174	50 150	1.014	0.891	0.054	-27 %	0.059	-38 %
8	Combination 2 + 5	1 057 450	64 758	1.022	0.857	0.042	-44 %	0.048	-49 %
9	Combination 3 + 6	1 337 911	71 453	0.933	0.788	0.042	-44 %	0.048	-49 %
10	Combination 4 + 7	1 466 934	91 864	0.731	0.628	0.043	-42 %	0.048	-49 %
	12 slabs, n8d12, Figure 4.5b								
1	Base	965 804	53 884	0.825	0.879	0.076	0 %	0.084	0 %
2	ρ doubled top floor	1 066 577	66 122	0.745	0.505	0.070	-8 %	0.080	-5 %
3	30% of live load as added mass	1 412 735	76 143	0.681	0.477	0.067	-11 %	0.074	-12 %
4	Cross section 280×900	1 168 658	63 987	1.139	0.893	0.044	-41 %	0.044	-48 %
5	Cross section 270×855	1 145 958	62 857	1.110	0.870	0.046	-39 %	0.046	-45 %
6	Combination 2 + 4	1 269 427	76 225	1.021	0.795	0.042	-44 %	0.042	-50 %
7	Combination 3 + 5	1 580 630	84 505	0.940	0.736	0.042	-44 %	0.042	-50 %
8	Combination 2 + 3 + 5	1 678 532	96 743	0.869	0.677	0.040	-47 %	0.040	-52 %
9	Combination 3 + 4	1 615 586	86 246	0.962	0.754	0.040	-47 %	0.040	-53 %

[7] Thickness and density of additional slab on roof: t = 250 mm, ρ= 1300 kg/m^3

Table 4.12: Frequencies and accelerations, n8d12-room

	Modification	**Mass** [kg]		**Frequency** [Hz]		**Acceleration** [m/s^2]			
		Total	m_e	x-dir	z-dir	x-dir	$\Delta a / a_{base}$	z-dir	$\Delta a / a_{base}$
	12 slabs, n8d12-room, Figure 4.5c								
1	Base	421 663	23 501	0.764	0.854	0.149	0 %	0.069	0 %
2	ρ doubled top floor	465 208	28 793	0.689	0.746	0.131	-12 %	0.062	-10 %
3	30 % of live load as added mass	620 843	33 422	0.628	0.702	0.134	-10 %	0.061	-11 %
4	Cross section 280×900	523 091	28 553	1.061	1.260	0.087	-41 %	0.038	-45 %
5	Cross section 270×855	511 740	27 988	1.031	1.237	0.092	-38 %	0.039	-43 %
6	Combination 2 + 4	566 661	37 511	0.949	1.129	0.076	-49 %	0.033	-53 %
7	Combination 3 + 5	705 230	37 624	0.873	1.047	0.084	-44 %	0.035	-49 %
8	Combination 2 + 3 + 5	747 567	42 916	0.806	0.966	0.081	-46 %	0.034	-51 %
9	Combination 3 + 4	722 271	38 473	0.896	1.064	0.079	-47 %	0.034	-51 %

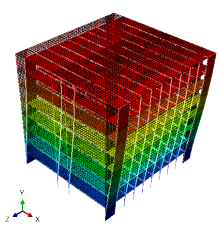

(a) 10 slab wide

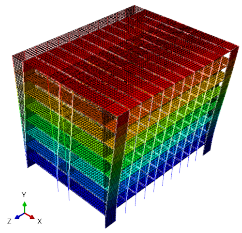

(b) 12 slab wide

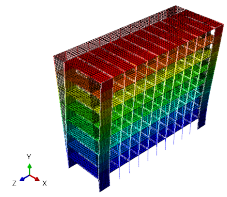

(c) 12 slab wide, only "room"

Figure 4.5: The first mode shapes (in x-direction) for variation of slabs

Deflection

The deflections for the base model and one modification from each design, alongside the deviation from the requirement of 48 mm, are listed in Table 4.13. The results from the main model are presented for comparison.

Table 4.13: Deflections, n8d12 and n8d12-room

Modification	**Deflection** [mm]			
	U1	$\Delta U1/_{max}$	U3	$\Delta U3/_{max}$
Main model (six slabs)	38.8	-19 %	61	27 %
n8d12, Figure 4.5b				
Base	33.7	-30 %	55.5	-16 %
Combination 3 + 4	16.0	-67 %	19.8	-59 %
n8d12-room, Figure 4.5c				
Base	92.6	93 %	26.6	-45 %
Combination 3 + 4	43.1	-10 %	10.2	-79 %

Fire design

The fire design loads are calculated for the n8d12 model, *Combination 3 + 4* (from Table 4.11). The worst effected columns are listed in Table 4.14, and the utilisation of the cross sections are found in Table 4.15. The RCR n8d10 and n8d12-room models have similar low utilisation and the tables for loads and utilisation are found in Appendix C.

Table 4.14: Fire design loads, **n8d12**, *Combination 3 + 4*

Column		M_z	M_y	V_z	V_y	N	P
eff. cross section [mm×mm]		[kNm]	[kNm]	[kN]	[kN]	[kN]	[kN]
Corridor, exterior, 210×760	x-dir	54.4	12.8	11.3	10.0	0.0	241.3
	z-dir	0.5	31.7	6.4	1.1	0.0	327.7
Outer corner, 210×830	x-dir	54.4	10.7	11.3	10.0	0.0	241.3
	z-dir	3.1	38.0	25.5	4.4	0.0	490.1

Table 4.15: Utilisation of cross section, **n8d12**, *Combination 3 + 4*

	Corridor, exterior		Outer corner	
	x-dir	**z-dir**	**x-dir**	**z-dir**
Shear				
C.7a	3 %	1 %	3 %	1 %
C.7b	4 %	0 %	4 %	0 %
Bending and tension				
C.9a	12 %	16 %	10 %	18 %
C.9b	12 %	12 %	10 %	13 %
Bending, comp. and buckling				
C.11a	18 %	25 %	15 %	30 %
C.11b	18 %	19 %	15 %	23 %

4.1.4 With shaft, n8-shaft

Acceleration

The model presented in Figure 4.6a has a shaft coupled to the structural system. Table 4.16 lists the frequencies and accelerations for the different modifications for the model with shaft. Table 4.17 shows the effect of removing the exterior shear walls, hence the stability is then only provided by the shaft and the moment resisting frames. This model is shown in Figure 4.6b

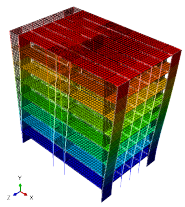

(a) With shaft and shear walls

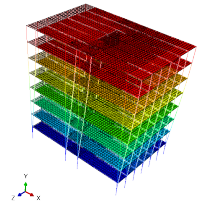

(b) Only shaft

Figure 4.6: The first mode shape (x-direction) of the RCR n8-shaft model, with and without shear walls

Table 4.16: Frequencies and accelerations, n8-shaft

	Modification	**Mass** [kg]		**Frequency** [Hz]		**Acceleration** [m/s^2]			
		Total	m_e	x-dir	z-dir	x-dir	$\Delta a / a_{base}$	z-dir	$\Delta a / a_{base}$
	Main model	494 298	27 334	0.827	0.796	0.080	31 %	0.134	67 %
1	**Base**	483 951	26 942	1.075	1.270	0.061	0 %	0.080	0 %
2	ρ doubled top floor	525 741	33 288	0.964	1.119	0.056	-8 %	0.076	-6 %
3	30 % of live load as added mass	708 919	38 199	0.885	1.044	0.054	-11 %	0.072	-11 %
4	Cross section 280×900	597 206	32 635	1.385	1.633	0.037	-38 %	0.050	-38 %
5	Cross section 270×675	547 667	30 168	1.263	1.568	0.045	-26 %	0.056	-30 %
6	Combination 2 + 4	637 584	38 929	1.236	1.463	0.036	-41 %	0.048	-41 %
7	Combination 3 + 5	777 837	41 631	1.054	1.308	0.041	-33 %	0.051	-37 %

Table 4.17: Relative change when exterior shear walls are removed

	Modification	**Mass** [kg]		**Frequency** [Hz]		**Acceleration** [m/s^2]	
		Δ total	Δ m_e	Δ x-dir	Δ z-dir	Δ x-dir	Δ z-dir
1	**Base**	-3 %	-2 %	2 %	-24 %	0 %	40 %
2	ρ doubled top floor	-1 %	-2 %	2 %	-24 %	0 %	40 %
3	30% live load as added mass	-1 %	-1 %	1 %	-25 %	-1 %	40 %
4	Cross section 280×900	-3 %	-3 %	2 %	-26 %	1 %	46 %
5	Cross section 270×675	-2 %	-1 %	2 %	-25 %	-1 %	43 %
6	Combination 2 + 4	-1 %	-2 %	3 %	-25 %	0 %	44 %
7	Combination 3 + 5	-1 %	-1 %	2 %	-25 %	-1 %	42 %

Deflection

The deflections for the base model and *Combination 3 + 5* (from Table 4.16), are listed in Table 4.18 alongside the deviation from the requirement of 48 mm. The results from the main model are also presented for comparison.

Table 4.18: Deflections, n8-shaft

Modification	**Deflection** [mm]			
	U1	$^{\Delta U1}/_{max}$	U3	$^{\Delta U3}/_{max}$
Main model	38.8	-19 %	61.0	27 %
Base	19.1	-60 %	22.9	-52 %
Combination 3 + 5	12.6	-74 %	13.2	-72 %

Fire design

The fire design loads for *Combination 3 + 5* (from Table 4.16) are listed in Table 4.19. Only the most vulnerable columns are listed. The utilisation of the capacity is shown in Table 4.20.

Table 4.19: Fire design loads, n8-shaft, *Combination 3 + 5*

Column		M_z	M_y	V_z	V_y	N	P
eff. cross section [mm×mm]		[kNm]	[kNm]	[kN]	[kN]	[kN]	[kN]
Corridor, exterior, 200×535	x-dir	29.9	10.5	11.2	6.5	0.0	294.4
	z-dir	0.7	26.5	6.0	1.1	0.0	185.2
Outer corner, 200×605	x-dir	29.9	7.0	11.1	5.2	0.0	294.4
	z-dir	2.9	26.5	24.1	4.5	0.0	416.6

Table 4.20: Utilisation of cross section, n8-shaft, *Combination 3 + 5*

	Corridor, ext.		Outer corner	
	x-dir	**z-dir**	**x-dir**	**z-dir**
Shear				
C.7a	3 %	2 %	2 %	2 %
C.7b	6 %	13 %	5 %	11 %
Bending and tension				
C.9a	15 %	12 %	10 %	20 %
C.9b	15 %	15 %	10 %	14 %
Bending, comp. and buckling				
C.11a	26 %	29 %	20 %	34 %
C.11b	25 %	21 %	19 %	26 %

4.1.5 With additional shear walls, n8d7-shear

Shear walls are added in both x- and z-direction in the exterior walls, presented in Figure 4.7.

(a) Mode shape 1 (b) Mode shape 2

Figure 4.7: The two first mode shapes of the RCR n8d7-shear model

Acceleration

The mass, frequency, acceleration and the deviation from the base model are listed in Table 4.21.

Table 4.21: Frequencies and accelerations, n8d7-shear

	Modification	**Mass** [kg]		**Frequency** [Hz]		**Acceleration** [m/s^2]			
		Total	m_e	x-dir	z-dir	x-dir	$\Delta a / a_{base}$	z-dir	$\Delta a / a_{base}$
	Main model	494 298	27 334	0.824	0.803	0.094	34 %	0.157	34 %
1	**Basis**	583 707	27 190	1.053	0.896	0.070	0 %	0.117	0 %
2	t_{shear} = 180 mm	601 194	27 919	1.098	0.956	0.065	-7 %	0.106	-6 %
3	ρ double top two floors	696 424	43 557	0.878	0.732	0.055	-21 %	0.094	-20 %
4	30 % live load as added mass	852 892	45 851	0.869	0.738	0.053	-24 %	0.088	-25 %
5	Cross section 270×675	662 474	36 368	1.282	1.222	0.042	-40 %	0.064	-45 %
6	Cross section 280×900	708 544	38 662	1.410	1.308	0.036	-49 %	0.054	-54 %
7	Combination 4 + 5	920 133	49 200	1.082	1.031	0.038	- 46 %	0.057	-51 %
8	Combination 4 + 6	977 729	52 069	1.193	1.105	0.032	- 54 %	0.049	-58 %
9	Combination 3 + 6	821 261	57 809	1.193	1.103	0.029	-59 %	0.045	-62 %
10	Combination 3 + 4 + 6	1 090 446	69 025	1.053	0.973	0.028	-60 %	0.043	-63 %

Deflection

The deflections for the base and *Combination 3 + 4 + 6* (from Table 4.21) are listed in Table 4.22, beside the deviation from the requirement of 48 mm.

Table 4.22: Deflection, n8d7-shear

Modification	**Deflection** [mm]			
	U1	$^{\Delta U1}/_{max}$	U3	$^{\Delta U3}/_{max}$
Main model	38.8	-19 %	61.0	27 %
Base	24.7	-49 %	40.7	-15 %
Combination 3 + 4 + 6	11.8	-75 %	16.0	-67 %

Fire design

The fire design load is for the modification with the lowest acceleration, *Combination 3 + 4 + 6* (from Table 4.21). The loads are listed in Table 4.23 and the utilisation of the cross section in Table 4.24.

Table 4.23: Fire design loads, n8d7-shear, *Combination 3 + 4 + 6*

Column		M_z	M_y	V_z	V_y	N	P
eff. cross section [mm×mm]		[kNm]	[kNm]	[kN]	[kN]	[kN]	[kN]
Corridor, exterior, 210×760	x-dir	44.9	12.6	9.6	19.8	0.0	463.1
	z-dir	1.7	29.7	9.8	2.1	0.0	286.0
Outer corner, 210×830	x-dir	42.5	8.5	11.3	10.1	0.0	284.6
	z-dir	3.8	33.1	23.6	5.4	0.0	483.7

Table 4.24: Utilisation of cross section, n8d7-shear, *Combination 3 + 4 + 6*

	Corridor, ext.		Outer corner	
	x-dir	**z-dir**	**x-dir**	**z-dir**
Shear				
C.7a	7%	1%	3%	2%
C.7b	3%	3%	4%	8%
Bending and tension				
C.9a	11%	16%	8%	16%
C.9b	11%	11%	8%	11%
Bending, comp. and buckling				
C.11a	23%	23%	14%	27%
C.11b	21%	17%	14%	21%

4.1.6 Special variation of Room Corridor Room

Open first floor

This section presents the results for the model where the slabs and beams for the first floor are removed, and for the model where only the slabs are removed. Table 4.25 list the mass, frequency and acceleration for the different modifications.

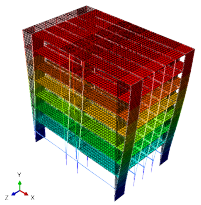

(a) With beams, n7-open1

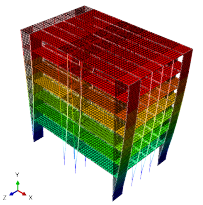

(b) first floor entirely stripped off, n7-open2

Figure 4.8: The first mode shape of the open first floor models

Table 4.25: Frequencies and accelerations, open first floor

	Modification	**Mass** [kg]		**Frequency** [Hz]		**Acceleration** [m/s^2]			
		Total	m_e	x-dir	z-dir	x-dir	$\Delta a / a_{main}$	z-dir	$\Delta a / a_{main}$
	Main model	494 298	27 334	0.824	0.793	0.080	0 %	0.134	0 %
1	n7-open1 (Fig. 4.8a)	435 211	27 939	0.824	0.799	0.081	~ 0 %	0.131	-2 %
2	n7-open2 (Fig. 4.8b)	433 245	27 825	0.755	0.799	0.087	8 %	0.131	-2 %
	Main model, ρ doubled top two floors	590 920	38 622	0.740	0.647	0.065	0 %	0.121	0 %
3	1 + ρ doubled top two floors	538 905	39 501	0.691	0.645	0.069	7 %	0.120	-1 %
4	2 + ρ doubled top two floors	535 928	38 938	0.640	0.646	0.075	16 %	0.120	~ 0 %

Four storeys on top of an existing building

This configuration is used to investigate the interaction between the existing building and the new four storey timber building. The following three cases are looked into:

1. Existing building has *lower* natural frequency than the added timber part
2. Existing building *in resonance* with the added timber part
3. Existing building has *higher* natural frequency than the added timber part

Only the results from case three are presented in Table 4.26, see Figure 4.9. The virtual existing building consist of five storeys.

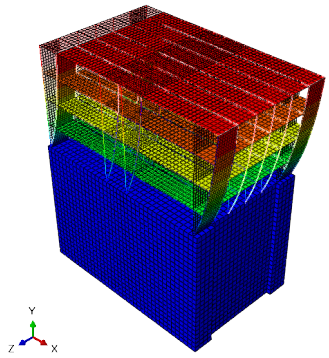

Figure 4.9: The first mode shape for the expanded building

Table 4.26: Frequencies and accelerations for four storeys on top of an existing building, n4-ontop

	Modification	**Mass** [kg]		**Frequency** [Hz]	**Acceleration** [m/s^2]	
		Total	m_e	x-dir	x-dir	$\Delta a / a_{base}$
1	**Base**	247 149	32 364	1.255	0.050	0 %
2	30 % live load as added mass	362 233	45 851	1.034	0.045	-11 %
3	Cross section 140×585	252 610	33 004	1.377	0.044	-12 %
4	Combination 2 + 3	367 694	46 491	1.137	0.040	- 21 %

4.2 Design: T-shape

The results for the T-design models are presented in this section. The main model is presented thoroughly with results for many modifications. The main model is followed by the most important results from the models with variation of number of slabs, additional shafts and a six storey model.

4.2.1 Main model

Acceleration

Table 4.27 presents the frequencies with corresponding acceleration for the main model. The three first eigenmodes are shown in Figure 4.10. The T-design models have torsional eigenmodes, which as mentioned in Section 2.5, should not be used in the acceleration calculation method from NS-EN 1991-1-4.

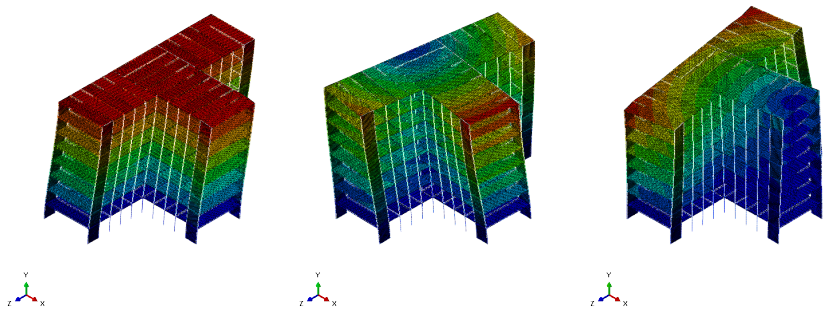

(a) Mode one, translation x (b) Mode two, torsion (c) Mode three, torsion

Figure 4.10: First three eigenmodes of the main model in T-design

Table 4.27: Frequencies and acceleration, T-design main model

Eigenmode	**Frequency** [Hz]	**Type**	**Acceleration**, a [m/s^2]
1	0.791	Translation	0.154
2	*0.844*	*Torsion*	-
3	*0.889*	*Torsion*	-

Table 4.28 presents the acceleration for different parametric changes from the main model, alongside the deviations from 0.04 m/s^2. The table also includes the values

for model total mass, effective mass and frequency for the translation eigenmode in x-direction.

Table 4.28: Frequencies and acceleration, T-design main model

	Modifications	**Mass** [kg]		**Frequency** [Hz]	**Acceleration, a** [m/s^2]		
		Total	m_e	x-dir	x-dir	$\Delta a / a_{0.040}$	$\Delta a / a_{main}$
1	**Base**[8]	698 123	29 088	0.791	0.154	285 %	0 %
2	t_{shear} = 180 mm	710 461	29 603	0.826	0.145	261 %	-6 %
3	k_{rot} = 20 000 kNm/rad	698 123	29 088	0.844	0.143	258 %	-7 %
4	ρ doubled top two floors	836 018	42 793	0.641	0.135	241 %	-11 %
5	30 % live load added as mass	1 019 412	42 475	0.639	0.137	238 %	-12 %
6	Cross section 210×675	759 889	31 662	0.942	0.117	193 %	-24 %
7	Cross section 280×900	846 360	35 265	1.088	0.090	125 %	-42 %
8	BC: k_{rot} = 10 000 kNm/rad	698 123	29 088	0.768	0.159	297 %	3 %
9	BC: pinned	698 123	29 088	0.741	0.165	313 %	7 %

Deflection

The deflections have been checked for the modifications with the lowest accelerations and are listed in Table 4.29. The deviation from the requirement of 48 mm for a 24 m high building is also included.

Table 4.29: Deflection, T-design main model

Modification	**Deflection** [mm]			
	U1	$\Delta U1 / max$	U3	$\Delta U3 / max$
Base	93.2	95.7 %	67.5	40.7 %
ρ doubled top two floors	92.9	93.5 %	69.1	44.0 %
Cross section 210×675	60.4	25.8 %	45.7	-4.8 %
Cross section 280×900	41.9	-12.7 %	32.0	-33.3 %

Fire design

The fire design loads are listed in Table 4.30. The worst effected columns are presented, and the utilisation of their cross sections are listed in Table 4.31. For the T-design models, the most vulnerable columns are the outer corner columns and the columns between the flange and the web, illustrated in Figure 4.11a. The corner columns have an initial cross section of 140 mm × 450 mm and are reduces by fire load on two sides. The

columns between flange and web have an initial cross section of 280 mm × 450 mm and are reduced by fire load on all four sides. Figure 4.11b illustrates the axis system used for fire design.

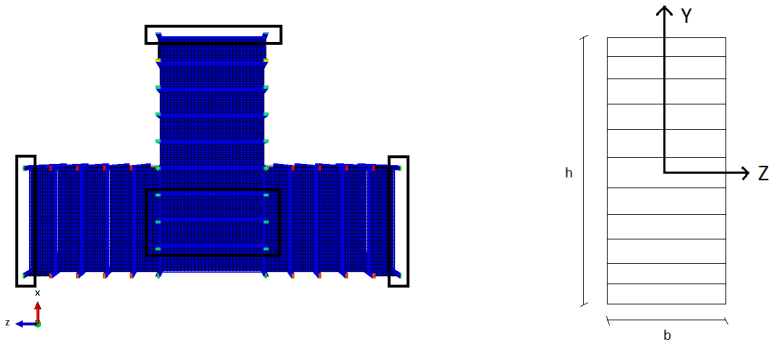

(a) The most vulnerable columns to fire load for the T-design models. Seen from below.

(b) Axis system of the cross section

Figure 4.11: Column grouping and axis system

Table 4.30: Fire design loads, T-design main model, *Base*

Column **eff. cross section** [mm×mm]		M_z [kNm]	M_y [kNm]	V_z [kN]	V_y [kN]	N [kN]	P [kN]
In between flange and web, 140×310	x-dir	42.1	14.5	58.0	18.8	231.0	405.0
	z-dir	32.3	14.8	47.1	15.5	0.0	600.0
Corner column, 70×380	x-dir	21.1	8.1	75.0	9.2	0.0	744.0
	z-dir	17.2	4.1	43.6	8.0	107.4	466.8

Table 4.31: Utilisation of cross section, T-design main model, *Base*

	In between flange and web		Outer corner	
	x-dir	**z-dir**	**x-dir**	**z-dir**
Shear				
C.7a	24 %	20 %	19 %	17 %
C.7b	74 %	60 %	157 %	91 %
Bending and tension				
C.9a	121 %	133 %	101 %	77 %
C.9b	125 %	133 %	89 %	75 %
Bending, comp. and buckling				
C.11a	138 %	158 %	743 %	462 %
C.11b	117 %	122 %	191 %	120 %
Lateral torsional instability				
C.14	123 %	139 %	684 %	437 %

4.2.2 Adding slabs, n8-long-web

Acceleration

The accelerations, mass and frequency for the different modifications of model n8-long-web, Figure 4.12, are presented in Table 4.32. The results from the main model are presented for comparison.

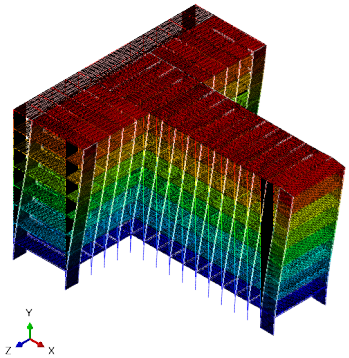

Figure 4.12: The first mode shape for the n8-long-web model

Table 4.32: Frequencies and accelerations, n8-long-web, see figure 4.12

	Modification	**Mass** [kg]		**Frequency** [Hz]	**Acceleration,** $\boldsymbol{a}$ [m/s^2]		
		Total	m_e	x-dir	x-dir	$\Delta a/_{0.040}$	$\Delta a/_{a_{base}}$
	Main	698 123	29 088	0.791	0.154	285 %	26 %
1	**Base**	914 687	38 112	0.669	0.122	206 %	0 %
2	ρ doubled top two floors	1 096 127	60 792	0.541	0.099	147 %	-19 %
3	Cross section 280×900	1 109 735	46 239	0.940	0.070	74 %	-43 %
4	Combination 2 + 3	1 291 175	68 919	0.773	0.059	48 %	-52 %

Deflection

The deflections for *Combination 2 + 3* (from Table 4.32) are listed in Table 4.33, alongside the deviation from the requirement of 48 mm. The results from the main model are also presented for comparison.

Table 4.33: Deflections, n8-long-web model

Modification	**Deflection** [mm]			
	U1	$^{\Delta U1}/_{max}$	U3	$^{\Delta U3}/_{max}$
Main model	93.2	96 %	67.5	41 %
Base	98.9	106 %	110.5	130 %
Combination 2 + 3	42.7	-11 %	52.6	10 %

Fire design

The fire design loads for *Combination 2 + 3* (from Table 4.32) are listed in Table 4.34. Only the most vulnerable columns are checked and the utilisation of the cross sections are listed in Table 4.35.

Table 4.34: Fire design load, n8-long-web, *Combination 2 + 3*

Column **eff. cross section** [mm×mm]		M_z [kNm]	M_y [kNm]	V_z [kN]	V_y [kN]	N [kN]	P [kN]
In between flange and web, 420×760	x-dir	114.0	67.8	33.2	21.6	45.7	471.6
	z-dir	134.4	41.8	28.7	24.4	0.0	648.0
Corner column, 210×830	x-dir	57.4	13.9	30.0	10.5	0.0	630.0
	z-dir	70.8	9.0	25.5	12.4	61.8	444.0

Table 4.35: Utilisation of cross section, n8-long-web, *Combination 2 + 3*

	In between flange and web		Outer corner	
	x-dir	**z-dir**	**x-dir**	**z-dir**
Shear				
C.7a	4 %	4 %	3 %	4 %
C.7b	6 %	5 %	10 %	7 %
Bending and tension				
C.9a	21 %	21 %	11 %	12 %
C.9b	21 %	22 %	12 %	13 %
Bending, comp. and buckling				
C.11a	20 %	19 %	26 %	20 %
C.11b	20 %	21 %	24 %	20 %

4.2.3 Adding shaft, n8-shaft

Acceleration

By adding a shaft to the T-design, the model becomes unsymmetrical about both axis. The eigenmodes of the model are therefore not pure translation. To calculate accelerations for the models with a shaft, the mode closest to translation in the x-direction is used. The mass activated is 64 % of the total mass, with 401 out of 623 tons. These numbers are extracted from *Abaqus*, and do not fluctuate much for the other modifications of the shafted models. Figure 4.13 shows the torsion modes for the basic model.

(a) Model n8-shaft (b) Model n8-shaft-shear

Figure 4.13: Torsional modes used as translation modes

The frequency, mass and acceleration for the modifications are presented in Table 4.36. The results from the main model are presented for comparison.

Table 4.36: Frequencies and accelerations, shear models, n8-shaft and n8-shaft-shear

	Modification	**Mass** [kg]		**Frequency** [Hz]	**Acceleration, a** [m/s^2]		
		Total	m_e	x-dir	x-dir	$\Delta a / a_{0.040}$	$\Delta a / a_{base}$
	Main model	698 123	29 088	0.791	0.154	285 %	85 %
1	**Base**	703 988	29 333	1.338	0.088	108 %	0 %
2	ρ doubled top two floors	836 439	45 889	1.098	0.068	71 %	-18 %
3	30 % live load added as mass	1 012 597	42 192	1.092	0.075	86 %	-11 %
4	Cross section 210×675	770 630	32 110	1.528	0.066	64 %	-21 %
5	Cross section 280×900	863 928	35 997	1.672	0.053	32 %	-37 %
6	Extra shear wall, Figure 4.13b	706 044	29 419	1.366	0.081	103 %	-3 %
7	Combination 2 + 4	903 081	48 666	1.269	0.055	36 %	-35 %
8	Combination 2 + 5	996 379	52 553	1.405	0.045	12 %	-46 %
9	Combination 2 + 4 + 6	905 137	48 752	1.299	0.053	32 %	-36 %
10	Combination 2 + 5 + 6	998 435	52 639	1.440	0.044	9 %	-48 %

Deflection

The deflections for *Combination 2 + 4* (from Table 4.36) for the n8-shaft model are listed in Table 4.37, alongside with the deviation from the requirement of 48 mm.

Table 4.37: Deflections, n8-shaft

Modification	**Deflection** [mm]			
	U1	$^{\Delta U1}/_{max}$	U3	$^{\Delta U3}/_{max}$
Main	93.2	96 %	67.5	41 %
Base	50.8	6 %	22.1	-54 %
Combination 2 + 4	35.1	-27 %	16.5	-66 %

Fire design

The fire design loads for *Combination 2 + 4* (from Table 4.36) for the model with shaft are listed in Table 4.38. Only the most vulnerable columns are listed. The utilisation of the capacity is shown in Table 4.39.

Table 4.38: Fire deign load, T-design, with shaft

Column **eff. cross section** [mm×mm]		M_z [kNm]	M_y [kNm]	V_z [kN]	V_y [kN]	N [kN]	P [kN]
In between flange and web, 280×535	x-dir	52.2	31.0	54.2	20.6	129.6	644.4
	z-dir	32.7	14.8	23.1	36.4	0.0	471.0
Corner column, 140×605	x-dir	27.0	7.4	31.7	8.2	0.0	441.0
	z-dir	17.0	3.6	19.1	6.6	0.0	298.8

Table 4.39: Utilisation of cross section, T-design, with shaft

	In between flange and web		Outer corner	
	x-dir	**z-dir**	**x-dir**	**z-dir**
Shear				
C.7a	8 %	14 %	5 %	4 %
C.7b	20 %	9 %	21 %	13 %
Bending and tension				
C.9a	40 %	25 %	17 %	9 %
C.9b	39 %	25 %	17 %	9 %
Bending, comp. and buckling				
C.11a	37 %	23 %	50 %	32 %
C.11b	36 %	23 %	35 %	22 %

4.2.4 Six storey models, n6

Acceleration

The mass, frequency and acceleration for models of six storeys are presented in Table 4.40.

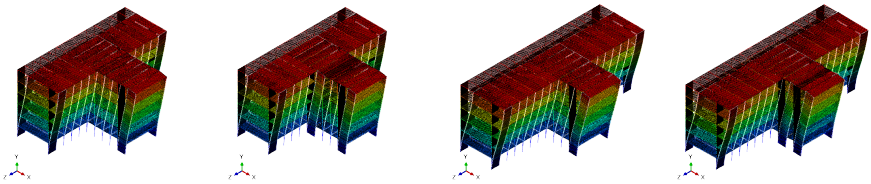

(a) Base model, n6 (b) n6-shear (c) n6-wide (d) n6-wide-shear

Figure 4.14: The first mode shapes for the six storey T-models

Table 4.40: Frequencies and accelerations, six storeys

	Modification	**Mass** [kg]		**Frequency** [Hz]	**Acceleration, *a*** [m/s^2]		
		Total	m_e	x-dir	x-dir	$\Delta a / a_{0.040}$	$\Delta a / a_{base}$
	Main model	698 123	29 088	0.791	0.154	285 %	33 %
1	**Base**, Figure 4.14a	523 593	29 088	1.123	0.116	189 %	0 %
2	ρ doubled top two floors	661 487	52 071	0.878	0.088	119 %	-24 %
3	30 % live load added as mass	764 559	42 475	0.906	0.103	157 %	-11 %
4	Cross section 210×625	569 917	31 662	1.376	0.085	111 %	-27 %
5	Cross section 280×900	634 770	35 265	1.629	0.063	56 %	-46 %
6	**Extra shear wall**, Figure 4.14b	526 677	29 260	1.469	0.083	106 %	-29 %
7	Combination 2 + 4	707 811	54 646	1.084	0.066	65 %	-43 %
8	Combination 2 + 5	772 664	58 247	1.297	0.050	26 %	-57 %
9	Combination 2 + 4 + 6	710 895	51 282	1.458	0.039	-2 %	-66 %
10	**n6-wide**, Figure 4.14c	604 804	33 600	1.139	0.103	157 %	-11 %
11	**n6-wide-shear**, Figure 4.14d	607 889	33 772	1.355	0.084	109 %	-28 %

Deflection

The deflections for *Combination 2 + 4 + 6* (from Table 4.40) are listed in Table 4.41, alongside with the deviation from the requirement, which is 36 mm for a 18 m high building. The results from the main model are also presented for comparison, here with the requirement of 48 mm.

Table 4.41: Deflections, six storey model

Modification	**Deflection** [mm]			
	U1	$^{\Delta U1}/_{max}$	U3	$^{\Delta U3}/_{max}$
Main	93.2	96 %	67.5	41 %
Base	38.7	8 %	29.1	-19 %
Combination 2 + 4 + 6	13.8	-62 %	15.7	-56 %

Fire design

The fire design loads for *Combination 2 + 4 + 6* (from Table 4.40) of the six storey model are listed in Table 4.42. Only the most vulnerable columns are checked. The utilisation of the capacity is shown in Table 4.43.

Table 4.42: The design load for fire design: T-design, six storeys

Column **eff. cross section** [mm×mm]		M_z [kNm]	M_y [kNm]	V_z [kN]	V_y [kN]	N [kN]	P [kN]
In between flange and web, 280×535	x-dir	33.9	21.5	28.7	13.6	0.0	489.6
	z-dir	33.9	16.2	22.2	12.6	0.0	390.0
Corner column, 140×605	x-dir	15.4	5.3	22.6	7.0	0.0	291.4
	z-dir	17.8	3.9	18.0	6.3	0.0	258.0

Table 4.43: Utilisation of cross section, T-design, six storeys

	In between flange and web		Outer corner	
	x-dir	**z-dir**	**x-dir**	**z-dir**
Shear				
C.7a	5 %	5 %	5 %	4 %
C.7b	11 %	8 %	15 %	12 %
Bending and tension				
C.9a	29 %	23 %	11 %	10 %
C.9b	28 %	24 %	11 %	10 %
Bending, comp. and buckling				
C.11a	26 %	22 %	33 %	29 %
C.11b	25 %	21 %	23 %	21 %

Chapter 5

Summary of Results and Discussion

This chapter includes a short summary of the results followed by discussion of the findings and a section on sources of error.

5.1 Summary of results

The results from the main model of each design show that the acceleration is far from the ISO-requirement of 0.04 m/s^2. The RCR base model has an acceleration of 0.080 m/s^2 in the x-direction and 0.134 m/s^2 in the z-direction (Table 4.1). The T-design base model has an acceleration of 0.154 m/s^2 (Table 4.28). For the same models, neither the deflection nor fire requirements are met. The deflection requirement is 48 mm for the 24 m building. For the RCR base model the deflection is no problem in the direction of the frames, but 61 mm in the shear wall direction (Table 4.2). For the T-design base model the deflection is 93.2 mm in x-direction and 67.5 mm in the z-direction (4.29). With the cross section dimensions of the base models, the capacity under fire load is exceeded (Table 4.4 and 4.31), and the cross sections need to be increased to meet the requirement.

Based on the results from the main models, the focus is to decrease the acceleration. The acceleration requirement is believed to be the most difficult to reach. This assumption is supported by experience from other projects on tall timber buildings [3] [40]. After achieving a lower value for the acceleration, the deflection and fire design are

checked with the same modification of parameters, and proven for most of the models to be satisfactory.

The results show that increasing the cross sections of the columns will have a large impact on the acceleration (Table 4.1 and 4.28). A large effect is also seen from adding shear walls, shafts and extra mass. Some modifications where only checked for the main models, e.g. the increase of rotational stiffness, change of boundary conditions, and changing the thickness of the shear walls. All parameters will be discussed to a greater or lesser extent in the following section.

5.2 Discussion

5.2.1 Parametric study

Cross section of columns

By increasing the height and width of the cross sections of the columns with a factor of n, the second moment of inertia, I, will increase by a factor of n^4. This can be seen from equation $I = \frac{b \cdot h^3}{12}$, for a rectangular cross section with sides h and b. By comparing the columns with cantilevers from the beam formulas, with stiffness $k = \frac{8EI}{L^4}$, it is clear that an increase in I will result in a larger stiffness contribution from the columns. The beam formula is shown in Figure 5.1. This can be seen in the eigenfrequencies and consequently the accelerations for all models in Chapter 4. E.g. for the RCR main model, where doubling the dimensions of the cross section leads to a decrease in accelerations of 41 % in the x-direction and 46 % in the z-direction (Table 4.1). Other welcomed effects of the increase of cross section are the reduced deflections in the top floor and higher capacity during fire.

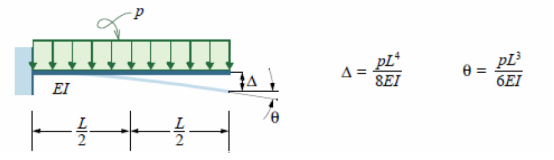

Figure 5.1: Formulas for a cantilever beam [2]

Mass

When the mass increases and the stiffness is kept unchanged, the eigenfrequency decreases. A lower eigenfrequency has a negative effect on the acceleration, while the in-

crease of mass has a positive effect. The contribution from increased mass has a greater impact on the acceleration than the decrease of frequency. The decrease of acceleration can be explained by Newtons second law; $F = m \cdot a$, where F is force, m is mass and a is acceleration. Newtons second law can be rewritten to $a = F/m$, where it becomes obvious that increasing mass decreases the acceleration, since the force at an arbitrary point is constant.

The results from Chapter 4 show that the relative decrease in acceleration is approximately the same if the density of the top two floors are doubled, as the effect of adding 30% of the live load as extra mass in the modal analysis. For the T-design main model, the acceleration decreased by 11 % when the density of the top two floors are doubled, and 12 % for including 30 % of the live load as extra mass (Table 4.28). The increase of total mass from these modifications are 138 and 321 tons, respectively. Even though the effect is more or less the same, it is advisable to add mass to the top of the building rather than a evenly distributed mass over the whole building. A low total mass means lower reaction forces, hence have a positive impact on the fire design as well as the amount of needed foundation.

The advantage of adding mass at the top of the building can be explained by the formula used to calculate the equivalent mass, m_e (Equation (2.7)). m_e is a function of the product of the mode shape and the distributed mass over the height of the building. The highest value of the mode shape is at the top of the building (Figure 5.2a), while the mass can be represented as evenly lumped mass to the floors, as illustrated in Figure 5.2b. Hence the mass added on the top of the building has a greater influence on the acceleration.

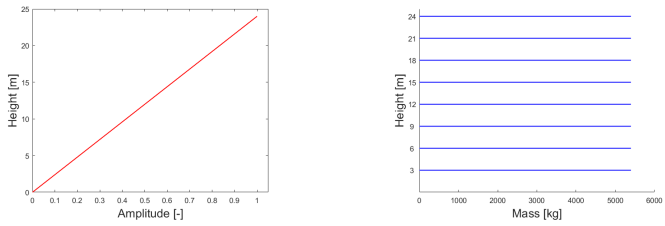

(a) Distributed mass (b) Fundamental mode shape

Figure 5.2: Illustration of distributed mass and mode shape

Shear walls and shaft

The adding of shear walls will greatly affect the stiffness in the plane direction of the wall. For the RCR main model it is shown that the acceleration in the x-direction decreases by 23 % when two shear walls are added (Table 4.1). The decrease is in the same

range for the T-design main model (Table 4.40). The effect can also be seen for the RCR model with shaft and shear walls, compared to the same model with only shaft. These results show that by removing the four shear walls, the acceleration increases by 40 % (Table 4.17). For the T-design model with added shaft, the adding of a shear wall have a modest influence of 2.6 % (Table 4.36). This is because the shaft is modelled with a 5 ply CLT, which takes up a large part of the forces due to its large capacity, thus dominating the stability contribution. Adding a shaft and connecting it to the support system will have a positive influence on the acceleration for all models, but there are some drawbacks connected to it. By adding a shaft to the model, some of the robustness is lost, as the results are dependent on the exact size and location of the shaft.

Doubling the thickness of the shear walls has a positive effect on the acceleration. 9 % for the RCR main model and 6.2 % for the T main model (Table 4.1 and 4.28). This contribution is not considered big enough compared to the alteration, and not investigated further. The shear walls have been placed in the corners of the buildings. This is not favourable as these areas can be used to let sunlight into the building, and thus should not be closed off by shear walls. The effect of placement of the shear walls has not been investigated in this thesis.

Rotational stiffness

To study the effect of the rotational stiffness in the connections between beams and columns, the RCR design is used. This model has columns all oriented the same way, making the discussion on the effect easier, while the T-design models have columns oriented orthogonal with respect to each other in the flange and the web part. Based on this, the results from Table 4.1 are used.

With a doubling of rotational stiffness, the acceleration decreases in the frame direction by 13 % and 1 % in the z-direction. This makes sense, given that the connections have rotational stiffness about the z-axis, and all other rotational degrees of freedom are released. The frequency rises with increased stiffness and makes the acceleration, as well as the deflection, decrease. This effect is welcomed, but as already stated, not taken into further investigation on the customised models. This decision is based on available knowledge on the matter, stating the possibility to achieve a rotational stiffness of about 10 000 kNm/rad [13] [20]. This is a topic under investigation, and if further research makes it possible to achieve higher rotational stiffness. This will have a positive effect on the acceleration and displacement in the frame direction of the building concept considered in this thesis. However, the connection can not be stiffer than a rigid connection, and a further increase of the rotational stiffness is assumed to stagnate when closing in on a rigid behaviour.

For the T-design main model, the decrease in acceleration for doubling k_{rot} is 6.9 % in the x-direction (Table 4.28). The deviation from RCR can be explained by number of effective moment resisting connections in the x-direction for the two models. The main model of RCR design has a total of 576 single connections to slabs in x-direction, while the main model of the T-design has 320. Hence the RCR design has 1.8 times more connections than the T-design. By multiplying the decrease in the T model by 1.8, the result is 12.4 %, which is about the same as the 13 % from the RCR design.

Number of storeys

The effective mass, m_e, (from Equation (2.8)) remains unchanged by adding or removing storeys of the building, given that all other parameters stays unaltered and that the simplified calculation m_e is used. From the beam formulas in Figure 5.1, it is clear that the stiffness will be influenced by the height, L, loosing stiffness for increasing height. This can be seen when comparing the building to a cantilever with stiffness $k = \frac{8EI}{L^4}$ for a uniform line load. This tendency is clear in the graph from Figure 5.3.

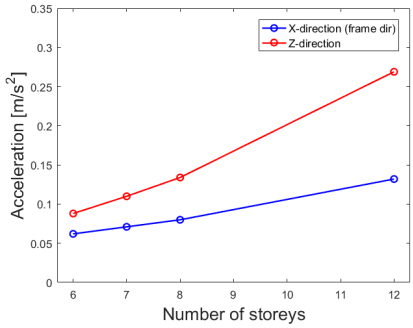

Figure 5.3: Graph of acceleration for the varying number of storeys

Variation of slabs

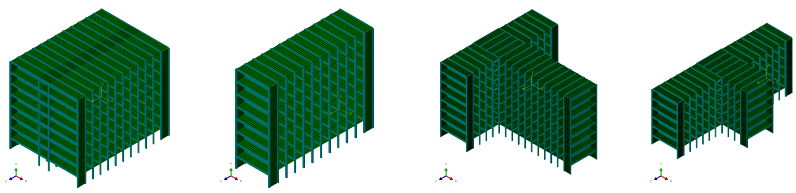

(a) RCR 12 slabs (b) Room 12 slabs (c) T long web (d) T long flange

Figure 5.4: Models with added slabs

The models in Figure 5.4 have in common that the footprints have been changed from the main model of their design type. This has been done by adding or removing frames and slabs. It is difficult to draw a conclusion of the effect of adding or removing slabs and frames alone. These changes affect a lot of parameters, like mass, stiffness, footprint and building slenderness, which again influence variables used in the formula for calculating the acceleration (Equation (B.1)).

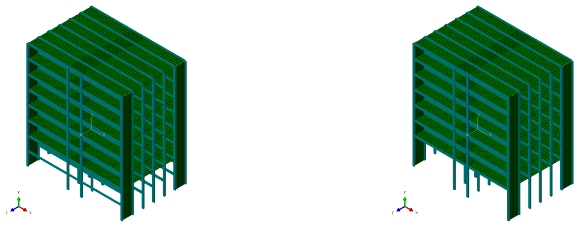

(a) n7-open1 (b) n7-open2

Figure 5.5: Models with open first floor

Figure 5.5 shows the RCR models with an open first floor, with results presented in Section 4.1.6. These models give a better view on the contributions from slabs. The results show that the acceleration is unaltered in the x-direction by removing only the slabs from the first floor (Table 4.25). To discuss the effect the removal of slabs have on the building, it is necessary to compare the global stiffness of the modified model with the main model. The global stiffness can be found by rearranging the basic formula for frequency to $K = \omega^2 \times M$. As mentioned, the acceleration is unaltered between the two models, but both the mass and the frequency have decreased by removing the slabs. As a consequence, K from the formula must have decreased as well, resulting in a lower global stiffness for the modified model. The reduced stiffness is caused by removing slabs, making utilisation of the slab stiffness impossible.

The acceleration increases with 8 % when both slab and beams are removed. The cause for the increased acceleration is the removal of connections with rotational stiffness, as discussed in the section for rotational stiffness. The effect of removing slabs and beams can be neglected in the z-direction, because the horizontal stability provided from the frames mainly affects the x-direction. This is supported by the findings summarised in Table 4.25, as the changes are in the magnitude of 1-2 %.

Boundary conditions

All base models are modelled with encastred boundary conditions for the columns. This is the stiffest connection type, and a change of the restrain have a negative ef-

fect on acceleration and deflection results. For the RCR main model, the acceleration is increased in the x-direction by 8 % for a semi-rigid condition with a rotational stiffness of 10 000 kNm/rad, and 21 % for the pinned connection (Table 4.1). In the z-direction, the effect is negligible. This is expected as the shear walls will distribute the forces into pressure and tension when the pinned connection prevents moment forces, and the stiffness in this direction is in a large extent due to the shear walls. In the x-direction however, the stiffness is only provided by the moment resisting frames, hence more influenced by the change of boundary condition. When the boundary condition is pinned, only the stiffness contribution from the frames are included. For the T-design main model, the increase in acceleration is 3.2 % for semi-rigid and 7.2 % for pinned (Table 4.28). The difference in impact for the T-design model can be explained by the shear walls spanning in both directions, giving a contribution to the stiffness and makes the boundary conditions less critical.

Fire design and deflection requirement

The calculation of capacity under fire is done, assuming no extra measures to gain fire protection of the columns. This is a conservative assumption as measures like fire paint or gypsum plates can be used to increase fire resistance. The fire capacity does not change drastically for some of the parametric changes, as e.g. increasing rotational stiffness or shear wall thickness. These changes will alter the force distribution, but not enough to make the big differences. However, by adding mass or increasing number of storeys, the forces will increase, and the fire requirements will be harder to reach. The change of most influence is the increase the columns cross sections. This will lead to a larger effective cross section after 90 minutes of fire, having a great impact on the second moment of inertia. The fire requirements are easily met by increasing the cross section. As seen in the fire capacity tables throughout Chapter 4 the increase of cross section is essential.

Increasing the cross section also has positive effect on deflections. By doubling the cross section dimensions, the deflection in the x-direction is reduced by 41 % for the RCR main model, and 42 % for the T-deign (Table 4.2 and 4.29). The same is seen for the z-direction. For other parameters, a decrease of stiffness in the structure will increase the deflections, while an increase of stiffness will have the opposite effect. Changing the boundary conditions from encastred to pinned, increased the deflection from 38.8 to 51.1 mm in the x-direction (Table 4.2). For simplicity, this effect can also be explained with the beam formula for a cantilever beam with uniform line load from Figure 5.1, where it becomes clear that an increase in stiffness will decrease the deflection.

5.2.2 Other interesting variables

The damping of the models, ξ, is set to 1.5% in the acceleration calculations, giving a structural damping $\delta_a = 0.0943$. This value is chosen based on results from comparable timber buildings like *Moholt 50|50* in Trondheim and *Treet* in Bergen [31]. If the actual damping is different from 1.5 %, the acceleration is affected. E.g. with a damping of 2.0 %, the acceleration for the RCR main model drops from 0.080 to 0.069 m/s^2 in the frame direction, a decrease of 12.7 %. In the z-direction, the acceleration drops from 0.134 to 0.117 m/s^2, a decrease of 12.6 %.

The reference wind speed has a large effect on the acceleration calculated. The reference wind speed from Trondheim is 26 m/s. If the building was set to Oslo, where the reference wind speed is 22 m/s (see Appendix A.4), the acceleration for the main model of the T-design would drop from 0.154 to 0.091 m/s^2, a decrease of 40.9 %, making this a very important parameter.

A few geometrical parameters have not been investigated. These include storey height, slab length and slab orientation. The storey height used in the analysis of 3 m can be too low, given that the slab thickness is yet to be decided and the lowest net height in a residential building is 2.4 m [42]. If the height increases, the stiffness will decrease, resulting in a higher acceleration. Increasing the storey height will also increase the buckling lengths of the columns, influencing the columns capacity.

Using shorter slabs will enable lower thickness, and ease satisfaction of serviceability requirements. The storey height is also less critical the thinner the slabs. If the slabs are oriented orthogonal with respect to the frames to get larger open column-free areas, they will not contribute to the horizontal bracing of the building. Another consequence is that there will be fewer columns per metre and fewer connections, making the structure less stiff in the frame direction. The accelerations and deflections will increase and the columns will have to take more forces, probably leading to the necessity of other measures to get the results within the requirements.

5.2.3 Adding storeys on existing building

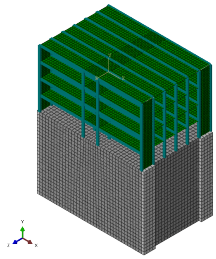

Figure 5.6: Four storeys on top of a virtual building

Adding storeys on an existing building is an interesting application due to the low density of wood. Figure 5.6 shows the model analysed. A four storey building was added on top of a building modelled to have a higher natural frequency. By increasing the cross section height of the column to 585 mm, and by using 30 % of the live load in the modal analysis, are sufficient to meet the acceleration criteria on 0.04 m/s^2 (Table 4.26). The base model with extra mass, with the original cross section of 140 × 450 mm, gives an acceleration of 0.045 m/s^2, which can be argued to be acceptable.

As mentioned in Section 4.1.6, three different cases where investigated. The natural frequency of the extended building is determined by the part with the lowest frequency. The most beneficial situation is when the added part has the lowest frequency. This case can be simplified to a situation where the added part behaves like the existing building is the ground foundation, due to the pinned connection between the two buildings. In other words, the added part behaves more or less independent from the existing one. When the frequency of the existing part is either lower or in resonance with the added part, the interacted frequency drops and thus makes it more difficult to meet the acceleration criteria. However, it has to be emphasised that this is a preliminary study, and a more detailed consideration is needed to find the exact interaction effect.

5.2.4 Acceleration requirement

As mentioned in Section 2.5.1, the acceleration requirement is not actually a *requirement*, but used as a guideline. It can be argued for designing buildings with an acceleration higher than the limits in the ISO-curve (see Figure 5.7). From Table 2.4, a new limit of 0.05 m/s^2 can be adopted. As the perception level limits work as a guideline, the construction client stands free to decide the requirement for each project. This means that for example the T-design model with shaft and modification 7 or 8 from Table 4.36

can be considered, giving a simulated acceleration of 0.055 m/s^2 and 0.045 m/s^2, respectively.

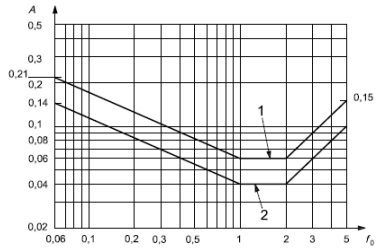

Figure 5.7: Evaluation curves for wind-induced vibrations [9]

5.2.5 Simplifications and sources of error

Slabs

The simplification of the slabs includes two steps, both bringing potential errors to the results of the calculations. First modelling the slab based on another model with possible errors of its own as explained in Section 3.3.5, and then the combining of several slabs with a weak partition in between slabs as one part in *Abaqus*.

The simplification of the slab is done for a single slab, this means that the frequencies and deflections that corresponded between the models might be altered when several slabs are put together as one part. However, the partition is so weak, that it is believed that the slabs are close to working independently. This is confirmed by checking the moment distribution for the RCR main model with wind in x-direction, where every column has the same moment about the z-axis. The connection between slabs will probably be made by screws in a constructed building, giving some stiffness between neighbouring slabs. This issue may cause a deviation between reality and simulation.

Shear walls and shaft

The shear walls are modelled in *Abaqus* by merging shear wall parts with full length columns. This results in a shear wall spanning over the entire height of the model. In reality the shear wall will probably consist of storey high parts, connected to each other and the rest of the structural system. This solution is better for the acoustic properties by reducing the flanking transmission. Storey high shear walls will cause a different force distribution and give a different stiffness which can impose errors in the acceleration and deflection simulations. Another limitation to the model is that only shear and

bending modes of the shear walls are simulated, not the anchorage slip, which is often governing [41]. The same limitations applies to the modelling of shafts. In addition, there has not been looked into openings in the shear walls or shafts for e.g. doors and windows, which will affect the stiffness contribution.

Wind modelling

The wind distribution used is in this work is a simplification of the distribution from NS-EN 1991-1-4. The simplification in the wind modelling gives a uniform wind field on each side of the building, with no variation over the height and no wind forces on the roof. A brief test was done including forces on the roof (see Appendix A.4.4). The results had little influence on the acceleration and deflection, thus making the wind forces on the roof negligible in this thesis. The other simplifications of distribution are considered conservative.

The details of the distribution are found in Section 2.4.4. It is also important to note that the method in the Eurocode is a simplification. Both with respect to simplification of the geometry for the building and the calculation of wind forces; assuming the wind to be a static load, only blowing orthogonal on one side of the building. Wind is a dynamic action, and the structural factor $c_s c_d$ is used to simplify the wind to be a static force.

The T-shape

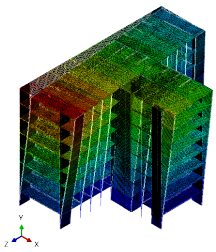

Figure 5.8: First mode of T-design n8-shaft

The T-design models that are symmetric about the x-axis, have an eigenmode dominated by translation and can be used in acceleration calculations. For the models with a shaft added, the eigenmode used in the acceleration calculations is less dominated by translation, hence the results from calculations can include errors. The eigenmode for one shaft model is shown in Figure 5.8 and has an activated mass of 64 % in the x-direction. This is not ideal, and wind tunnel testing is recommended.

The T-design has a too complicated geometry for the simplified method in NS-EN 1991-1-4. To calculate wind loads for these models, a fictive rectangular shape encapsulating the building has been used. The actual wind distribution for the building will be different from the one used and this can cause deviations between the simulations and the reality.

Abaqus mesh

The investigation on the effect of different mesh sizes in the finite element analyses has been brief. There has been run a few simple models with finer mesh to learn how the results was influenced. The frequencies did not change with more than a few percent for a finer mesh. For the amount of simulations done during this thesis, it was of great importance that the computational time was low. This was done by keeping the mesh size relatively coarse, with a possible consequence of reduction in exactness of the solutions.

Chapter 6

Conclusions and Further Work

Based on the results from Chapter 4 and the discussion from Chapter 5, some conclusive remarks on the work are made, followed by some recommendations for further work.

6.1 Conclusion

As expected, the main obstacle to overcome working with these timber buildings was the acceleration requirements. For the main model of each design, the best result was 0.08 m/s^2 for the RCR design, being the exact double of the requirement from the ISO curve, of 0.04 m/s^2.

The parametric study showed that a lot can be done to decrease the accelerations to better levels. The response of a building is dependent on the typology, as well as design solutions like connections and boundary conditions. It has been shown that the most effective change is to increase the size of the column sections, represented by the results for the T-design main model, which had its acceleration drop by 41.5 % by doubling the dimension of both sides of the columns. By adding shear walls to a design, an effective improvement of the results has been seen. This is represented by the main model of the RCR design, where the acceleration decreased by 23 % after adding a shear wall pair. Shafts also have an important contribution, as they work similarly to shear walls if connected to the support system. The RCR main model has 31 % higher acceleration in the x-direction compared to the same model with a connected shaft. In the z-direction, the acceleration is 67 % higher.

For deflections, the results of this thesis show that the requirements are met as long

as the acceleration requirements are. Besides lowering the number of storeys, the increasing of the column sections is the most important factor to decrease the deflection. These parameters are also the most important regarding the fire capacity, which is satisfactory for the models and modifications where the acceleration and deflections are within their requirements.

An important remark is that the acceleration requirements are considered a guideline, and the construction client has to set the limits for the individual project. Also, the effect of the reference wind speed and the damping ratio has a great impact on accelerations, and should be considered for the individual project.

Based on the results from this thesis, it can be concluded that it will be possible to build high-rise timber buildings using the structural system with moment resisting frames bracing the building in one direction. With the requirements for acceleration, deflection and fire capacity met. By combining different modifications, like increasing column cross sections, including a shaft as a part of the support system or adding mass to the higher floors, the system can be used to build eight storeys high buildings, and probably higher.

6.2 Recommendations for further work

The structural system based on moment resisting frames for timber buildings has not been investigated to a great extent in the past, hence there are a lot of parameters which influence can be mapped. During the work of this thesis, some parameters have been investigated more than others. To improve the exactness of the results, and to get a better understanding on the issues investigated in this thesis, recommendations on topics to look further into are presented here.

Geometrical changes

The storey height of the models investigated are all 3 m high. Changing the height of the columns will influence both capacity and results on acceleration and deflection. The impact of this parameter should be studied in greater detail as it is believed that this is a parameter that might be changed, as discussed in Section 5.2.2.

The span length and span orientation of the slabs will influence the dynamic properties of the models. The effect of using shorter or longer slabs have not been considered in this thesis, but is not believed to be negligible. Investigating the effect from using shorter slabs might not be that interesting, given the goal of large open spaces for the WoodSol project. Orienting the slabs so that the span direction is orthogonal to the frame span is more interesting, as this will rise the possibility for larger open areas. The negative effects discussed previously of this change are important to map.

Shear walls and bracing

The effect of the placement of shear walls have not been investigated. The problems on loss of daylight in valuable areas for apartments makes this a topic worth looking into. In addition to the placement of the walls, it should be investigated other ways of bracing. Glass plates used to stiffen a building is a possibility, or multi-storey spanning timber trusses.

It is recommended to look further into the modelling of the connection between shear walls and columns. This should be done to investigate the influence of the anchorage slip mode, and maybe get more accurate results on shear wall contribution.

Seismic performance

The seismic actions have not been given any consideration in this thesis due to the assumption that the governing horizontal load action arises from the wind. The seismic

performance will be of greater importance for low-rise buildings due to higher natural frequency and thus lower natural period, which is more likely to coincide with the natural period of an earthquake. However, due to Eurocode regulations, new building projects must include seismic design considerations.

Assembly and model testing

Assembly on site is of great interest for realisation of this project. One of the goals stated for the WoodSol project is *rapid erection on site*.

In addition to rapid erection, the tolerance requirements for the assembly of frames and slabs should be emphasised. Some sort of temporary bracing may be needed to assure the required tolerance limit, even though the rotational stiffness of the boundary condition are approaching an clamped situation.

Model testing of a full scale model would be useful to ensure that the structural system behaves like it is modelled. This full scale model could for instance include two storeys and two slabs. In a potential model testing, one should emphasise the behaviour of the moment resisting frames, stabilisation effect from the slabs and contribution from the shear walls.

Bibliography

[1] Aarstad, J., Glasø, G., and Bunkholt, A. (2008). Massivtre. *Fokus på tre*, 20.

[2] Bell, K. (2010). *Matrisestatikk*. tapir akademisk forlag.

[3] Bjertnæs, M. A. and Malo, K. A. (2014). Wind-induced motion of treet - a 14 storey timber residential building in norway. *World Conference of Timber Engineering*.

[4] Bjørge, H. and Kristoffersen, T. (2017). Konseptstudie av trebaserte kompositttdekker med mulighet for innspenning til limtresøyler. Master's thesis, NTNU.

[5] Boggs, D. (1995). Acceleration indexes for human comfort in tall buildings - peak or rms. *CTBUH Monograph Chpt. 13: Motion Perception Tolerance and Mitigation 1997*.

[6] Dahl, K. B. (2009). *Mechanical properties of clear wood from Norway spruce*. PhD thesis, NTNU.

[7] David R. H. Jones, M. F. A. (2012). *Engineering Materials 2*. Elsevier Ltd.

[8] Garathun, M. G. (2017). I april starter byggingen av verdens høyeste trehus. *Teknisk Ukeblad, Avaliable from: https://www.tu.no/artikler/i-april-starter-byggingen-av-verdens-hoyeste-trehus-i-brumunddal/376266*.

[9] ISO-10137 (2007). *Bases for design of structures - Serviceability of buildings and walkways against vibrations*. International Standard.

[10] Kristjansdottir, T., Fjeldheim, H., Selvig, E., Risholt, B., Time, B., Georges, L., Dokka, T. H., Bourelle, J., Bohne, R., and Cervenka, Z. (2014). A norwegian zeb-definition embodied emission. *ZEB Project report 17*.

[11] Kuzman, M. K. and Sanberg, D. (2016). A new era for multi-storey timber buildings in europe. *Forest Products Society International Convention*.

[12] Labonnote, N. and Malo, K. A. (2010). Vibration properties of coss laminated timber floors.

[13] Malo, K. A. and Stamatopoulos, H. (2016). Connections with threaded rods in moment resisting frames. *World Conference on Timer Engineering*.

[14] Malo, K. A., Stamatopoulos, H., Nesheim, S., and Solem, B. (2017). Requirements, lay-out and design considerations of a building system. WP 2.

[15] Martinsons. Kl-trä: Prosjektera och bygg. *Avaliable from. http://www.martinsons.se/byggprodukter/kl-tra/projektera-och-bygg*. Sortiment, , Avaliable from: http://www.martinsons.se/byggprodukter/kl-tra/projektera-och-bygg.

[16] Mendis, P., Ngo, T., Haritos, N., Hira, A., Samali, B., and Cheung, J. (2007). Wind loading in tall buildings.

[17] Merakerås, G. K. (2016). Hel ved på moholt 50|50, massivtreprosjekt. *Veidekke, Avaliable from: http://veidekke.no/om-oss/nyheter-og-media/temasaker/article21354.ece*.

[18] Moelven (2011). Teknisk godkjenning, fasthetsverdier kerto. *Avaliable from: http://www.moelven.com/no/Produkter-og-tjenester/Limtre-og-Kerto/Kerto/*.

[19] Moelven (2015). Teknisk godkjenning,. fasthetsverdier limtre og smalt limtre. *Avaliable from: http://www.moelven.com/no/Produkter-og-tjenester/Limtre-og-Kerto/Standard-Limtre/*.

[20] Nordal, K. I. and Lied, K. S. (2016). A conseptual study of gluam connections using thresded rods and connection circular steel profiles. Master's thesis, NTNU.

[21] NS-EN 13501-2 (2009). *Brannklassifisering av byggevarer og bygningsdeler, del 2*. Standard Norge.

[22] NS-EN 14080 (2013). *Trekonstruksjoner - Limtre og limt laminert heltre*. Norsk Standars.

[23] NS-EN 1990 (2016). *Eurokode 0: Grunnlag for prosjektering av konstruksjoner*. Standard Norge.

[24] NS-EN 1991-1-1 (2002). *Eurokode 1: Laster på konstruksjoner - Del 1-1: Allmenne laster - Tettehet, egenvekt og nyttelater i bygninger*. Standard Norge.

[25] NS-EN 1991-1-3 (2003). *Eurokode 1: Laster på konstruksjoner - Del 1-3: Allmenne laster - Snølaster*. Standard Norge.

[26] NS-EN 1991-1-4 (2005). *Eurokode 1: Laster på konstruksjoner - Del: 1-4: Allmenne laster - Vindlaster*. Standard Norge.

[27] NS-EN 1995-1-1 (2004). *Eurokode 5: Prosjektering av trekonstruksjoner - Del 1-1: Allmenne regler og regler for bygninger*. Standard Norge.

[28] NS-EN 1995-1-2 (2004). *Eurokode 5: Prosjektering av trekonstruksjoner - Del 1-2: Brannteknisk dimensjonering*. Standard Norge.

[29] NS-EN 338 (2016). *Konstruksjonstrevirke: Fasthetsklasser*. Norsk Standard.

[30] NTNU (2014). *fap2D user manual*, 3.1 edition. Developed by: Department of structural engineering.

[31] Olsen, M. F. and Hansen, O. (2016). Measuring vibrations and assessing dynamic properties of tall timber building. Master's thesis, NTNU.

[32] Reynolds, T., Harris, R., and Chang, W.-S. (2012). Dynamic response to tall timber buildings to wind load.

[33] Simulia (2014a). *Abaqus Analysis User's Guide*, 6.14 edition.

[34] Simulia (2014b). *Abaqus Theory Guide*, 6.14 edition.

[35] SINTEF (2016). Martinsons kl-trä. *Teknisk Godkjenning*.

[36] Stamatopoulos, H. and Malo, K. A. (2016). Withdrawal stiffness of threaded rods embedded in timber elements.

[37] Statsbygg (2013). Tre for bygg og bygg for tre. kunnskapsgrunlag for økt bruk av tre i offentlige bygg. Technical report, Landbruks- og matedepartementet, Oslo, Norway.

[38] TEK10 (2010). *Byggteknisk forskrift*. Avaliable from: https://dibk.no/byggeregler/tek/.

[39] Torp, K. U. (2016). Climate gas analysis and building solutions in wood.

[40] Utne, I. (2012). Numerical models for dynamic properties of a 14 storey timber building. Master's thesis, NTNU.

[41] Vessby, J. (2011). Analysis of shear walls for multi-storey timber buildings. Master's thesis, Linnaeus University.

[42] WOODSOLS (2016). Project description. Wood frame solutions for free space design in urban buildings.

Appendix A

Loads

A.1 Load cases

Table A.1 gives an overview of the ψ-factors, while Table A.2 gives load combinations.

Table A.1: Overview ψ_0, from NS-EN 1990 [23]

		ψ_0	ψ_1	ψ_2
A	Residential areas	0.7	0.5	0.3
B	Office areas	0.7	0.5	0.3
C	Congregation areas	0.7	0.7	0.6
D	Shopping areas	0.7	0.7	0.6
	Snow	0.7	0.5	0.2
	Wind	0.6	0.2	0.0

Table A.2: Load combination from NS-EN 1990 [23]

	Permanent load		**Dominant variable**	**Remaing variable**
	Favorable	Unfavorable	load	loads
Eq (2.3a)	$1.35 \cdot G_{kj,sup}$	$1.00 \cdot G_{kj,inf}$	$1.50/0^{1} \cdot \psi_{0,1} Q_{k,1}$	$1.50/0 \cdot \psi_{0,i} Q_{k,i}$
Eq (2.3b)	$1.20 \cdot G_{kj,sup}$	$1.00 \cdot G_{kj,inf}$	$1.50/0 \cdot Q_{k,1}$	$1.50/0 \cdot \psi_{0,i} Q_{k,i}$

[1] 1.50 if favorable, 0 if unfavorable

A.2 Live load

Table A.3 show examples of a buildings intended use and the associated live load.

Table A.3: Live loads, from NS-EN 1991-1-1 [24]

	Distributed load kg/m^2>kg/m^2	**Concentrated load** [kN]
Residential, floor	2	2
Office building	3	2
Schools, restaurants	3	4
Shopping areas	5	4

A.3 Snow load

The Equation (A.1) for snow load is found in NS-EN 1991-1-3 [25]. The shape of the roof decides the reduction factor μ_1. For this work, the assumption of a flat roof is used, which gives μ_1 equal 0.8, see Figure A.1. Snow loads for a selection of Norwegian cities are listed in Table A.4. Further investigations are required for either pitched or multi-span roofs. **Note**: s is referenced to as s_k in Section 2.4

$$s = \mu_1 \cdot C_e \cdot C_t \cdot s_k \tag{A.1}$$

where

$$s_k = \begin{cases} s_{k,0} & \text{if } H < H_g \\ s_{k,0} + n\Delta s_k & \text{if } H > H_g \end{cases} \tag{A.2}$$

$$n = \frac{H - H_g}{100}$$

where

μ_1	is the shape factor, equal 0.8 for a flat roof
C_e	is the exposure factor, $C_e = 1$
C_t	is the thermal factor, $C_t = 1$
H	is the metres above sea level, see Table A.4
H_g	is the ground height, equal 150 m

Table A.4: Snow loads from NS-EN 1991-1-3 [25]

City	H / H_g metres above sea level	$s_{k,0}$ [kN/m^2]	Δs_k [kN/m^2]
Oslo	0-150	3.5	
	151-250	4.5	
	251-350	5.5	
	>350	6.5	
Bergen	150	2.0	0.5
Trondheim	150	3.5	1.0
Tromsø	150	6.0	1.0

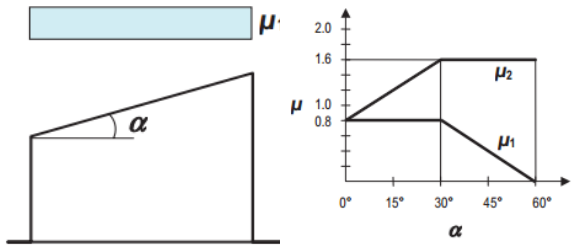

Figure A.1: Shape factor for snow load on roof, from NS-EN 1991-1-3 [25]

A.4 Wind load

The wind force is calculated by using Equations from NS-EN 1991-1-4 [26].

The internal and external forces, Equation (A.3), are added to find the resulting force on the building.

External and internal forces:

$$F_{w,e} = c_s c_d \sum_{surfaces} w_e A_{ref} \tag{A.3a}$$

$$F_{w,i} = \sum_{surfaces} w_i A_{ref} \tag{A.3b}$$

where

$c_s c_d$	is the structural factor, formulas for calculation in Section A.4.2
w_e	is the wind pressure on external surface at reference height z_e
w_i	is the wind pressure on internal surface at reference height z_i
A_{ref}	is the reference area

External and internal wind pressure:

$$w_e = q_p(z_e) c_{pe} \tag{A.4a}$$

$$w_i = q_p(z_i) c_{pi} \tag{A.4b}$$

where:

$q_p(z)$	is peak velocity pressure at reference height, formulas for calculation in Section A.4.1
c_p	is the pressure coefficient, formulas for calculation in Section A.4.3

A.4.1 The peak velocity pressure

The peak velocity pressure q_p is a function of the height and depends on the turbulence intensity I_v. The peak velocity pressure for a reference speed of 26 m/s is shown in

Figure A.2.

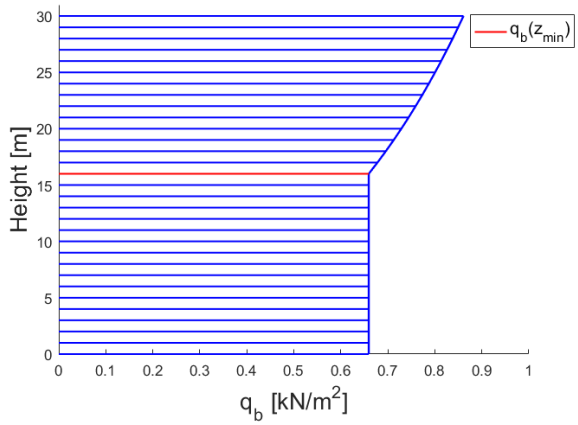

Figure A.2: The calculated peak velocity pressure for a reference speed of 26 m/s

$$q_p = [1 + 7 \cdot I_v] \cdot \frac{1}{2} \cdot \rho \cdot v_m^2 \tag{A.5}$$

where

ρ is the air density, $\rho = 1.25$ kg/m^3

I_v is the turbulence intensity

v_m is the mean wind velocity

$$I_v(z) = \frac{\sigma_v}{v_m} = \frac{k_l}{c_0 \cdot \ln(\frac{z}{z_0})} \qquad z_{min} < z < z_{max} \tag{A.6}$$

$$I_v(z) = \frac{\sigma_v}{v_m} = \frac{k_l}{c_0 \cdot \ln(\frac{z_{min}}{z_0})} \qquad z < z_{min} \tag{A.7}$$

where

σ_v is the standard deviation of the wind velocity

k_l is the turbulence factor

z is the height for where the wind load is calculated

z_0 for terrain category IV, $z_0 = 1$

z_{min} is decided by min[16m; $0.6 \times H$], for terrain category IV

The mean wind velocity v_m, is based on the reference wind velocity, v_b, at site. v_b, is dependent on the terrain, altitude, season etc. Most factors equal 1, which is a conservative assumption [26].

$$v_m = c_r \cdot c_0 \cdot v_b \tag{A.8a}$$

$$v_b = c_{dir} \cdot c_{season} \cdot c_{alt} \cdot c_{prob} \cdot v_{b,0} \tag{A.8b}$$

where

c_r is the roughness coefficient

c_0 is the terrain form factor, $c_0 = 1$

c_{dir} is the directional factor, $c_{dir} = 1$

c_{season} is the seasonal factor, $c_{season} = 1$

c_{alt} is the altitude factor, $c_{alt} = 1$

c_{prob} is the probability factor, $c_{prob} = 1$ when return periode 50 years, equivalent to 2 % annual probability

$v_{b,0}$ is the reference wind velocity, Table A.5

Table A.5: Reference wind velocity for selected Norwegian cities

	$v_{b,0}$ [m/s]
Oslo	22
Bergen	26
Trondheim	26
Max Norway (Træna et al.)	31

Terrain factor is IV represent city areas where 15 % of the area is covered with building with average height over 15 metre. The terrain roughness decides the roughness coefficient, c_r

$$c_r(z) = k_r \cdot \ln\left(\frac{z}{z_0}\right) \qquad z_{min} < z < z_{max} \tag{A.9}$$

$$c_r(z) = k_r \cdot \ln\left(\frac{z_{min}}{z_0}\right) \qquad z < z_{min} \tag{A.10}$$

where

k_r is the roughness for the terrain, $k_r = 0,24$ for terrian category IV

A.4.2 The structural factor

The structural factor takes into account the dynamic response of the structure due to wind, a simplified method is to use the structural factor $c_s c_d$. The factor takes the effect of non-simultaneous occurrence of peak wind pressures on the surface together with the effect of the vibrations of the structure due to turbulence [26]. The procedure in Annex B in NS-EN 1991-1-4 is used the determine $c_s c_d$.

$$c_s c_d = \frac{1 + 2 \cdot k_p \cdot I_v(z_s) \cdot \sqrt{B^2 + R^2}}{1 + 7 \cdot I_v(z_s)} \tag{A.11}$$

where:

z_s is the reference height, $z_s = 0.6 \cdot h \geq z_{min}$, see Figure A.3

k_p is the peak factor

I_v is the turbulence intensity

B^2 is the background factor, allowing the lack of full correlation of the pressure on the structure surface

R^2 is the resonance response factor, allowing for turbulence in resonance with the vibration mode

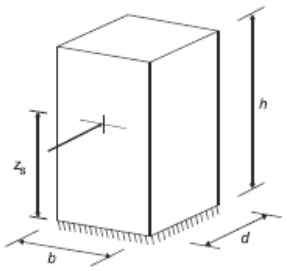

Figure A.3: Structural dimentions and reference height [26]

The background factor:

$$B^2 = \frac{1}{1 + 0.9 \cdot \left(\frac{b+h}{L(z_s)}\right)^{0.63}} \tag{A.12a}$$

$$L(z_s) = L_t \cdot \left(\frac{z}{z_t}\right)^{\alpha} \tag{A.12b}$$

where

$L(z_s)$	is the turbulence length scale
b, h	is the width and height of the structure
L_t	is the reference length scale, $L_t = 300m$
z_t	is the reference height, $z_t = 200m$
α	is $\alpha = 0.67 + 0.05\ln(z_0)$, where z_0 is the roughness length. $\alpha = 0.67$ for $z_0 = 1$

The resonance response factor:

$$R^2 = \frac{\pi^2}{2 \cdot \delta} \cdot S_L(z_s, n_{1,x}) \cdot R_h(\eta_h) \cdot R_b(\eta_b) \tag{A.13}$$

where

δ	is the total logarithmic decrement of damping
S_L	is the non-dimensional power spectral density function
R_h, R_b	is the aerodynamic admittance functions

It is difficult to calculate the correct damping of a system. To know the exact damping of a structure a vibration experiment must be executed on the actual structure. Equation (A.14) gives an approximation of the damping:

$$\delta = \delta_s + \delta_a + \delta_d \tag{A.14}$$

where

δ_s	is the logarithmic decrement of structural damping. Where ξ is the

damping ratio for the building

$$\delta_s = 2\pi \cdot \frac{\xi}{\sqrt{1-\xi^2}}$$

δ_a is the logarithmic decrement of aerodynamic damping for the fundamental mode. Where c_f, $n_{1,x}$ and m_e are defined in Appendix B

$$\delta_a = \frac{c_f \cdot \rho \cdot v_m(z_s)}{2 \cdot n_{1,x} \cdot m_e}$$

δ_d is the logarithmic decrement of damping due to special devices, $\delta_d = 0$ for this project

$$R_h = \frac{1}{\eta_h} - \frac{1}{2 \cdot \eta_h^2}\left(1 - e^{-2\eta_h}\right) \tag{A.15a}$$

$$R_b = \frac{1}{\eta_b} - \frac{1}{2 \cdot \eta_b^2}\left(1 - e^{-2\eta_b}\right) \tag{A.15b}$$

with

$$\eta_h = \frac{4.6 \cdot h}{L(z_s)} \cdot f_L(z_s, n_{1,x}) \tag{A.16a}$$

$$\eta_b = \frac{4.6 \cdot b}{L(z_s)} \cdot f_L(z_s, n_{1,x})[0.3cm] \tag{A.16b}$$

$$S_L(z,n) = \frac{6.8 \cdot f_L(z,n)}{\left(1 + 10.2 \cdot f_L(z,n)\right)^{5/3}} \tag{A.17a}$$

$$f_L(z,n) = \frac{n \cdot L(z)}{v_m(z)} \tag{A.17b}$$

$f_L(z,n)$ is a non-dimensional frequency determined by the fundamental frequency $n = n_{1,x}$ of the structure in [Hz].

A.4.3 The pressure coefficient

The velocity pressure profile vary both vertically and horizontally. Each zone has a pressure coefficient c_p, see Table A.6. Figure A.4 illustrate the different zones. A conservative simplification in this work, is not to vary the pressure profile over the height of the building and only use q for h. Another simplification is to use only the zone with the highest wind pressure coefficient on the walls parallel to the wind direction. The wind pressure on the roof is neglected.

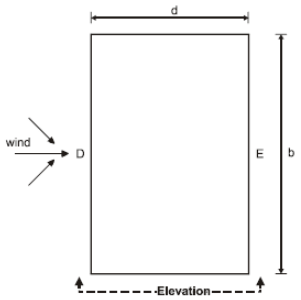

(a) Wind zones orthogonal to wind direction

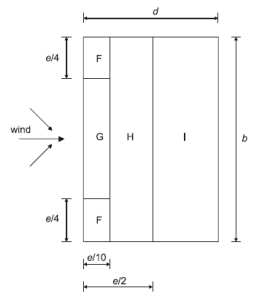

(b) Wind zones for roof

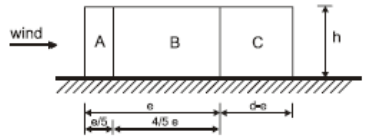

(c) Wind zones perpendicular to wind direction

Figure A.4: Wind zones

Table A.6: External and internal pressure coefficients [26]

	A	B	C	D	E	F	G	H	I
$c_{pe,10}$	-1.2	-0.8	-0.5	0.8	-0.5 to -0.7	-1.8	-1.2	-0.7	-0.2
$c_{pi,10}$	-0.3	-0.3	-0.3	0.2	-0.3	-0.3	-0.3	-0.3	-0.3

A.4.4 The calculated wind loads for each model

The wind loads for the models in this thesis, with some of the factors used for calculation and the resulting line load on the columns, are presented in this Appendix through Tables A.8 to A.31. The wind loads presented are used for all modifications for the given model, and models with similar geometric properties. E.g. the loads from Table A.29 are used for all modifications of the T-design with a shaft added to the support system, as well as for the model with a shaft *and* an extra shear wall added.

Note that the structural factor, $c_s c_d$, will have small variations with change of parameters within a typology. The structural factor affect the resulting wind load, but a new calculation of wind load for each modification is seen unnecessary, as the changes are small.

A brief check for the effect on including wind loads on the roof is also presented.

Wind load on roof

The main model including wind load on the roof was checked. The deviation in deflections for wind in x-direction from the main model without wind load on the roof is presented in Table A.7.

Table A.7: Deflection with and without wind load on roof, RCR main

	Deflection [mm]	
x-dir		
With wind on roof	38.7	
No wind on roof	38.8	+0.26%

RCR: Main model, n8-shaft and n8d7-shear

Table A.8: Geometric properties, RCR main

Wind direction		**x-dir**	**z-dir**
Structural factor	$c_s c_d$	0.90	0.87
Force coefficient	$c_{f,0}$	1.80	2.37
End-effect factor	ψ_λ	0.64	0.63

Table A.9: Wind load for RCR main, n8-shaft and n8d7-shear

		A	D	E	F	G	H	I
x-dir								
Wind pressure [kN/m^2]		1.09	0.72	0.62	1.51	1.09	0.73	0.30
Line force on columns [kN/m]	inner	6.8	1.7	1.1				
	outer	5.2	0.9	0.5				
z-dir								
Wind pressure [kN/m^2]		1.06	0.71	0.63	1.47	1.06	0.72	0.29
Line force on columns [kN/m]	inner	2.5	4.5	2.8				
	outer	1.3	3.4	2.1				

RCR: Variation of storeys

12 storeys.

Table A.10: Geometric properties, RCR n12d6

Wind direction		**x-dir**	**z-dir**
Structural factor	$c_s c_d$	0.915	0.903
Force coefficient	$c_{f,0}$	1.8	2.37
End-effect factor	ψ_λ	0.66	0.63

Table A.11: Wind load, RCR n12d6

		A	D	E
x-direction				
Wind pressure [kN/m^2]		1.29	0.82	0.75
Line force on columns [kN/m]	inner	8.1	2.1	1.6
	outer	6.2	1.0	0.8
z-direction				
Wind pressure [kN/m^2]		1.28	0.85	0.78
Line force on columns [kN/m]	inner	3.1	5.4	4.2
	outer	1.5	4.1	3.2

Seven storeys.

Table A.12: Geometric properties, RCR n7d6

Wind direction		**x-dir**	**z-dir**
Structural factor	$c_s c_d$	0.915	0.883
Force coefficient	$c_{f,0}$	1.8	2.37
End-effect factor	ψ_λ	0.64	0.63

Table A.13: Wind load, RCR n7d6

		A	D	E
x-direction				
Wind pressure [kN/m^2]		1.04	0.69	0.58
Line force on columns [kN/m]	inner	6.5	1.7	1.0
	outer	5.0	0.8	0.5
z-direction				
Wind pressure [kN/m^2]		1.04	0.69	0.60
Line force on columns [kN/m]	inner	2.5	4.4	2.6
	outer	1.2	3.3	2.0

Six storeys.

Table A.14: Geometric properties, RCR n6d6

Wind direction		**x-dir**	**z-dir**
Structural factor	$c_s c_d$	0.918	0.887
Force coefficient	$c_{f,0}$	1.8	2.37
End-effect factor	ψ_λ	0.64	0.63

Table A.15: Wind load, RCR n6d6

		A	D	E
x-direction				
Wind pressure [kN/m^2]		0.97	0.64	0.55
Line force on columns [kN/m]	inner	6.1	1.5	0.8
	outer	4.6	0.8	0.4
z-direction				
Wind pressure [kN/m^2]		0.97	0.64	0.56
Line force on columns [kN/m]	inner	2.3	4.1	2.3
	outer	1.2	3.1	1.7

RCR: Variation of slabs

12 slabs.

Table A.16: Geometric properties, RCR n8d12

Wind direction		**x-dir**	**z-dir**
Structural factor	$c_s c_d$	0.859	0.893
Force coefficient	$c_{f,0}$	2.3	2.0
End-effect factor	ψ_λ	0.64	0.63

Table A.17: Wind load, RCR n8d12

		A	D	E
x-direction				
Wind pressure [kN/m^2]		1.02	0.68	0.57
Line force on columns [kN/m]	inner	6.1	1.6	1.4
	outer	4.6	0.8	0.7
z-direction				
Wind pressure [kN/m^2]		1.05	0.70	0.59
Line force on columns [kN/m]	inner	2.5	4.2	3.5
	outer	1.3	3.2	2.6

10 slabs.

Table A.18: Geometric properties, RCR n8d10

Wind direction		**x-dir**	**z-dir**
Structural factor	$c_s c_d$	0.868	0.873
Force coefficient	$c_{f,0}$	2.1	2.10
End-effect factor	ψ_λ	0.64	0.63

Table A.19: Wind load, RCR n8d10

		A	D	E
x-direction				
Wind pressure [kN/m^2]		1.02	0.68	0.57
Line force on columns [kN/m]	inner	6.1	1.6	1.4
	outer	4.6	0.8	0.7
z-direction				
Wind pressure [kN/m^2]		1.03	0.69	0.58
Line force on columns [kN/m]	inner	2.5	4.1	3.5
	outer	1.2	3.1	2.6

12 slabs, only room.

Table A.20: Geometric properties, R n8d12-room

Wind direction		**x-dir**	**z-dir**
Structural factor	$c_s c_d$	0.851	0.914
Force coefficient	$c_{f,0}$	2.0	1.8
End-effect factor	ψ_λ	0.61	0.63

Table A.21: Wind load, R n8d12-room

		A	D	E
x-direction				
Wind pressure [kN/m^2]		1.02	0.68	0.61
Line force on columns [kN/m]	inner	4.6	1.6	1.5
	outer	-	0.8	0.7
z-direction				
Wind pressure [kN/m^2]		1.08	0.72	0.65
Line force on columns [kN/m]	inner	2.6	3.2	2.9
	outer	1.3	-	-

RCR: With shaft or additional shear walls

Table A.22: Geometric properties, RCR n8d7-shear

Wind direction		**x-dir**	**z-dir**
Structural factor	$c_s c_d$	0.886	0.872
Force coefficient	$c_{f,0}$	1.9	2.37
End-effect factor	ψ_λ	0.64	0.625

Table A.23: Wind load, RCR n8d7-shear

		A	D	E
x-direction				
Wind pressure [kN/m^2]		1.07	0.72	0.62
Line force on columns [kN/m]	inner	6.8	1.7	1.1
	outer	5.2	0.9	0.5
z-direction				
Wind pressure [kN/m^2]		1.06	0.71	0.62
Line force on columns [kN/m]	inner	2.5	4.5	2.8
	outer	1.3	3.4	2.1

T-design: main model

Values for z-direction based on torsional mode with most mass contribution in z direction, as mentioned in Section 3.6.

Table A.24: Geometric properties, T-design main

Wind direction		**x-dir**	**z-dir**
Structural factor	$c_s c_d$	0.85	0.87
Force coefficient	$c_{f,0}$	1.80	2.40
End-effect factor	ψ_λ	0.63	0.62

Table A.25: Wind forces and line loads, T-design main

		A	D	E
x-direction				
Wind pressure [kN/m^2]		1.04	0.69	0.60
Line force on columns [kN/m]	body inner	2.5	0.0	0.0
	body outer	1.2	4.2	3.6
	wing outer	5.0	0.8	0.7
	wing inner	0.0	1.7	1.4
z-direction				
Wind pressure [kN/m^2]		1.07	0.71	0.60
Line force on columns [kN/m]	body inner	0.0	1.7	1.4
	body outer	6.4	0.9	0.7
	wing outer	1.3	3.4	2.9
	wing inner	2.6	0.0	0.0

Adding slabs

Table A.26: Geometric properties, T-design n8-long-web

Wind direction		**x-dir**	**z-dir**
Structural factor	$c_s c_d$	0.85	0.84
Force coefficient	$c_{f,0}$	2.05	2.15
End-effect factor	ψ_λ	0.61	0.61

Table A.27: Wind forces and line loads, T-design n8-long-web

		A	D	E
x-direction				
Wind pressure [kN/m^2]		1.04	0.70	0.59
Line force on columns [kN/m]	body inner	2.5	0.0	0.0
	body outer	1.3	4.2	3.5
	wing outer	5.0	0.8	0.7
	wing inner	0.0	1.7	1.4
z-direction				
Wind pressure [kN/m^2]		1.04	0.69	0.59
Line force on columns [kN/m]	body inner	0.0	1.7	1.4
	body outer	6.2	0.8	0.7
	wing outer	1.2	3.3	2.8
	wing inner	2.5	0.0	0.0

Adding shaft

Table A.28: Geometric properties, T-design n8-shaft

Wind direction		**x-dir**	**z-dir**
Structural factor	$c_s c_d$	0.85	0.88
Force coefficient	$c_{f,0}$	2.4	1.8
End-effect factor	ψ_λ	0.61	0.63

Table A.29: Wind forces and line loads for T-design n8-shaft and n8-shaft-shear

		A	D	E
x-direction				
Wind pressure [kN/m^2]		1.05	0.70	0.60
Line force on columns [kN/m]	body inner	2.5	0.0	0.0
	body outer	1.3	4.2	3.6
	wing outer	5.0	0.8	0.7
	wing inner	0.0	1.7	1.5
z-direction				
Wind pressure [kN/m^2]		1.07	0.71	0.60
Line force on columns [kN/m]	body inner	0.0	1.7	1.4
	body outer	6.4	0.9	0.7
	wing outer	1.3	3.4	2.9
	wing inner	2.6	0.0	0.0

Six storey models

Table A.30: Geometric properties, T-design n6

Wind direction		**x-dir**	**z-dir**
Structural factor	$c_s c_d$	0.86	0.89
Force coefficient	$c_{f,0}$	2.4	1.8
End-effect factor	ψ_λ	0.60	0.63

Table A.31: Wind forces and line loads for T-design n6, n6-shear, n6-wide and n6-wide-shear

		A	D	E
x-direction				
Wind pressure [kN/m^2]		0.93	0.62	0.54
Line force on columns [kN/m]	body inner	2.2	0.0	0.0
	body outer	1.1	3.7	3.2
	wing outer	4.5	0.7	0.6
	wing inner	0.0	1.5	1.3
z-direction				
Wind pressure [kN/m^2]		0.96	0.64	0.54
Line force on columns [kN/m]	body inner	0.0	1.5	1.3
	body outer	5.8	0.8	0.6
	wing outer	1.2	3.1	2.6
	wing inner	2.3	0.0	0.0

Appendix B

Acceleration

The acceleration of the building can be calculated from Equation (B.1) from Annex B in NS-EN 1994-1-4 [26].

$$a = \sigma_{a,x} \cdot k_p \tag{B.1}$$

where

$\sigma_{a,x}$ is the standard deviation of the wind induced acceleration

k_p is the peak velocity factor, with $\nu = n_{1,x}$

$$\sigma_{a,x}(z) = \frac{c_f \cdot \rho \cdot b \cdot I_v(z_s) \cdot v_m^2}{m_e} \cdot R \cdot K_x \cdot \phi_{1,x}(z) \tag{B.2}$$

where

c_f is the force coefficient

ρ is the air density, $\rho = 1.25$ kg/m^3

b is the width of the structure

$I_v(z_s)$ is the turbulence intensity, Equation (A.7)

$v_m(z_s)$ is the mean wind velocity, Equation (A.8a), calculated with a return period of 2 years

R is the square root of the resonance response, Equation (A.13)

K_x is the non-dimensional coefficient

m_e is the along wind fundamental equivalent mass

$n_{1,x}$ is the fundamental frequency of along wind vibration of the structure

$\Phi_{1,x}(z)$ is the fundamental along wind modal shape

z_s is the reference height, $z_s = 0.6 \cdot h \geq z_{min}$, see Figure A.3

The force coefficient is dependent on the geometry of the building.

$$c_f = c_{f,0} \cdot \Psi_r \cdot \Psi_\lambda \tag{B.3}$$

where

$c_{f,0}$ is the force coefficient of rectangular sections with sharp corners, and dependent on the depth and with ratio. $c_{f,0}$ is found in Figure 7.23 in NS-EN 1991-1-4

Ψ_r is the reduction factor for round corners, assuming sharp corners $\Psi_r = 1$

Ψ_λ is the end-effect factor and a function of the solidity ratio φ and the slenderness, see Section 7.6 in NS-EN 1991-1-4

Assuming $\Phi_{1,x}(z) = (z/h)^\zeta$ and $c_0 = 1$, K_x can be approximated:

$$K_x = \frac{(2 \cdot \zeta + 1) \cdot \left\{ (\zeta + 1) \cdot \left[\ln\left(\frac{z_s}{z_0}\right) + 0.5 \right] - 1 \right\}}{(\zeta + 1)^2 \cdot \ln\left(\frac{z_s}{z_0}\right)} \tag{B.4}$$

ζ is the exponent of the mode shape

z_0 is the roughness length, $z_0 = 1$ for terrain category IV

For acceleration calculation the mean wind velocity, v_m, should be calculated with a return period of 1 year, and not 50 years as for the wind force [9]. Sine $p = 1$ is not valid in the formula for the probability factor, 2 years is used as the return period.

$$c_{prob} = \left(\frac{1 - K \cdot \ln(-\ln(1-p))}{1 - K \cdot \ln(-\ln(0.98))} \right)^n \tag{B.5}$$

where

p $p = \frac{1}{retur}$, where $retur = 2$

K is the shape parameter, $K = 0.2$

n is the exponent, $n = 0.5$

The peak factor k_p:

$$k_p = \sqrt{2 \cdot \ln(\nu \cdot T)} + \frac{0.6}{\sqrt{2 \cdot \ln(\nu \cdot T)}}; \qquad k_p \geq 3 \tag{B.6}$$

where

ν	is the up-crossing frequency, if $\nu < n_{1,x}$, $\nu = n_{1,x}$
T	is the averaging time for the mean wind velocity, T = 600

The up-crossing frequency ν:

$$\nu = n_{1,x} \cdot \sqrt{\frac{R^2}{B^2 + R^2}}; \qquad \nu \geq 0.08 Hz \tag{B.7}$$

The equivalent mass, m_e, can be calculated in two different ways. Either with the exact integral i Equation (B.8), or in a simplified manner based on properties of the upper third of the building, shown in Equation (B.9).

$$m_e = \frac{\int_0^l m(s) \cdot \Phi^2(s)\,\mathrm{d}s}{\int_0^l \Phi^2(s)\,\mathrm{d}s} \tag{B.8}$$

where

$m(s)$	is the mass per unit length
$\Phi(s)$	is the considered mode shape

$$m_e = \frac{m_3}{h_3} \tag{B.9}$$

where

m_3	is the average value of the mass over the upper third of the building
h_3	is the height of the upper third of the building

Appendix C

Fire Design

Formulas for structural fire design are found in NS-EN 1995-1-1[27] and NS-EN 1995-1-2 [28].

C.1 Load actions

The load actions are gathered from *Abaqus* for each model and reduced by a factor 0.6 . The effect of actions:

$$E_{d,fi} = \eta_{fi} \cdot E_d \tag{C.1}$$

where

E_d is the design effect of actions for normal temperature design, see limit states from Section 2.4.5

η_{fi} is the reduction factor of design load in the fire situation, as a simplification $\eta_{fi} = 0.6$ [28]

C.2 Strength and stiffness

To verify mechanical resistance under fire loading, following formulas are used:

$$f_{d,fi} = k_{mod,fi} \cdot \frac{f_{20}}{\gamma_{M,fi}} \tag{C.2}$$

$$S_{d,fi} = k_{mod,fi} \cdot \frac{S_{20}}{\gamma_{M,fi}} \tag{C.3}$$

where

$f_{d,fi}$ is the design strength in fire

$S_{d,fi}$ is the design stiffness property, modulus of elasticity, $E_{d,fi}$, or shear modulus, $G_{d,fi}$

f_{20} is the 20 % fractile of the strength property at normal temperature

S_{20} is the 20 % fractile of the stiffness property at normal temperature

$k_{mod,fi}$ is the modification factor for fire, $k_{mod,fi} = 1$

$\gamma_{M,fi}$ is the partial safety factor, $\gamma_{M,fi} = 1$

$$f_{20} = k_{fl} \cdot f_k \tag{C.4}$$

$$S_{20} = k_{fl} \cdot S_{05} \tag{C.5}$$

where

S_{05} is the 5 % fractile of the stiffness property at normal temperature

k_{fl} for glue laminated timber $k_{fl} = 1.15$

$\gamma_{M,fi}$ is the partial safety factor, $\gamma_{M,fi} = 1$

Table C.1 gives and overview over the characteristic strength and stiffness properties [22] and the calculated strength and stiffness properties for fire design.

Table C.1: Strength and stiffness properties for GL30c

	Characteristic	[N/mm^2]	**Design in fire**	[N/mm^2]
Bending strength	$f_{m,g,k}$	30.0	$f_{m,fi}$	34.500
Tensile strength	$f_{t,0,g,k}$	19.5	$f_{t,0,fi}$	22.425
	$f_{t,90,g,k}$	0.5	$f_{t,90,fi}$	0.575
Compression strength	$f_{c,0,g,k}$	24.5	$f_{c,0,fi}$	28.175
	$f_{c,90,g,k}$	2.5	$f_{c,90,fi}$	2.875
Shear strength	$f_{v,g,k}$	3.5	$f_{v,fi}$	4.025
Modulus of elasticity	$E_{0,g,05}$	10 800.0	$E_{0,fi}$	12 420.000

C.3 Capacity of cross section

The remaining effective cross section are calculated by using Equation (2.9) in Section 2.6. When exposed to fire on only one sides, the remaining dimensions of the cross section are:

$$h_{ef} = h - d_{ef}$$
$$b_{ef} = b - d_{ef}$$

where

h is the initial height of the cross section

b is the initial width of the cross section

d_{ef} is the charred and in-effective part of the cross section

Equations from NS-EN 1995-1-1 are used to calculate the capacity of the cross section when exposed to the fire load [27]. Figure C.1 defines the directions used for the column cross section.

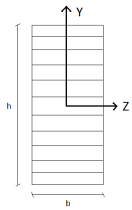

Figure C.1: Definition of y- and z-direction for the column cross section

C.3.1 Shear capacity

$$\frac{\tau_{d,y,fi}}{f_{v,fi}} \leq 1 \tag{C.7a}$$
$$\frac{\tau_{d,z,fi}}{f_{v,fi}} \leq 1 \tag{C.7b}$$

where

$$\tau_{d,fi} = \frac{3}{2} \cdot \frac{V_d}{b_{ef,cr} \cdot h_{ef}}$$

$$b_{ef,cr} = k_{cr} \cdot b_{ef}$$

$\tau_{d,fi}$ is the design shear stress

$V_{d,fi}$ is the design shear load

$b_{ef,cr}$ is the effective width to account for fracture in the cross sections

h_{ef} is the effective height of the cross sections

k_{cr} for glulam $k_{cr} = 0.67$

C.3.2 Combined bending and axial tension

$$\frac{\sigma_{t,0,fi}}{f_{t,0,fi}} + \frac{\sigma_{m,y,fi}}{f_{m,y,fi}} + k_m \cdot \frac{\sigma_{m,z,fi}}{f_{m,z,fi}} \leq 1 \quad \text{(C.9a)}$$

$$\frac{\sigma_{t,0,fi}}{f_{t,0,fi}} + k_m \cdot \frac{\sigma_{m,y,fi}}{f_{m,y,fi}} + \frac{\sigma_{m,z,fi}}{f_{m,z,fi}} \leq 1 \quad \text{(C.9b)}$$

where

k_m for rectangular cross sections $k_m = 0.7$

The bending stresses and axial tension are calculated with the reduced forces and effective cross section.

$$\sigma_{c,fi} = \frac{N_{Rd,fi}}{A_{ef}}$$

$$\sigma_{m,y,fi} = \frac{M_{Rd,y,fi}}{W_{y,ef}}$$

$$\sigma_{m,z,fi} = \frac{M_{Rd,z,fi}}{W_{z,ef}}$$

C.3.3 Combined bending, axial compression and buckling

$$\frac{\sigma_{c,0,fi}}{k_{c,y} \cdot f_{c,0,fi}} + \frac{\sigma_{m,y,fi}}{f_{m,y,fi}} + k_m \cdot \frac{\sigma_{m,z,fi}}{f_{m,z,fi}} \leq 1 \tag{C.11a}$$

$$\frac{\sigma_{c,0,fi}}{k_{c,z} \cdot f_{c,0,fi}} + k_m \cdot \frac{\sigma_{m,y,fi}}{f_{m,y,fi}} + \frac{\sigma_{m,z,fi}}{f_{m,z,fi}} \leq 1 \tag{C.11b}$$

where

k_m for rectangular cross sections $k_m = 0.7$

Formulas for calculating buckling. Calculate for y-axis and z-axis:

$$k_c = \frac{1}{k + \sqrt{k^2 - \lambda_{rel}^2}} \tag{C.12a}$$

$$k = 0.5 \cdot \left(1 + \beta_c \cdot (\lambda_{rel} - 0.3) + \lambda_{rel}^2\right) \tag{C.12b}$$

$$\lambda_{rel} = \frac{\lambda}{\pi} \cdot \sqrt{\frac{f_{c,0,k}}{E_{0.05}}} \tag{C.13a}$$

$$\lambda = \frac{l_{ef}}{i} \tag{C.13b}$$

where

l_{ef} is the buckling length, conservatively assuming $l_{ef} = 3$ m, which is the height of one storey. This assumption is conservative[1]

i $i = \frac{h_{ef}}{\sqrt{12}}$, $i = \frac{b_{ef}}{\sqrt{12}}$, where h_{ef} and b_{ef} are the dimensions of the effective cross section

β_c for glulam $\beta_c = 0.1$

[1] As the column has to be pinned in both ends to get this buckling length. The columns of the model are encastred in one end, and partially stiff in the other, decreasing the buckling length.

C.3.4 Lateral torsional instability

$$\left(\frac{\sigma_{m,y,fi}}{k_{crit}\cdot f_{m,y,fi}}\right)^2+\frac{\sigma_{c,0,fi}}{k_{c,z}\cdot f_{c,0,fi}}\leq 1 \tag{C.14}$$

where

k_{crit} is a factor which takes into account the reduced bending strength due to lateral buckling

$$k_{crit}=\begin{cases}1.0 & \text{for } \lambda_{rel,m}\leq 0.75\\ 1.56-0.75\cdot\lambda_{rel,m} & \text{for } 0.75<\lambda_{rel,m}\leq 1.4\\ \frac{1.0}{\lambda^2_{rel,m}} & \text{for } 1.4<\lambda_{rel,m}\end{cases} \tag{C.15}$$

$\lambda_{rel,m}$ is the relative slenderness, and is calculated in accordance to Equation (C.16).

$$\lambda_{rel,m}=\sqrt{\frac{f_{m,y,fi}}{\sigma_{m,crit}}} \tag{C.16}$$

where

$\sigma_{m,crit}$ is the critical bending stress

$$\sigma_{m,crit}=\frac{0.78\cdot b^2_{fi}}{h_{fi}\cdot l_{ef}}\cdot E_{0.05} \tag{C.17}$$

b_{fi} is the effective cross sectional width due to fire

h_{fi} is the effective cross sectional height due to fire

l_{ef} is the effective lateral buckling length, l_{ef} = 3 m[2]

[2]Conservative assumption, as the column has to be pinned in both ends to get this buckling length

Control of lateral buckling

Lateral buckling may occurs when the second moment of inertia is considerable larger about the strong axis than the weak axis, making slender columns critical. For all increased cross sections in this thesis, $\lambda_{rel,m}$ is less than 0.75, and lateral buckling will then not occur. Table C.2 list k_{crit} and $\lambda_{rel,m}$ for the main models and the most slender column for a increased cross section.

Table C.2: k_{crit} and $\lambda_{rel,m}$ for different cross sections

Effective cross section [mm]	k_{crit}	$\lambda_{rel,m}$
70 × 380 (T-design, outer corner column)	0.85	0.94
70 × 310 (RCR, corridor column)	0.92	0.85
140 × 605 (T-design, outer corner column)	1.00	0.60

C.4 Resulting fire design

The tables not listed in Chapter 4 are presented here, from Table C.3 to C.8. In this section the resulting fire loads are listed, together with the calculated utilisation of the cross sections.

C.4.1 Design: Room Cooridor Room

C.4.2 Variation of storeys

Six storeys.

Table C.3: Fire design loads, **six storeys** n6d6, *Combination 3 + 4*

Column **eff. cross section** [mm×mm]		M_z [kNm]	M_y [kNm]	V_z [kN]	V_y [kN]	N [kN]	P [kN]
Corridor, exterior, 200×535	x-dir	20.7	9.0	10.1	6.5	0.0	246.4
	z-dir	0.6	19.2	5.2	2.4	0.0	244.7
Outer corner, 200×605	x-dir	20.7	6.0	10.1	6.5	0.0	316.9
	z-dir	3.2	23.0	20.9	4.7	0.0	349.5

Table C.4: Utilisation of cross section, **six storeys**, *Combination 3 + 4*

	Corridor, ext.		Outer corner	
	x-dir	**z-dir**	**x-dir**	**z-dir**
Shear				
C.7a	3 %	2 %	3 %	2 %
C.7b	5 %	2 %	5 %	2 %
Bending and tension				
C.9a	12 %	16 %	8 %	17 %
C.9b	11 %	11 %	8 %	12 %
Bending, comp. and buckling				
C.11a	21 %	25 %	16 %	30 %
C.11b	20 %	19 %	15 %	23 %

Seven storeys.

Table C.5: Fire design loads, **seven storeys**, *Combination 3 + 4*

Column **eff. cross section** [mm×mm]		M_z [kNm]	M_y [kNm]	V_z [kN]	V_y [kN]	N [kN]	P [kN]
Corridor, exterior, 200×670	x-dir	35.5	10.6	10.7	8.6	0.0	291.7
	z-dir	0.5	30.3	6.4	2.4	0.0	180.8
Outer corner, 200×740	x-dir	35.5	7.1	10.6	8.6	0.0	291.7
	z-dir	3.2	33.0	25.8	4.9	0.0	407.0

Table C.6: Utilisation of cross section, **seven storeys**, *Combination 3 + 4*

	Corridor, ext.		Outer corner	
	x-dir	**z-dir**	**x-dir**	**z-dir**
Shear				
C.7a	4 %	2 %	3 %	2 %
C.7b	4 %	4 %	4 %	3 %
Bending and tension				
C.9a	12 %	20 %	8 %	20 %
C.9b	12 %	14 %	9 %	14 %
Bending, comp. and buckling				
C.11a	21 %	25 %	16 %	31 %
C.11b	19 %	19 %	15 %	24 %

Variation of slabs

12 slabs, only room part

Table C.7: Fire design loads, **n8d12-room**, *Combination 3 + 4*

Column **eff. cross section** [mm×mm]		M_z [kNm]	M_y [kNm]	V_z [kN]	V_y [kN]	N [kN]	P [kN]
Exterior mid., 210×760	x-dir	132.8	9.7	11.8	21.0	0.0	281.9
	z-dir	1.7	24.0	18.4	4.2	0.0	438.8
Outer corner, 210×830	x-dir	132.8	9.7	7.9	22.9	0.0	375.8
	z-dir	1.7	24.0	15.4	6.2	0.0	478.7

Table C.8: Utilisation of cross section, **n8d12-room**, *Combination 3 + 4*

	Exterior mid.		Outer corner	
	x-dir	**z-dir**	**x-dir**	**z-dir**
Shear				
C.7a	7 %	0 %	4 %	0 %
C.7b	4 %	0 %	1 %	0 %
Bending and tension				
C.9a	16 %	12 %	7 %	3 %
C.9b	19 %	8 %	9 %	2 %
Bending, comp. and buckling				
C.11a	22 %	22 %	11 %	8 %
C.11b	25 %	17 %	13 %	7 %

Appendix D

Slab Partition

Since the connection properties between the slabs are unknown, they are modelled as a partition with properties resembling 1/10 of the bending stiffness of the slab about the strong axis. The partition is modelled as an isotropic material and the poission ratio is set to $\nu = 0.3$.

The bending stiffness for a plate:

$$D = \frac{Et^3}{12 \cdot (1 - \nu^2)} \tag{D.1}$$

For the slab $t = 350\,\text{mm}$ and $E_1 = 15000\ \text{N/m}^2$ and $\nu_{12} = 0.6$ in the longitudinal direction. The resulting stiffness $D = 8.374 \cdot 10^{10}\text{N mm}$.

The bending stiffness for a beam:

$$EI = \frac{E \cdot bh^3}{12} \tag{D.2}$$

The dimensions for the partition are set to: $b = 100\,\text{mm}$ and $h = 350\,\text{mm}$.

$EI \approx 1/10 \cdot D$, resulting elastic modulus for the partition $E = 23.4\,\text{MPa}$ rounded up to be $E = 30\,\text{MPa}$.